UNIVERSITY OF SOUTHAMPTON

FACULTY OF PHYSICAL SCIENCES AND ENGINEERING

Optoelectronics Research Centre

The Rotating Cavity Laser

by

Matthew Eckold

Thesis for the degree of Doctor of Philosophy

January 2015

UNIVERSITY OF SOUTHAMPTON

ABSTRACT

FACULTY OF PHYSICAL SCIENCES AND ENGINEERING
Optoelectronics Research Centre

Doctor of Philosophy

THE ROTATING CAVITY LASER

by Matthew Eckold

This thesis describes a new technique for mitigating the detrimental thermal phenomena that often limit the power scaling potential of solid state lasers. The unavoidable heating effect that arises from the quantum defect leads to a degradation in beam quality, reduced efficiency and, eventually catastrophic failure. However, lasing processes occur on a faster time scale than those associated with heat flow through a typical laser gain medium. This is made use of whenever a laser is operated in a QCW mode, the laser is operated within an adiabatic window then turned off whilst the gain medium cools. This adds a constraint to the maximum duty cycle of the laser and thus reduces the average power output. Alternatively to separating the two processes in time they can be separated in space.

The thermal process can be separated from lasing with the introduction of motion to the system. By passing a collinear pump beam and laser mode through a rotating periscope placed in front of a gain medium the lasing spot can be moved into cold material before heat is able to flow. We call this arrangement the Rotating Cavity Laser (RCL). Unlike previously demonstrated solid state lasers which make use of motion, the RCL keeps the gain medium stationary. This allows it to be heat sunk directly, simplifying the mechanical arrangement.

Within this thesis the first results from an RCL are presented with theoretical predictions of the influence motion has both on the lasing and thermal properties of the system. Attention is paid to the regime where stimulated emission is negligible and the losses due to motion are therefore greatest. The analysis of this regime allowed the threshold under motion to be calculated and the approach was verified experimentally.

The RCL architecture allowed 120 W of 1064 nm light to be generated from a single end pumped Nd:YAG ceramic slab. The presence of moving intracavity components was found to have consequences for the stability of the power output. When producing 72 W the output power varied with a standard deviation of 2.8%, importantly this variation was cyclic suggesting it would be straightforward to correct by modulating the pump source. Whilst excellent beam quality was found at low powers the M^2 became poor as the pump power increased. At output powers less than 51 W the beam quality was found to be constant over a rotation period. It is postulated that the increase in M^2 at high pump powers, as well as the increase in variation in beam quality over a rotation period, is partly due to the presence of a thermally induced wedge compromising the alignment of the resonator.

A number of experiments are also presented that demonstrate the effectiveness of introducing motion as a method to reduce the thermal load within a laser gain medium. Losses due to stress induced birefringence were reduced from 8% for the stationary case to less than 0.5% by rotating the periscope. The aberrating nature of the thermal lens present in the RCL was also investigated by passing a 1064 nm probe beam through it. When the periscope was stationary the probe beam degraded from an M^2 of 1.1 to 2.0 under 16.3 W of pump power. Introducing motion and pumping the slab with 180 W resulted in the M^2 increasing to 1.4, clearly demonstrated the greater resilience a system with motion has to detrimental thermal effects.

Contents

List of Figures

List of Tables

Declaration of Authorship

I, Matthew Eckold, declare that the thesis entitled *The Rotating Cavity Laser* and the work presented in the thesis are both my own, and have been generated by me as the result of my own original research. I confirm that:

- this work was done wholly or mainly while in candidature for a research degree at this University;
- where any part of this thesis has previously been submitted for a degree or any other qualification at this University or any other institution, this has been clearly stated;
- where I have consulted the published work of others, this is always clearly attributed;
- where I have quoted from the work of others, the source is always given. With the exception of such quotations, this thesis is entirely my own work;
- I have acknowledged all main sources of help;
- where the thesis is based on work done by myself jointly with others, I have made clear exactly what was done by others and what I have contributed myself;
- none of this work has been published before submission

Signed:.....

Date:14/1/15.....

Acknowledgements

After four years at the ORC there is not enough space to mention everyone whose help and support I have benefited from. I am fortunate enough to include people on this list who are not just colleagues, but friends.

I would like to thank my supervisors Professor Andy Clarkson and Dr Jacob Mackenzie for inspiration, support, and guidance. Group members past and present Masaki Tokurakawa, Jae Daniel, Kristian Thaller, Nikita Simakov, Di Lin, Stan Vassilev, Antonin Bilaud, and Callum Smith. Simon Butler, without whom the mechanical elements of my project would not have been as successful as they were. A special mention to the 'handsome' of post docs I have had the pleasure of working, drinking, eating, and cycling with; Drs Alex Butler (in part for coining the collective noun), Stephen Beecher, Jaclyn Chan, and Peter Shardlow.

My parents, siblings, and house mates; Dave, Lloyd, Patrick and Poppy for being around when I need them.

Nomenclature

η	Efficiency
λ	Wavelength
ν	Lasing frequency
ϕ	Photon density
$\rho(\nu)$	Energy density of a photon flux with central wavelength ν
σ	Stimulated emission cross section
A_{ij}	The Einstein A coefficient for the transition i to j
B_{ij}	The Einstein B coefficient for the transition i to j
c	Speed of light
g	Gain coefficient
g_0	Small signal gain coefficient
h	Planck's constant
I_{circ}	Circulating electric field intensity
k	Boltzmann's constant
l	Length of gain medium
n	Population inversion
n	Refractive index
n_1	The population density of the lower electronic laser level
n_2	The population density of the upper electronic laser level
P_{ij}	Pump rate from level i to level j
P_{pump}	Pump power
q	Complex beam parameter
R	Radius of curvature
T	Temperature
w	Beam waist (radius)
W_{ij}	Absorption and stimulated emission coefficient for the transition i to j, this is directly proportional to the Einstein B coefficient

Chapter 1

Introduction

1.1 Overview

A laser is an unusual light source. In nature photons are produced somewhat randomly with no relation between the phase and direction of subsequent photons. A laser on the other hand produces a uniform, directional stream of photons that can be readily manipulated. Since their invention in 1958 by Schawlow and Townes lasers have become ubiquitous and are now found across the modern world [1]. Their unique properties have resulted in a myriad of applications for a device that initially had none. They have found uses within the manufacturing industry as a tool, as the backbone of telecommunication networks, within consumer electronics and are now even used in surgery - both elective and emergency.

Lasers have not just replaced other technologies in the manufacturing sector, they have triggered the development of processes not previously possible. In particular, laser sintering of powdered materials has not only reduced the time required for prototyping components but allows parts not previously manufacturable to be made. For example, it is not possible to machine components with internal moving parts with traditional techniques but it is with additive manufacturing such as laser sintering [2].

There has been rapid development in the laser field since their first demonstration and now lasers are responsible for the shortest controllable events [3] and designs have been produced for systems intense enough to interact with the vacuum [4]. However, throughout their history how the excess heat that is generated by the lasing process is handled has been a reoccurring problem. This heat can manifest itself as a performance limitation or in more severe cases it can lead to catastrophic failure of the laser device.

The thermal management of laser devices has thus been the motivation behind the design of many high power laser systems. For example thin disk lasers were specifically designed to manage the direction of heat flow to allow power scaling [5], and the small

temperature rise found along the length of a typical fibre laser has contributed to an orders of magnitude increase in output power within ten years [6].

While thin disk and fibre geometries overcome thermally induced problems this is often at the expense of other aspects of the laser's operation. In particular the high intensities associated with laser pulses are of particular concern when constrained to a small mode size like in a fibre laser. Extreme peak intensities can damage the optical fibre they are propagating through, but adverse effects are typically encountered at considerably smaller intensities [6].

For example, the large intensities found in fibre lasers trigger the onset of nonlinear effects which can act to impair the performance of the laser device. Furthermore the large pumped volumes in both fibres and thin disks makes it difficult to store energy. If an excited laser ion spontaneously decays it is possible for the generated photon to travel a considerable distance through the active region, all the while stimulating the emission of further photons which in turn extract more energy. The smaller pumped volumes associated with solid state lasers avoid this problem, allowing the energy storage potential of laser ions to be better utilized [6].

Solid state lasers, whilst no longer competitive for the generation of raw average power, are thus still very much of interest for the generation of high peak powers. However, generating them alongside high average power by running at high repetition rates is not straightforward due to their susceptibility to thermal effects. The thermal gradients present in a solid state gain medium create a variety of problems including lensing and the modification of the material's refractive index in a non-uniform manner [7].

Many different approaches have thus been tried to improve the rate of heat extraction from a solid state laser gain medium, some more extreme than others. For example for optimum cooling a fluid can be passed directly over the laser crystal, however if this coolant passes through the beam path consideration has to be given to its optical properties. For this reason heavy water, D_2O, has been suggested, and demonstrated, as a coolant for 1 μm laser sources as it shows an order of magnitude less absorption than water [8]. Diamond has also been used been used as a cooling surface for the same reasons [9].

This thesis explores a new concept for the removal of the thermal load within a solid state laser crystal that takes advantage of the difference in time scales associated with heat flow and the lasing processes. Whilst this difference is commonly used within a QCW laser to separate the two processes in time, here motion is introduced to separate them in space to allow CW laser operation independently of thermal processes.

1.2 Thesis Structure

The following chapter introduces the concept of optical gain and shows how it can be extended to produce a laser resonator. An outline is then given of what has already been achieved in the field of high power lasers, in particular the different laser designs used will be explored. The challenges currently facing the laser community as they try and power scale further will then be explained. Particular emphasis is placed on the constraints thermal effects place on the operation of high average power solid state sources.

§3 introduces the Rotating Cavity Laser (RCL), the development of which is the subject of this thesis. The RCL makes use of intracavity motion to both separate heat flow from the lasing processes and provide a larger thermal mass without changing the optical properties of the system. A discussion on the consequences of including motion and examples of prior art is included.

The next chapter describes the first demonstration of an RCL and includes discussion of an initial prototype which was constrained to low speed operation as well as a device capable of introducing motion of the order of multiple beam waists per upper state lifetime. The low speed device confirmed that the consequences of introducing motion were less severe than the thermal effects they over came. The high speed device was used to confirm the predicted effect motion can have on the lasing processes. In the process of characterising this now pump limited system it was found that traditional beam profilers were unable to temporally resolve any variation in beam quality over a rotation cycle. A profiler capable of doing this is then described.

In §5 the pump source used previously was replaced with a more powerful unit to allow the capabilities of the RCL to be more fully explored. A discussion of results found in both a resonator and amplifier configuration are presented. Preliminary amplifier results revealed a fault in the thermal interface between the gain medium and the heat sink. A description of a procedure to improve this interface that made use of both ultrasonic soldering and an oxygen free environment is then included. Amplifier results with improved heat sinking indicated a larger than expected thermal wedge was being produced by the pump spot, FEA analysis was then conducted to attempt to identity the source of this wedge.

The final experimental chapter includes a number of experiments conducted to demonstrate the improved thermal load handling ability motion allows. Stress induced birefringence is used to determine the strength of any thermally induced stresses inside the pumped spot. The aberating quality of the thermal profile created by the moving pump spot is then investigated with a probe beam. An approach to predict the thermal lens strength under rotation is also presented with a comparison with experimental data. Finally, a discussion of the ultimate power scaling limit of the RCL is presented.

References

[1] A. Schawlow and C. Townes, "Infrared and optical masers," *Physical Review*, vol. 112, no. 6, p. 1940, 1958.

[2] A. Lou and C. Grosvenor, "Selective Laser Sintering, Birth of an Industry." http://www.me.utexas.edu/news/2012/0712_sls_history.php#ch4. Accessed: 04/01/2015.

[3] R. Trebino, "Measuring the seemingly immeasurable," *Nature Photonics*, vol. 5, pp. 189–192, Apr. 2011.

[4] E. Gerstner, "Laser physics: Extreme light," *Nature*, vol. 446, pp. 16–18, Mar. 2007.

[5] A. Giesen, H. Hügel, A. Voss, and K. Wittig, "Scalable concept for diode-pumped high-power solid-state lasers," *Applied Physics B*, vol. 372, pp. 365–372, 1994.

[6] D. J. Richardson, J. Nilsson, and W. A. Clarkson, "High power fiber lasers: current status and future perspectives [Invited]," *Journal of the Optical Society of America B*, vol. 27, p. B63, Oct. 2010.

[7] W. A. Clarkson, "Thermal effects and their mitigation in end-pumped solid-state lasers," *Journal of Physics D: Applied Physics*, vol. 34, p. 2381, 2001.

[8] M. Siebold, M. Loeser, G. Harzendorf, H. Nehring, I. Tsybin, F. Roeser, D. Albach, and U. Schramm, "High-energy diode-pumped D¡sub¿2¡/sub¿O-cooled multislab Yb:YAG and Yb:QX-glass lasers.," *Optics letters*, vol. 39, pp. 3611–4, June 2014.

[9] Y. Tzuk, A. Tal, S. Goldring, Y. Glick, E. Lebiush, G. Kaufman, and R. Lavi, "Diamond Cooling of High-Power Diode-Pumped Solid-State Lasers," *IEEE Journal of Quantum Electronics*, vol. 40, pp. 262–269, Mar. 2004.

Chapter 2

Background

2.1 Introduction

To produce a beam of light made of coherent photons a device must first be constructed that allows stimulated emission to become dominant over spontaneous emission. This device must also ensure this beam can propagate inside it whilst satisfying the wave equation. A laser resonator is such a device, and its success relies on the existence of optical gain.

This chapter introduces the concept of optical gain and provides the theory behind how it can be used to form an optical resonator and thus laser action. Equations to predict key laser performance properties, namely threshold and slope efficiency are then derived. A comparison of the thermal and optical processes that can occur concurrently in a laser gain medium is then presented, with a particular focus on their differing time scales.

The definition of 'brightness' is then provided as it can than be used as a quality factor to compare different laser sources. The different mechanisms that can limit not only the output power of a resonator but the brightness of the laser's output are then introduced. Finally, a brief overview of different laser designs that attempt to overcome some of these power limiting phenomena is then given along with some state of the art results.

2.2 Gain

The concept of optical gain is integral to how a laser operates, the fundamental mechanism behind this phenomenon was described by Einstein in 1917 [1]. In this paper Einstein describes the three processes photons can undergo when they interact with a material's electronic structure. They are shown by Figure 2.1 and were described with probabilistic constants, the Einstein A and B coefficients, in Einstein's paper.

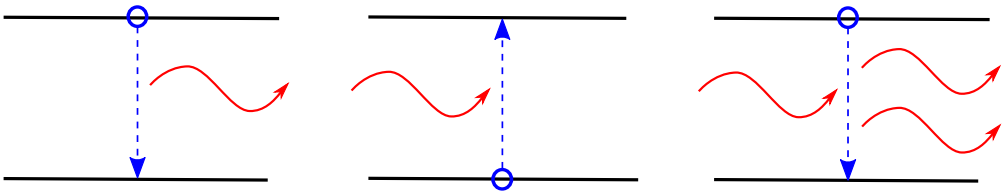

Figure 2.1: Spontaneous emission, absorption and stimulated emission are the three photon-matter processes

The A coefficient is the probability an electron will spontaneously decay to a lower energy level, releasing a photon of a frequency which is related to the energy gap between the two electron levels by Planck's Relation. The B coefficients deal with the case of an external photon interacting with the atom. When a photon interacts with an atom there is a chance that it will be absorbed, however if the atom already has excited electrons there is a chance that another photon will be instead emitted through a process known as stimulated emission. The probability of these two events happening is linked to the electron population of each of the levels by the B coefficients. These are related to one another via the degeneracy of the electronic levels involved. If neither state is degenerate the ratio between the rate of stimulated emission and absorption events is equal to the ratio of the electron populations.

When an atom releases energy via stimulated emission the generated photon is indistinguishable from the incident photon; it has the same phase, polarization, direction, and energy. The incident light is therefore amplified by this process, however if there is an electron population in the lower level absorption will also occur. For a net amplification effect to take place there must therefore be more electrons in the excited state than in the lower state, this is known as population inversion.

Population inversion cannot happen without the input of energy. If a system is in thermal equilibrium thermodynamics shows the population of different energy states will be given by Boltzmann's distribution, Equation 2.1. Here n_2 is the electron population density of the upper state, n_1 the population density of the lower state, k is Boltzmann's constant, T is the temperature, and ΔE is the energy difference between the two levels. This clearly does not allow a higher energy level to have a larger population than a lower one.

$$\frac{n_2}{n_1} = \exp\left(\frac{-\Delta E}{kT}\right) \tag{2.1}$$

If the system is not in thermal equilibrium the population of electrons no longer obeys Boltzmann's distribution, but spontaneous emission and absorption must first be overcome before gain can be realised. If only two energy levels are considered Equation 2.2 gives the change in population of the upper state, where A_{21} is the Einstein A coefficient for the transition from the level 2 to 1. W_{21} and W_{12} are the absorption and stimulated emission rates respectively, these rates are simply the Einstein B coefficients

multiplied by the energy density of the part of the incident photon flux that interacts with this transition, $\rho(\nu)$, and give the proportion of an energy level's population that is transferred per unit time [2].

$$\frac{dn_2}{dt} = -n_2 A_{21} - n_2 W_{21} + n_1 W_{12} \tag{2.2}$$

If it is assumed the entire electron population can be described by $n = n_1 + n_2$, and that neither state is degenerate so that $W_{12} = W_{21} = W$ the solution to Equation 2.2 is given by Equation 2.3. If the photon flux is large so $W >> A_{21}$ and in the limit $t \to \infty$ this reduces to Equation 2.4.

$$n_2(t) = \left(n_2(0) - \frac{nW}{A_{21} + 2W} \right) e^{-(A_{21}+2W)t} + \frac{nW}{A_{21} + 2W} \tag{2.3}$$

$$n_2 = \frac{n}{2} \tag{2.4}$$

Clearly it is not possible to achieve inversion with just two electronic levels. The most a two level system can do is become transparent to the incoming photon flux.

A more complicated electronic structure is thus needed to support population inversion and produce optical gain. By making use of energy levels with different A coefficients, and therefore different electron lifetimes, it is possible to indirectly populate a higher energy level from a lower one and achieve population inversion.

The simplest electronic structure that population inversion can exist under requires three levels, shown schematically in Figure 2.2(a). Some of these levels can be within the same Stark manifold, as is the case with in-band pumping [3], or they can all be in separate manifolds. Here electrons are pumped from the ground state to a level with a short lifetime. From this energetic state the electrons drop into an intermediate long

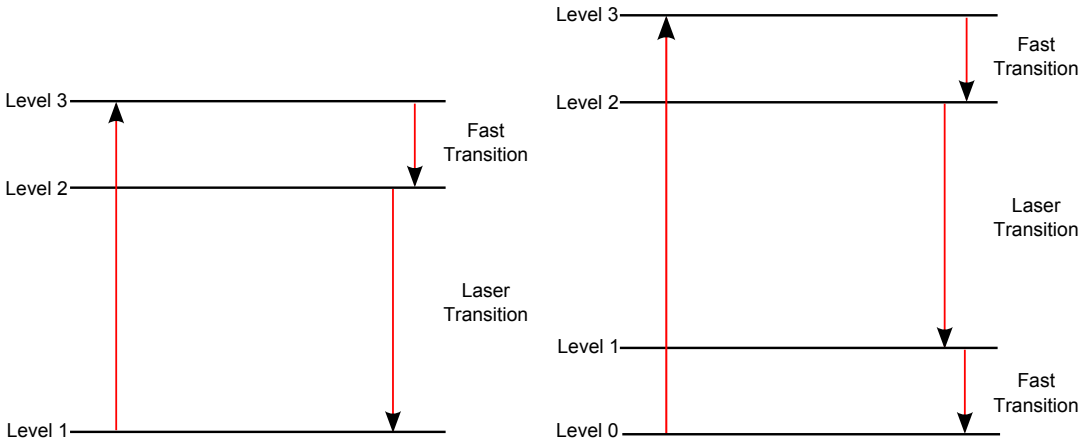

(a) 3 level (b) 4 level

Figure 2.2: Energy levels required for population inversion

lifetime level and thereby produce a population inversion relative to the ground state. The populations of these levels change as described by Equation 2.5 when P_{13} is the proportion of an energy level promoted per unit time by pump photons.

$$\begin{aligned}\frac{dn_3}{dt} &= P_{13}n_1 - (A_{31} + A_{32})n_3 \\ \frac{dn_2}{dt} &= A_{32}n_3 - (W_{21} + A_{21})n_2 + W_{12}n_1 \\ \frac{dn_1}{dt} &= -P_{13}n_1 - W_{12}n_1 + (W_{21} + A_{21})n_2\end{aligned} \tag{2.5}$$

As stated above a 3 level system requires the transition between the most energetic level and the intermediate level to be fast, Equation 2.5 can therefore be simplified by setting $A_{32} >> A_{31}$ and $A_{32} >> P_{13}$. Like the 2 level case previously the probabilistic constants related to stimulated emission and absorption are taken to be equal so $W_{12} = W_{21} = W$. If a steady state is considered and neither state is degenerate Equation 2.6 can then be found.

$$\begin{aligned}P_{13}n_1 &= A_{32}n_3 \\ A_{32}n_3 - (W + A_{21})n_2 + Wn_1 &= -P_{13}n_1 - Wn_1 + (W + A_{21})n_2\end{aligned} \tag{2.6}$$

With Equation 2.6 it is straightforward to find Equation 2.7.

$$\frac{n_2}{n_1} = \frac{P_{13} + W}{A_{21} + W} \tag{2.7}$$

Using the approximation $n = n_1 + n_2$, which is appropriate if $A_{32} >> A_{21}$, and Equation 2.7 it is now possible to find the difference in population between the intermediate level and the ground state. This is given in Equation 2.8.

$$\begin{aligned}\Delta n &= n_2 - n_1 \\ &= n\left(\frac{P_{13} - A_{21}}{P_{13} + A_{21} + 2W}\right)\end{aligned} \tag{2.8}$$

If $\Delta n > 0$ there is a population inversion and an incident photon flux with a wavelength corresponding to the energy difference between the intermediate state and the ground state will experience gain. This situation occurs if the pump rate, P_{13}, is greater than the spontaneous emission rate of the intermediate energy level. It should also be noted that as the photon flux, embedded in W, increases $\Delta n \to 0$. Physically this means if the photon flux is large enough it will not experience gain as there is not enough energy available to amplify it but equally it will not experience reabsorption.

If $A_{21} > P_{31}$ in Equation 2.8 there is no inversion and the material will act as an attenuator. This is a key characteristic of 3 level laser materials, they must be pumped to be transmissive. By introducing a fourth energy level to the system, illustrated by

Figure 2.2(b), it is possible to have a material that can support a population inversion whilst being transparent to the incident photon flux at all times.

A 4 level system can be described by Equation 2.9, where once again it is assumed A_{32} is sufficiently large to make the other transitions out of level 3 negligible and that the probabilistic constants associated with absorption and stimulated emission are equal.

$$\begin{aligned}
\frac{dn_3}{dt} &= P_{03}n_0 - A_{32}n_3 \\
\frac{dn_2}{dt} &= A_{32}n_3 - n_2A_{21} - W\Delta n \\
\frac{dn_1}{dt} &= -A_{01}n_1 + n_2A_{21} + W\Delta n \\
\frac{dn_0}{dt} &= -P_{03}n_0 + A_{10}n_1
\end{aligned} \tag{2.9}$$

To find the condition for population inversion the case where the photon flux is small can be considered as, unlike the 3 level case, the depopulation of level 1 caused by this flux is assumed to be negligible so $W \to 0$. Again the steady state is considered and the population of level 3 is assumed to be small. The proportion of the total population in each level can then be found, and is given in Equation 2.10.

$$\begin{aligned}
n_2 &= n\left(\frac{P_{03}A_{10}}{A_{21}A_{10} + A_{21}P_{03} + P_{03}A_{10}}\right) \\
n_1 &= n\left(\frac{P_{03}A_{21}}{A_{21}A_{10} + A_{21}P_{03} + P_{03}A_{10}}\right) \\
n_0 &= n\left(\frac{A_{10}A_{21}}{A_{21}A_{10} + A_{21}P_{03} + P_{03}A_{10}}\right)
\end{aligned} \tag{2.10}$$

The condition for population inversion and therefore gain is thus given by Equation 2.11.

$$\Delta n = \frac{nP_{03}(A_{10} - A_{21})}{A_{21}A_{10} + A_{21}P_{03} + P_{03}A_{10}} \tag{2.11}$$

If $A_{10} > A_{21}$ any pump rate will create an inversion in a 4 level system as the pump does not have to overcome any absorbing property of the system. The threshold pump rate for gain can therefore be considerably lower in a 4 level system than that in a 3 level system.

2.3 The Laser Resonator

2.3.1 Laser Modes

If a pumped gain medium is placed near a mirror so that a spontaneously emitted photon is passed back through the medium it is possible for the emission of a second, identical, photon to be stimulated. If a second mirror is placed to feed these photons through the gain medium again it is straight forward to see how the process of repeated stimulated emission can lead to a build up of indistinguishable photons, as shown in Figure 2.3. This is the basic principle behind a laser resonator.

For the photon flux to continue to see gain on each round trip, each trip must overlap spatially on the previous one. The spatial profile of the optical wave described by these photons must therefore reproduce itself after each round trip. By constraining the wave equation in this way it is possible to find the forms of the profiles that can be supported by a resonator. The simplest, and lowest order, of these modes is a Gaussian. Further solutions in Cartesian coordinates are known as the Hermite-Gaussian modes and the solutions found using radial coordinates are the Laguerre-Gaussian modes [4].

Fox and Li found that a resonator can support many of these self-reproducing optical modes in their numerical study [5]. They go on to say that after many round trips the spatial profile of the photon flux stops evolving and the field stops receiving a net amplification as all the available energy is used to counter act losses experienced by the oscillating photons.

The modes that initially come into existence within the resonator depend on the initial electromagnetic field distribution within the resonator. This initial distribution is created by noise due to spontaneous emission. However, as there is finite gain within the gain medium and the modes have different diffraction losses associated with them, not all the modes will survive long enough to reach a steady state.

Each laser mode effectively competes for gain, and those that experience greater losses on each round trip diminish and are eventually extinguished. This leaves those that are able to extract enough energy from the gain medium to overcome any losses they

Figure 2.3: A flux of indistinguishable photons can be created by passing photons repeatedly through a gain medium

experience. The modes that survive are typically of low order, their exact form and number depends on the spatial distribution of the available gain within the resonator and its overlap with the propagating photon flux. It is possible to design a resonator so that the gain overlap with a desired mode is maximised, resulting in the chosen mode surviving into the steady state. This can be done with ABCD matrix analysis.

ABCD matrix analysis describes optical elements as a simple 2x2 matrix, some of which are given in Table 2.1. By applying these matrices to the complex beam parameter, Equation 2.12, it is possible to calculate how a Gaussian beam propagates through an optical system. Here R is the radius of curvature of the beam, w is the beam waist, λ is the wavelength and n is the refractive index of the medium the light is propagating through. By enforcing the condition that the beam must reproduce itself after a round trip, with this system it is possible to determine whether a given resonator can support a laser mode [4].

$$\frac{1}{q} = \frac{1}{R} - \frac{i\lambda}{\pi n w^2} \tag{2.12}$$

A further condition on the form the oscillating beam can take is imparted by the need to have a standing wave pattern within this type of simple resonator. This leads to a comb of frequencies that the resonator can support. As typical cavity lengths are large when compared with the wavelength of the oscillating light, multiple longitudinal modes are typically within the gain envelope; a notable exception being the HeNe laser [6]. No energy extraction can occur at the nodes of the standing wave pattern, this leads to a phenomenon known as spatial hole burning. These residual areas of gain allow other

Optical Element	Ray Transfer Matrix
Free space	$\begin{pmatrix} 1 & d \\ 0 & 1 \end{pmatrix}$
Reflection from a mirror	$\begin{pmatrix} 1 & 0 \\ 0 & 1 \end{pmatrix}$
Reflection from a curved mirror	$\begin{pmatrix} 1 & 0 \\ -\frac{2}{R} & 1 \end{pmatrix}$
Thin lens	$\begin{pmatrix} 1 & 0 \\ -\frac{1}{f} & 1 \end{pmatrix}$

Table 2.1: Ray transfer matrices for some common optical elements [4]

frequencies within the gain band to exist within the resonator leading to an output made of a range of discrete wavelengths. The requirement to have a standing wave inside the resonator can be removed by feeding emitted photons back into a gain medium with a ring [7].

2.3.2 Predicting Resonator Performance

If a laser mode is to survive inside a laser resonator it needs to undergo enough amplification per round trip to counteract any losses it experiences. These round trip losses are a combination of diffraction effects, absorption, scattering, and the finite reflectivity of the resonator mirrors, in fact it is the finite reflectivity of the mirrors that provides the laser's output. The lowest pump rate that satisfies this condition is know as the threshold power, and it is possible to calculate this value with the laser rate equations. The efficiency the resonator converts pump energy to laser photons can also be determined by considering the rate equations.

If electron population densities are now considered it is convenient to expresses the Einstein B coefficients as part of a cross-section term. The definition of this term, which is known as the stimulated emission cross section, is given in Equation 2.13. Here h is Planck's constant. and c is the speed of light

$$\sigma = \frac{h\nu_s g(\nu_s, \nu_0) B_{21}}{c} \tag{2.13}$$

In reality the energy associated with an atomic transition can take a range of values described by a linewidth function. This is due to a number of broadening mechanisms, for example in a typical solid state gain medium vibrations of the host lattice shift the resonance frequency of the embedded ions at a high frequency, effectively broadening the transition. This particular form of broadening has a characteristic Lorentzian linewidth [7]. In Equation 2.13 this is taken into account by $g(\nu_s, \nu_0)$ where ν_S is the photon frequency and ν_0 is the linewidth centre frequency.

For a real system it is also more convenient to express the interacting photon flux energy density as a photon density, this is straightforward and the relationship is given by Equation 2.14 [2].

$$\phi = \frac{\rho(\nu)}{h\nu g(\nu)} \tag{2.14}$$

The probability of a stimulated emission event occurring can now be written as

$$W = \rho(\nu) B_{21} = c\sigma\phi \tag{2.15}$$

And, with the pump rate, P_{13}, rewritten as R_p for convenience and the degeneracy of levels 1 and 2 expressed with g_1 and g_2 the rate equations can be written as follows [2].

$$\frac{dn_2}{dt} = R_p n_0 - \left(n_2 - \frac{g_2}{g_1} n_1\right) \sigma \phi c - \left(\frac{n_2}{\tau_f}\right) \tag{2.16}$$

$$\frac{dn_1}{dt} = \left(n_2 - \frac{g_2}{g_1} n_1\right) \sigma \phi c + \frac{n_2}{\tau_{21}} - \frac{n_1}{\tau_{10}} \tag{2.17}$$

In a 4 level laser the transition between levels 1 and 0 is fast so the population in level 1 can be assumed to be 0. Thus the population inversion, n, can be taken to be the population of the second energy level. In a steady state $\frac{dn_2}{dt} = 0$ so Equation 2.16 can be simplified to

$$n = R_p n_0 \left(\sigma \phi c + \frac{1}{\tau_f}\right)^{-1} \tag{2.18}$$

When operated near threshold $\phi = 0$, thus Equation 2.16 can be further reduced to

$$R_p n_0 \ = \frac{n}{\tau_f} \tag{2.19}$$

As the optical gain coefficient is the stimulated emission cross section, σ, multiplied by the population inversion it is possible to write an expression for the gain coefficient near threshold, known as the small signal gain coefficient, g_0, this is

$$g_0 = \sigma R_p n_0 \tau_f \tag{2.20}$$

and therefore the single pass gain coefficient as

$$g = g_0 \left(\sigma \phi c \tau_f + 1\right)^{-1} \tag{2.21}$$

This coefficient can be converted to the gain of medium with Equation 2.22 where l is the length of the gain medium.

$$G = \exp(gl) \tag{2.22}$$

As $R_p n_o$ is the number of electrons excited per unit time, per unit volume it is straight forward to relate this to the number of pump photons.

$$g_0 = \eta \frac{\sigma \tau_f P_{pump}}{h \nu_l V} \tag{2.23}$$

Here η is an efficiency factor relating the energy emitted by the pump to the energy stored in the crystal in the form of excited atoms, P_{pump} is the pump power, h is Planck's constant, ν_l is the frequency of the laser, and V is the volume of the pumped region.

The only parameter in Equation 2.21 that is not a property of the material is ϕ. ϕ can be determined from the output power of the resonator. Equation 2.24 relates the photon density to the circulating intensity, I_{circ} [2].

$$\phi = \frac{I_{circ}}{ch\nu_l} \tag{2.24}$$

Combining Equations 2.21 and 2.24 and introducing $I_s = h\nu_l/\sigma\tau_f$ gives

$$g = g_0 \left(1 + \frac{I_{circ}}{I_s}\right)^{-1} \tag{2.25}$$

Equation 2.26 is the lasing condition for a resonator, R_{oc} is the reflectivity of the output coupler, R_l is the combined reflectivity of any other cavity mirrors, and α is the loss associated with the length of the gain medium, for example those due to scattering losses and reabsorption. This has been derived by realising that a resonator operating in a steady state will have its round trip losses matched by the gain.

$$R_{oc}R_l \exp\left[2l(g - \alpha)\right] = 1 \tag{2.26}$$

Equation 2.26 can be rewritten as

$$2gl = -\ln(R_{oc}R_l) + 2\alpha l \tag{2.27}$$

Substituting this into Equation 2.25, and rearranging leaves

$$I_{circ} = I_s \left(\frac{2lg_o}{\delta - \ln R} - 1\right) \tag{2.28}$$

Here R_{oc} has been rewritten as R and all the other losses have been combined into δ.

Figure 2.4 shows how the output power is related to the two circulating intensities. With the assumption that the total circulating power is constant throughout the resonator, and is the sum of the two components, Equation 2.29 can be found. This assumption is valid when $(1 - R) << 1$. The cross-sectional area of the laser mode has been used to convert the intensity into a power [2].

$$\begin{aligned} P_{out} &= \pi w_l^2 \frac{1 - R}{1 + R} I_{circ} \\ &\simeq -\frac{\pi w_l^2}{2} \ln R I_{circ} \end{aligned} \tag{2.29}$$

Using Equations 2.23, 2.28 and 2.29 it is now possible to write

$$P_{out} = \frac{-\eta \ln R}{(\delta - \ln R)} \left(P_{pump} - \frac{(\delta - \ln R)\pi w_l^2 h\nu_l}{2\eta\sigma\tau_f}\right) \tag{2.30}$$

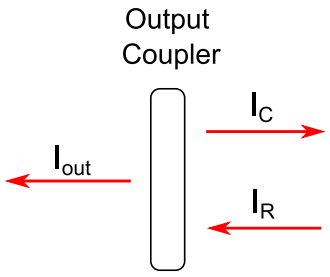

Figure 2.4: Intracavity power can be related to the output power

The efficiency factor η used above gives the proportion of the pump energy converted into excited electrons. This can be broken down into a series of efficiency factors based on the properties of the resonator [7].

$$\eta = \eta_o \eta_{qd} \eta_a \eta_q \tag{2.31}$$

η_o is the overlap between the laser mode and the inversion profile. For a Gaussian pump beam and laser mode this is given by Equation 2.32 if the pump beam is larger than the laser mode, otherwise it is 1 [7].

$$\eta_o = \frac{2w_l^2}{w_p^2 + w_l^2} \tag{2.32}$$

Equation 2.33 gives the proportion of the pump power absorbed by the crystal, a pre-requisite for a photon to promote an electron. Here l is the interaction length between pump and crystal and α is the absorption coefficient of the gain medium.

$$\eta_a = 1 - \exp(-\alpha l) \tag{2.33}$$

The energy difference between a pump and signal photons gives the efficiency factor due to the quantum defect, η_{qd}. This is equivalent to the ratio of the pump wavelength, λ_p, and laser wavelength, λ_l.

$$\eta_{qd} = \frac{\lambda_p}{\lambda_l} = \frac{\nu_l}{\nu_p} \tag{2.34}$$

Not all the absorbed pump photons result in an election being excited to the upper energy level. It can can trigger transitions between other energy levels or some other non-radiative process and this is included in η with η_q, the quantum efficiency. However, in most solid state media it can be assumed to be 1 [7].

The efficiency factors described by Equations 2.34 and 2.32 can be included in Equation 2.30 to leave

$$\begin{aligned} P_{out} &= \frac{-\eta \ln R}{(\delta - \ln R)} \left(P_{pump} - \frac{\pi(\delta - \ln R)(w_l^2 + w_p^2) h\nu_p}{4\eta_q \eta_a \sigma \tau_f} \right) \\ &= \eta_{slope}(P_{pump} - P_{th}) \end{aligned} \tag{2.35}$$

With this it is straightforward to predict the threshold and slope efficiency of a four level laser.

2.4 Heat Flow

The quantum defect, Equation 2.34, mandates that some of the energy deposited into a laser gain medium is removed via some mechanism other than that of stimulated or spontaneous emission; most often this energy is dissipated as heat. This heat not only affects the physical properties of a gain medium but can also change its optical properties. Knowing how this heat moves within the gain medium, and the time scales associated with it, is therefore important to ensuring successful operation of a laser device.

Heat flow is governed by the heat equation, given below, and is a direct consequence of Fourier's Law of conduction. Here α is the thermal diffusivity which is a measure of the thermal inertia of a material. The higher a material's diffusivity the more readily heat flows through it [8].

$$\frac{\partial T}{\partial t} = \alpha \nabla^2 T \tag{2.36}$$

Comparing Equation 2.36 with Equation 2.16 suggests that $\sigma\phi c$ and τ_f^{-1} can be used to predict the time scales associated with lasing, whilst α can be used to do the same for heat flow. α has the units $\mathrm{m}^2\ \mathrm{s}^{-1}$ so a characteristic length scale needs to be chosen before the rates of these two processes can be compared. In a solid state laser operating at 1 μm beam radii are typically of the order of a 500 μm so this length has been used in Table 2.2.

The reciprocal of the upper state lifetime given in Table 2.2 gives a minimum rate for the lasing process as Equation 2.16 also has a stimulated emission term. If laser action is to be efficient clearly this term has to be larger than the spontaneous term, or the majority of the pump energy would be lost spontaneously. The upper state lifetime therefore gives a measure of the minimum rate lasing process can occur at. Even so, this rate is orders of magnitude faster than that associated with heat flow.

[1] Schott LG-760 phosphate glass used as an example

	Nd:YAG	Nd:YVO_4	Nd:$GdVO_4$	Yb:YAG	Nd:glass[1]
Typical Lasing Wavelength [nm]	1064	1064	1064	1030	1054
Thermal Conductivity [W m^{-1} K^{-1}]	14	5.23	11.7	14	0.57
Density [kg m^{-3}]	4560	4240	5470	4560	2600
Specific Heat Capacity [J kg^{-1} K^{-1}]	590	800	1000	590	750
Thermal Diffusivity [(500 μm)^2 s^{-1}]	20	6	8	20	1
Upper state lifetime^{-1} [s^{-1}]	4248	11111	11111	769	3096

Table 2.2: The reciprocal of upper state lifetimes and thermal properties of some common laser materials, for birefringent materials the value parallel to the c-axis has been given [9–12]

2.5 Modes of Laser Operation

A laser can operate in a number of different modes, these allow some laser systems to produce average powers in the kW region whilst others produce peak powers of GWs with a relatively low average power output.

2.5.1 Continuous Wave

If a laser resonator can support a laser mode and the available gain can overcome any round trip losses the circulating intracavity power will stabilise to a value that extracts as much energy from the gain medium as is lost each round trip. When a laser operates in this regime it is said to be 'continuous wave' or CW. In this mode the laser outputs a beam of constant power. The first example of a functioning CW laser was a HeNe built by Javan et al in 1961 [13].

If a laser is allowed to enter this steady state but the pump light source is turned on and off, for example to reduce the thermal loading experienced by the gain medium, the laser is said to be in a 'quasi continuous wave', QCW, mode.

2.5.2 Pulsed

A number of different strategies exist to make use of the energy storage offered by a gain medium's upper state lifetime. By storing energy here, and then extracting it as

quickly as possible it is possible to generate extremely high peak powers.

2.5.2.1 Gain Switching

Before a laser enters a steady state after it is switched on the coupled system made up of the available gain and circulating power undergo relaxation oscillations as the system tends towards a stable output. As it takes a number of resonator round trips for a laser mode to come into existence, the population of the upper state can be increased to a level considerably above the threshold gain. This results in the large initial relaxation spike and if the pump source is turned off at the appropriate point further relaxation oscillations can be suppressed as the available gain is reduced below threshold by the initial spike. The Nd:YAG laser presented by Owyoung et al was capable of producing 60 mW of peak power via gain switching even though it's CW output was limited to the order of 10s of micro Watts [14].

2.5.2.2 Q-Switching

Q-switching leads to similar pulse lengths as gain switching, typically equivalent to a few resonator round trips, but often leads to greater pulse energies. This is due to ability to better utilise the upper state lifetime as an energy storage mechanism in this regime. Instead of relying on quickly filling the upper state laser action is instead impeded by lowering the cavity Q. This allows the pump period to be longer than the upper state lifetime allowing it to be filled, in fact the pump source can sometimes be run continuously [7]. By raising the cavity Q laser action can then extract the energy stored in the gain medium in a single, large pulse.

Clearly, the cavity Q needs to be switched quickly for this regime to be used successfully, and a number of different mechanisms exist to do this. The first demonstrated Q-switched laser made use of the Kerr effect to alter the polarisation state of the laser mode and thus change the cavity Q [15]. More modern Q-switches often make use of the Pockels effect as this allows lower electric fields to be used and thus faster switching times.

Q-switches can also be made from materials that don't respond to the electro-optical effect and instead use acoustic waves in the form of acouto-optic modulators or AOMs. Here a material such as fused silica has an acoustic wave induced inside it. This variation in pressure over the substrate induces a variation in refractive index that acts as a Bragg grating. This grating diffracts any laser mode passing through it providing a switchable loss mechanism that can be placed inside a laser resonator [7].

Historically Q-switches constructed from moving optical elements have been used, the first of which was demonstrated by Collins et al in 1962 [16]. This consisted of a spinning,

opaque, disk with a small aperture cut into it to provide the low loss state. Other mechanical systems based on rotating porro prisms have also been demonstrated [17]. In situations where the simplicity of the laser device are critical mechanical Q-switches are preferable over the electronic methods outlined above are more commonly even though the mechanical techniques suffer from both being less flexible when choosing a duty cycle and slower rise times [18].

Q-switching can also be achieved without any active elements and can instead be enacted passively. Inserting a saturable absorber into a resonator will increase its threshold. However, once laser action is achieved the absorber saturates and becomes a low less element, reducing the Q of the resonator. This then results in the generation of a Q-switched pulse. Whilst this technique is simpler than the active methods above it offers less control, with the maximum pulse energy being set by the properties of the absorber whilst the repetition rate is controlled by the pump power [7].

2.5.2.3 Mode Locking

Laser pluses of length of the order of 10^{-15} s can be generated by mode locking. Much like Q-switching mode locking relies on the modulation of the resonator losses, but in this case the modulation is synchronised to the round trip time of the oscillator. A pulse that arrives at the modulating element as it is switching to its low loss state will experience shorting of its leading edge whilst the centre of the pulse sees the most gain. This modulation can be provided by an active element, such as an AOM, or if particularly short pulses are required a passive saturable absorber can be used.

2.6 High Power Lasers

Since its formation the laser community has been developing ever more powerful, and brighter, laser devices. High power lasers have many uses in both research and industry, including materials processing, producing guide stars for astronomy, medical applications, military countermeasures and laser based particle acceleration. This range of applications provides the demand for ever more powerful and brighter sources.

2.6.1 Brightness and Beam Quality

Whilst the absolute power output of laser is an important defining characteristic, on its own it cannot be used to determine any potential uses for the laser system. To better understand the capabilities of a laser its 'brightness' must also be considered. Brightness can be defined by Equation 2.37 where P is the output power, A_e is the emitting area and Ω is the solid angle divergence of the beam [7].

$$B = \frac{P}{A_e \Omega_e} \tag{2.37}$$

Higher brightness sources are capable of producing more intense focused spots of light. Effectively, brighter sources are capable of delivering more 'power on target', which is the critical parameter for most applications.

There is a physical limit to the maximum brightness beam that can be produced by a laser resonator, these diffraction limited beams are the lowest order self-propagating solution to the wave equation and can be described by Equation 2.38 [2]. Here $E_0 = |E(0,0)|$, r is the radial distance from the central axis, z is the distance from the beam waist, w_o is the waist size, $w(z)$ is the radial distance the field amplitude drops to e^{-1} of the on axis value, $R(z)$ is the radius of curvature of the wavefront and $\zeta(z)$ is a term relented to the phase change when the beam passes through a focus, known as the Gouy phase shift.

$$E(r,z) = E_0 \frac{w_0}{w(z)} \exp\left[\left(\frac{-r}{w(z)}\right)^2 - iz\frac{2\pi}{\lambda} - iz\frac{2\pi}{\lambda}\frac{r^2}{2R(z)} + i\zeta(z)\right] \tag{2.38}$$

This electric field results in the transverse field amplitude given by Equation 2.39, which is in the form of a Gaussian. Hence, beams of this type are known as Gaussian beams.

$$I(r,z) = I_0 \left(\frac{w_0}{w(z)}\right)^2 \exp\left(\frac{-2r^2}{w(z)^2}\right) \tag{2.39}$$

The above intensity profile is asymptotic towards 0, this makes the definition of a measure of the beam radius important. Commonly the point where the intensity is e^{-2} of the axial intensity is used. It can be calculated with Equation 2.40, where z_R is the Rayleigh range which is the distance from a waist over which the radius increases by a factor of $\sqrt{2}$. This length can in turn be calculated with Equation 2.41

$$w(z) = w_0 \sqrt{1 + \left(\frac{z}{z_R}\right)^2} \tag{2.40}$$

$$z_R = \frac{\pi w_0^2}{\lambda} \tag{2.41}$$

The divergence angle of a Gaussian beam in the limit $z >> z_R$, known as the far field, can be approximated by considering Figure 2.5 and Equation 2.40. In this limit the beam waist reduces to $w = \frac{\lambda z}{\pi w_0}$, thus the divergence angle is given by Equation 2.42.

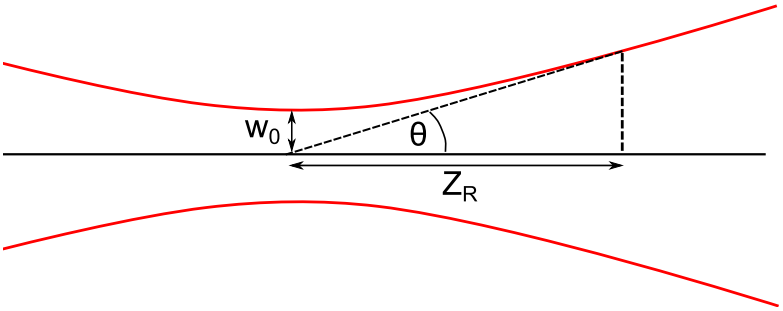

Figure 2.5: Propagation of a Gaussian beam

$$\theta = \frac{\lambda}{\pi w_0} \tag{2.42}$$

It is convenient to use a parameter independent of beam waist to describe a laser when comparing laser devices as the waist can be changed by external focusing optics. Thus the Beam Parameter Product (BPP) is defined as the product of the beam waist and the divergence angle. The larger the BPP the faster it diverges, the minimum focused spot size also increases with BPP. The smallest possible BPP is $\frac{\lambda}{\pi}$ as outlined above.

The 'quality' of a given laser beam is often determined by comparing it with an ideal Gaussian beam of the same wavelength, and is known as either the beam propagation factor or the M^2. This factor is simply the ratio of the ideal BPP and the measured BPP, Equation 2.43. Clearly, an M^2 of 1 is the lowest achievable and the M^2 increases is beam quality goes down.

$$M^2 = \frac{\theta \pi w_0}{\lambda} \tag{2.43}$$

Both the speed of divergence and minimum spot size are key when applying a laser system to an application, making M^2 one of the key measures of a laser's performance. The slower the divergence, the longer the Rayleigh range. This means the target can be further away from the focusing lens; allowing, for example, longer working distance confocal microscopes and reducing the risk of damage to delivery optics in machining lasers. The longer Rayleigh range also reduces the tolerance on positioning items for machining as the intensity of the beam is higher over a longer axial distance. Smaller spot sizes allow higher intensities to be reached for a given output power which may allow a lower power device, and thus one with a lower power draw, to be used. Smaller spot sizes also allow for more accurate machining and smaller objects to be resolved in microscopy applications.

2.6.2 Pumping Schemes

Efficient pumping is essential for practical high power lasers. The pump radiation produced by flashlamps typically has a far larger bandwidth than the absorption line in the gain medium. A significant proportion of the flashlamps radiation is therefore wasted; lowering the total, or 'wall plug', efficiency of the device. In high power systems where the energy demands are considerable the wall plug efficiency becomes particularly important when determining if a given system is practical.

As the capital cost of flashlamps is considerably less than the alternatives they are still used when extremely high peak powers are needed. For example, both the Laser Megajoule and National Ignition Facility make use of flashlamps [19, 20].

Gas lasers are often electrically pumped. If a gas is placed between electrodes with a high potential difference between them electrons flowing between the electrodes can hit a gas molecule. These impacts trigger the gas molecules to enter an excited state, and if enough impacts occur inversion can be achieved. However this approach is not possible in traditional, insulating, solid-state media.

Semiconductor diode lasers can be electrically pumped, but rely on a different mechanism to gas lasers. Here the potential difference promotes electrons to the semiconductor's conduction band. If the material has an appropriate band gap photons can be released when an electron returns to the valence band, either via spontaneous decay or after being stimulated by an incident photon.

Diode lasers are capable of producing very high powers at a range of wavelengths. However, for many applications they cannot be used directly due to their low brightness. The output power of a single diode emitter is limited to prevent the semiconductor material breaking down, so they are often combined in arrays. The spatial separation between the individual emitters creates a lower limit on the beam size and thus their brightness. By using them as optical pumps for a second laser medium, such as in a diode-pumped solid state laser (DPSS), the brightness of the final output can be increased dramatically for a small cost in both efficiency and simplicity.

2.6.3 Limitations of Laser Performance

Whilst Equation 2.35 suggests the output power of a laser scales linearly with pump power in reality this is true only up to a limit. A laser resonator is sensitive to a number of power related phenomena that can effectively cap the output brightness of a given system. Some of these power capping effects can be related to the increase in heat deposited inside the laser crystal as the pump power is increased. Others are due to the increase in signal flux interacting with the laser gain medium.

Many of a lasers limitations are related to the heat generated by the lasing process. In any laser the pump and signal wavelengths must be different, see §2.2, there is therefore a energy difference between pump and laser wavelengths; this is known as the quantum defect. This means a heating effect proportional to the pump power within the gain medium is unavoidable as electrons undergo the fast transitions in Figure 2.2 via non-radiative decay. Clearly this heating effect can be reduced by minimising the quantum defect; however this is not always possible, or desirable, if a specific wavelength is required. The temperature gradient that is produced by this heating effect is the source of a number of problems. This is due to a number of phenomena, including the temperature dependence of a materials refractive index, which creates a lensing effect. The thermal gradient also introduces stresses in the gain medium as the material tries to expand. These stresses also effect the refractive index creating both lensing and birefringence effects. In high power systems these effects can become extreme and not only limit the performance of the system but also cause the catastrophic failure of the device.

2.6.3.1 Thermally Induced Lensing Effects

A material's refractive index is determined by the interaction a photon flux has with the electronic structure of that material. As this electronic structure is temperature dependant it follows that the refractive index also changes with temperature. Typically electronic bonds weaken with an increase in temperature increasing their interaction with an incident photon flux and thus increasing the refractive index. The change in a materials density with temperature also contributes to the temperature dependence of the refractive index. A less dense material will have a lower refractive index. The sign and magnitude of $\frac{dn}{dT}$ is thus determined by the relative sizes of these two effects. It should be noted that it is possible to design a material to experience a minimal refractive index change with temperature and become 'athermal'. This is the case for some laser glasses; for example Kigre QX [21].

Laser pumping schemes typically try to match the gain profile to the desired laser mode to maximise the pump-laser mode overlap and therefore the efficiency. This often results in a higher pumping density in the centre of the laser mode and thus a higher heat load. This leads to a formation of a lens like refractive index profile. If $\frac{dn}{dT}$ is positive this will be a focusing lens otherwise it will cause the mode to diverge. Furthermore, the resulting refractive index profile is different enough from an ideal lens to introduce aberrations and therefore reduce the purity of the laser mode and the brightness of the resonator's output [22].

The density variation of the gain medium can also physically alter the shape of a rod or slabs end faces, this can also effect the quality of any laser mode passing through it. In [22] Koechner shows how the end faces of a Nd:YAG rod, if optically pumped from one if its ends, bulge producing a curved, and therefore lensing, surface. This end face

bulging is due to the expanding material being constrained by the surrounding, cooler material; thus it can only expand outwards. The temperature profile inside a laser gain medium is a function of the pump power, therefore the strength of these lensing effects is varies with the operating power. This variable lens can have severe consequences on the ability of the laser mode to reproduce after a round trip, and can drive the resonator unstable impeding laser action.

In [23] Magni presents an analysis on a resonator's stability when a lens of varying focal length is included. Under the assumption that the thermal lens acts as a thin lens and that it is positioned between two mirrors Magni found two zones of stability where a laser mode can exist. These zones are shown in Figure 2.6.

In Figure 2.6 X is a function of thermal lens focal length, f, and w_{30} is the waist at the lens. u_1 is a function of the distance from end mirror and the thermal lens and the mirror's radius of curvature, u_2 is the same but for the other mirror. If a plane mirror is used they simplify to the separation, thus if the thermal lens is at a plane end mirror, such as in an 'active mirror' arrangement, one of these values will be zero. This has the important ramification that in this type of resonator only one stability zone will exist. The lack of a stability zone limits the operating range of given laser, which may or may not be significant depending on the application.

Clearly when designing a laser resonator care needs to be taken to ensure the desired operating regime is within a stability zone. The resulting resonator may not be able to support a mode at its predicted threshold value, particularly of a large beam waist is being used, leaving a small window of stable operation at a higher power level.

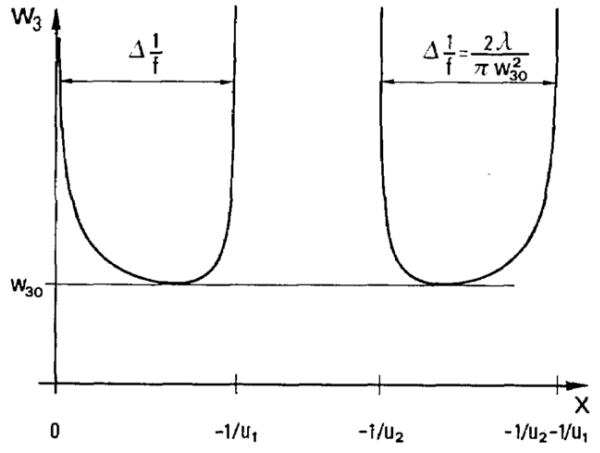

Figure 2.6: The stability zones calculated by Magni, taken from [23]

2.6.3.2 Thermally Induced Mechanical Effects

A material's density is related to its temperature via its thermal expansion coefficient, Invar being a notable exception with a very small expansion coefficient over an approximately 40 K temperature range [24]. If only part of an object is heated, and its thermal conductivity is low, only part of the object will undergo a density change. This density change will then impart a stress on the object, and if it is transparent these stresses will effect its optical properties.

In [22] Koechner describes the refractive index change in a Nd:YAG rod due to the stress created by the thermal gradient produced by the uniform pumping. He found that these stresses produce a parabolic, polarization dependent, refractive index profile across the pumped region. This polarization dependence confers birefringence onto the Nd:YAG rod which can then increase losses if polarization selective elements are being used elsewhere in the resonator. Furthermore, as the refractive index profile is parabolic it will have a lensing effect on any laser mode passing through it. Not only can this once again alter the stability of the resonator, but as the stress induced lens is not ideal it will also aberrate the laser mode reducing the brightness of the output. The birefringence also means different polarizations experience thermal lenses of different strengths which results in different stability zones for each polarization, this effect is known as 'bifocusing' [25].

If the heat induced stress exceeds the mechanical strength of the gain medium it will fracture, causing the catastrophic failure of the laser device. Whilst the size of the laser rod is not significant when determining the fracture point of a given material, the absorption depth is critical. The shorter the absorption depth the smaller, and more concentrated, the heated zone. This leads to greater stresses and lowers the thermal fracture limit [26]. The exact point of failure is not straightforward to calculate as it is heavily dependent on the surface quality of the heated surface.

2.6.3.3 Optical Damage

Intense laser beams can damage materials, indeed their ability to modify materials is one of the reasons lasers have such a large range of applications. However, if the laser mode modifies the surfaces forming the optical resonator, further laser action will be impeded. Whilst materials that are deliberately machined by a laser mode are typically absorbing at the laser's wavelength, resonator components are typically transparent or act as reflecting surfaces (a notable exception being modulators whose properties can be switched, but in this case the impedance of laser action is deliberate).

If the laser is operating in a CW mode, or the pulses are long, if a material absorbs any of the incident radiation it will undergo a heating effect and can fail due to the mechanisms

outlined above if the laser intensity is high enough. However, if the laser is running in a pulsed regime the large electric field intensity involved can trigger an electron avalanche which then transfers energy to the substance in a form that can cause rapid heating, and thus fracturing. Clearly these mechanisms are a function of a lasers intensity and so are of greater concern in lasers with smaller laser mode sizes, in particular if they are being used in a pulsed mode [27].

2.6.3.4 Nonlinear Processes

The photon flux inside a laser resonator can be very large. This can make non-linear processes significant and in some cases they can limit the performance of a given resonator. These processes are typically weak at low intensities and only manifest when the photon flux is high.

Stimulated Brillouin Scattering Stimulated Brillouin Scattering (SBS) is an acousto-optical phenomenon. A lattice has a number of vibrational modes with corresponding phonons, these phonons can interact with photons passing through the material. If the vibrational mode of the lattice corresponds to an in phase movement of the lattice atoms the associated phonons are know as 'acoustical'. These in phase vibrations are trigged by the electrostriction effect, this is where a dielectric changes shape in the presence of an electric field. These vibrations modulate the material's refractive index creating a travelling wave Bragg grating [28].

A propagating laser mode can be partially reflected by this Bragg grating and in the process receive a Doppler shift lowering its frequency. This can lead to a considerable quantity of backwards propagating power and if it is contained within a guiding medium, such as an optical fibre, it will be constrained to the excited region were it can extract energy. Not only does this reduce the gain available for the laser mode but it amplifies the backwards propagating wave, in high gain systems this can be of particular concern. For example in a fibre amplifier this backwards propagating, frequency shifted, amplified wave can result in the destruction of pump diode and other fiberised components [29].

The relatively small gain bandwidth of SBS, typically 50-10 MHz in silica [30], means this effect is of special concern in narrow linewidth, high gain, guiding lasers and amplifiers. In effect it is normally only detrimental in fibre lasers and amplifiers, and indeed when they are run in a single frequency mode it can be the main performance limiting effect [31].

Stimulated Raman Scattering Stimulated Raman Scattering (SRS) is another acousto-optical phenomenon, in this case the phonons in question are 'optical'. An optical phonon corresponds to an out of phase atomic vibration within the lattice. These

are of higher energy than the acoustical phonons associated with SBS. The existence of these vibrational modes allow the absorption of a laser photon followed by the emission of a lower energy photon and an optical phonon. This lower energy photon is said to be 'Stokes shifted'. It is also possible for a photon to interact with a pre-existing phonon to form a photon of higher energy, the resultant photon is known as 'anti-Stokes shifted'. However, anti-Stokes shifting is typically an inefficient process.

For this process to be significant large optical intensities and interaction lengths are required. Its effect is therefore normally once again seen within guiding laser architectures and in particular fibre lasers. Whilst the Raman gain coefficient is low compared to that of Birillouin scattering, in silica 10^{-13} W m^{-1} as opposed to 5×10^{-11} W m^{-1} [32, 33], its bandwidth is far larger. For systems with larger bandwidths it is therefore SRS rather than SBS that should be considered.

In a laser SRS can be detrimental for two reasons. Firstly, the resultant phonon after a Stokes shift leads to heating within the gain medium. Secondly, the frequency shift may remove the photon from the gain bandwidth, effectively reducing the gain available to the laser mode and thus reducing efficiency. For fibre lasers with a bandwidth that is considerably larger than the SBS bandwidth SRS often becomes the main performance limitation [31].

Self-Focusing A dielectric's refractive index is a function of an applied electric field. If the materials response to an electric field is a positive refractive index change a Gaussian beam can create a lens like refractive index profile, similar to that created by the thermal lens associated with gain extraction. This is due to the Kerr effect, which modifies the refractive index proportional to the square of an incident electric field.

Once a critical power is reached a laser mode will start collapsing in on itself, this value can be found with Equation 2.44 where n_2 is the nonlinear refractive index [34]. Whilst this critical power level is high, pulsed lasers are capable of surpassing it. Importantly, this value is independent of the size of the laser mode, the original size of the beam only effects the propagation distance required for the beam to collapse. Systems that require long interaction lengths are therefore more susceptible to damage due to self-focussing, particularly if the laser mode is contained within a dielectric with a higher nonlinear index than air for a considerable length.

$$P_{crit} = \frac{1.46\lambda^2}{n.n_2} \tag{2.44}$$

2.6.3.5 Amplified Spontaneous Emission

Amplified Spontaneous Emission, ASE, is of particular concern in lasers with large volumes of excited material. The spontaneous emission term in Equation 2.9 means there is always some likelihood of an electron in the upper state releasing a photon without interacting with a laser photon. In this situation the emitted photon can travel in any direction. If this photon then passes through excited material it can extract energy via stimulated emission, reducing the available gain for any laser mode. Clearly this problem is exacerbated if energy is not being extracted by a resonant mode, for example between laser pulses. The longer the available path length the more energy that can be extracted through this process.

2.6.3.6 Quenching

Quenching manifests as a reduction in the upper state lifetime of the laser ions as their concentration within the host is increased. Whilst decreasing the upper state lifetime leads to an increase in the required threshold power, see Equation 2.35, this can be partly counter acted by the increase pump absorption and the resulting increase in inversion denisty. However, the potential for energy storage within the gain medium is reduced, this is of particular concern if the system is to be operated in a pulsed mode as this directly effects the maximum achievable pulse energy [35].

This effect is due to a number of different mechanisms, one of which is the result of energy transfer from one ion to another. This mechanism is known as energy migration. It is possible for a excited state to move from one ion to another, the likelihood of this happening is related to the distance between the ions, thus it is more likely to occur at higher concentrations. If the energy is moved to a defect in the lattice it can be lost as the defect acts as an energy sink. If energy is transferred to these energy sinks fast enough the upper state life time is effectively reduced [36].

If an intermediate energy level exists between the ground state and the excited state it is possible for an electron to enter this state and transfer some of the energy to the intermediate state of a second ion, see Figure 2.7. This is known as cross relaxation. As this is once again a probabilistic event the rate of it occurring increases with the population of laser ions. A further mechanism which can cause energy to be lost from the excited state is Auger upconversion. Under this process the energy stored by an excited electron is used to promote a second excited electron to an even higher energy level and the rate of this process is again related to the ion concentration [37].

Whilst cross-relaxation and Auger recombination are only relevant in ions with a complicated energy level structure, the loss due to energy migration can affect simpler ions such as Yb [38]. Consideration therefore must be paid to the dopant level of the laser gain medium to ensure it is appropriate for a given application.

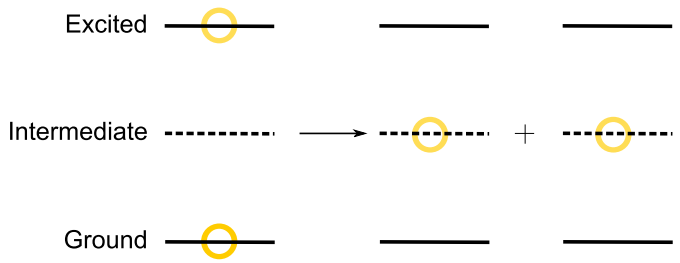

Figure 2.7: Excited electrons can be lost to an intermediate energy level via cross relaxation

2.6.4 Laser Architectures

A number of different laser architectures have been developed since the invention of the laser and their effect on a device's performance can be profound. Therefore the requirements of the application typically determine type of laser used. Some examples of high power laser architectures are outlined here.

2.6.4.1 End Pumped Rods

A common example of a laser geometry is the end pumped rod, Figure 2.8. Here a cylindrical laser rod is placed inside a heat sink and is pumped via one of its exposed end faces. The laser mode propagates along the axis of the rod extracting gain before reaching mirrors placed either side of the rod to form a resonator.

This geometry can lead to very efficient operation as the laser mode can travel the entire length of the pumped region. However, as there is often a large brightness mismatch between the laser mode and the pump light, an order of magnitude or more is not uncommon, care must be taken to ensure the laser mode is properly matched to the pumped region. If there is a large spatial mismatch higher order transverse modes can

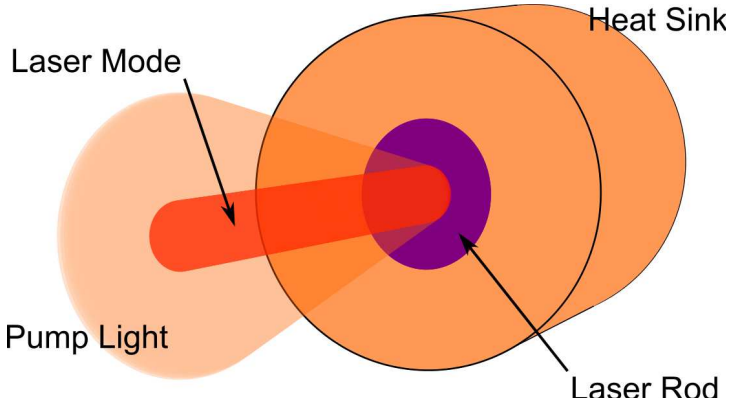

Figure 2.8: An end pumped laser rod

come into existence to extract the gain in the wings, of the pump severely reducing the beam quality of the system [39].

This geometry encourages heat flow radially through the laser rod and laser mode. This creates a radial refractive index variation and thus a thermal lensing effect which can render a resonator unstable as well as aberrating the laser mode, which will reduce the beam quality [7].

As the laser power is increased so is the thermal load within the rod, this causes it to expand. This hot material is surrounded by cooler sections of gain medium which will not undergo the same expansion, this expansion mismatch results in stresses forming inside the rod. This can induce radial birefringence in the gain medium which can act as a loss mechanism for polarized sources. The thermal expansion mismatch can also lead to bulging of the rod's faces which will lead to unwanted focusing inside the resonator [40].

Whilst the radial nature of the heat flow makes it is possible to compensate for some of the induced effects, eventuality aberrations introduced by them will reduce the brightness of the lasers output. For example, by introducing a quarter wave plate between the laser rod and a cavity mirror it is possible to drastically reduce depolarization losses [41].

When operating at high power the stresses induced in the laser material by the expansion mismatch between the hot and cold areas of the gain medium can increase beyond the material's fracture limit. If this happens the material will crack causing the catastrophic failure of the laser system. This can be partly compensated for by reducing the dopant level (and thus the absorption coefficient of the pump) and increasing the length of the rod. This increases the volume over which the heat is deposited, reducing the temperature rise. This approach has been extended to include varying the dopant concentration along the length of the rod to encourage a more even heat distribution [42]. However, longer rods require brighter pumps that are capable of delivering a small spot size along the length of the rod to avoid the generation of higher order modes. This typically limits the maximum length of the laser rod.

2.6.4.2 Side Pumped

An alternative to a end pumped geometry is a side pumped configuration. The distinguishing feature of this architecture is that the laser mode propagates in the orthogonal direction to the pump beam. This has one immediate advantage over end pumped systems; as the pump spot no longer needs to be of a similar size and shape to the laser mode the brightness requirements of the pump source are drastically reduced. Furthermore, if consideration is paid to the aspect ratio of the slab when the system is beginning designed it is possible to remove the need for pump shaping optics simplifying the optical set up.

If pumped from just one side it is straightforward to extract heat from the gain medium from the other sides via a heat sink. However, it is possible to pump from multiple sides, further relaxing the required brightness from the pump source. This arrangement can make heat sinking the gain medium more challenging as line of sight is required for the pump source. In this case the gain medium might need to be encased in a transparent water jacket or a diamond heat spreader can be used [43].

The low pump requirements make it possible to use flash lamps as the pump source. As it is possible to produce a large population inversion at low rep rates for a relatively low initial capital cost, side pumped systems are well suited to produce very energetic pulses. For example, a large proportion of the beam line at NIF consists of side pumped amplifier slabs [20].

The large spatial mismatch that can occur between the laser mode and the gain region can lead to a low extraction efficiency and poor beam quality. One way to overcome this limitation is to use a gain medium with a very short absorption length. This ensures the gain region is limited to the edge of the slab. If the laser mode is allowed to totally internal reflect off this high gain face, see Figure 2.9, it is possible to achieve efficient operation with good beam quality with this 'bounce geometry' [44].

In a side pumped geometry there is a gain gradient across the beam which can lead to aberrations. A further advantage of making use of a total internal reflection is it acts to average out any effects due to this gradient. After the refection the laser mode flips so each side of the laser mode experiences the same amplification after a full pass of the gain medium.

The bounce geometry can be extended to include multiple internal reflections through the gain medium. This allows the size of the slab to be increased with the potential for more low brightness pumping. Very high power levels are therefore possible with this geometry, for example kilowatt level power levels have been demonstrated by Comaskey et al [45].

In addition to the gain gradient across the laser mode there is a thermal gradient, as heat is again extracted from the sides of the gain medium. However, if a slab rather

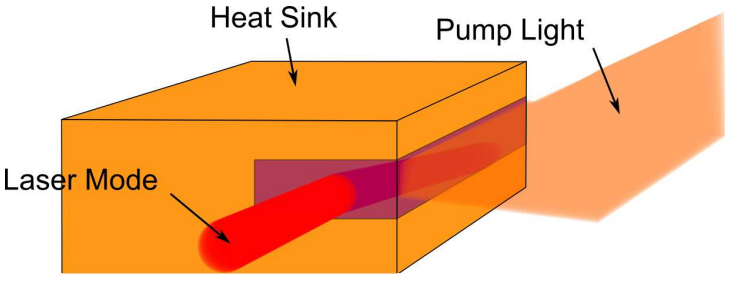

Figure 2.9: A side pumped, bounce geometry, laser

than a rod is used this gradient is no longer radially symmetric. If heat is extracted from the top and bottom of the slab, as is common in bounce geometry lasers, the thermal lens strength is different in the x and y directions leading to astigmatic beams [44].

2.6.4.3 Fibre Lasers

The significance of thermal effects in a laser gain medium is clearly related to the temperature rise inside it. Thus if the temperature rise can be reduced these detrimental phenomenon can be avoided and brighter, more powerful devices can be realised. As mentioned above, if a laser rod is lengthened the pump density can be reduced whilst maintaining the available gain. The fibre laser is an extension of this concept.

The length of a traditional laser rod is limited by the brightness of the pump source, as both the pump light and laser mode are allowed to propagate freely through the gain medium. Any brightness mismatch between the pump and laser mode will thus result in a reduction in overlap as the two beams diverge. It should also be noted that the shorter wavelength pump will diverge more quickly than the laser mode even if it is single mode. In a fibre laser this is not the case, and instead the structure is designed to guide both the laser mode and the pump light along its length, maintaining overlap. This therefore removes the pump brightness limitation found in the non-guiding, rod case.

To create this guiding structure a refractive index profile is embedded into a glass preform by controlling the deposition of dopants. The preform is then drawn to produce a fibre with a core that can be of the order of microns in diameter. By carefully selecting the core size and the refractive index change, a fibre can be designed to only support the propagation of a single mode for a given wavelength, ensuring a high brightness output [46].

To pump a fibre laser the pump light can be coupled directly into the central core. However, to get a high coupling efficiency a high brightness pump is required if the core is designed to only allow a single mode to propagate. This negates one of the advantages a fibre has over a 'long rod'. It is possible to remove this restriction if the pump is coupled into the fibre cladding instead. In this case pump light is guided by the interface between the fibre and the air, or a external polymer cladding. A polymer cladding is often added to fibres to provide mechanical strength. Whenever pump light passes through the active central core it is partially absorbed, providing gain for the laser mode, see Figure 2.10 [47].

If a cladding pumped fibre laser is radially symmetric it is possible for some of the pump light to travel through the fibre without interacting with the core. This has serious implications for the efficiency of the laser, as well as being problematic if the unabsorbed pump is allowed to feed back into the pump source. This problem is exacerbated if a large cladding to core area ratio is needed to facilitate the use of a lower brightness

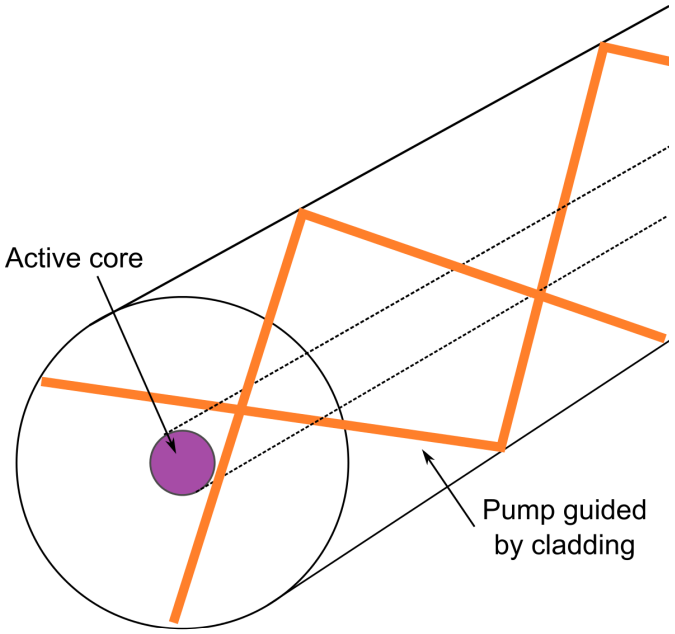

Figure 2.10: A cladding pumped fibre laser

pump source. To avoid these problems the symmetry of the fibre can be broken, this can be achieved by using an off axis core or by shaping the outside of the cladding into a different shape; for example a 'D' shape fibre can be created by polishing a flat edge onto the preform before it is drawn [48].

A resonator can be constructed out of a fibre by placing free space optics at either end of the fibre. However, this approach is typically very sensitive to misalignment. An alternative is write a Bragg grating within the fibre to act as a mirror. This has the immediate advantage that the laser can be completely fibrised providing resilience against misalignment and a robust overall package. The wavelength reflected by the Bragg grating can also be very well defined, allowing a narrow linewidth to be selected from the fibre's gain bandwidth [49].

Whilst the gain per unit length is typically low inside the fibre, the total gain offered by it can be extremely high. Fresnel reflection at the end of a fibre can therefore give enough feedback to trigger lasing. This can be a problem if a particular wavelength within the gain bandwidth is desired, but can often be solved by ensuring the end of the fibre is cleaved at an angle or by adding an end cap. An end cap is a short length of fibre without a guiding core attached to the end of a fibre. This allows the laser mode to expand within the glass before it reaches the air glass interface. Any light Fresnel reflected back into the core will therefore be of a much lower intensity than would otherwise be the case [50].

The large amount of gain inside the fibre coupled with its guiding property makes ASE a problem. Spontaneous emission can also be guided along the length of the fibre so it can

extract a substantial proportion of the gain, lowering the overall efficiency of the device. This as in addition to the potential of the ASE causing damage to optical components within the laser system [51].

While increasing the interaction length of the gain medium is beneficial with respect to thermal effects, it also it provides an opportunity for nonlinear effects to present themselves. For example, in gain media with a large bandwidth stimulated Raman scattering is the non linear limitation, for the narrow bandwidth case the nonlinear limitation is stimulated Brillouin scattering [31]. This susceptibility to nonlinear effects is a particular problem when generating high pulse energies.

The ultimate limit on the output power of a fibre laser is given by the optical intensity that can be transmitted by the fibre core without damaging it. By increasing the area of the fibre core the maximum optical power can be increased but if it is increased too far higher order modes will also be guided; this has a detrimental effect on the brightness of the laser's output. Again the chance of breaching the fibre's damage threshold is increased when handling laser pulses as the peak powers are typically orders of magnitude higher than the average power produced when running in a CW mode [31].

2.6.4.4 Planar and Channel Waveguides

Optical fibres are not the only structure that can guide an optical mode, refractive index changes can be embedded in slab like structures to producing a guiding structure. By surrounding active material with lower refractive index material it is possible to ensure any generated laser light can be constrained to the gain containing region. This low index material can be a combination of air and a supporting substrate such as in a channel waveguide, Figure 2.11(a). The structure offered by a channel waveguide offers guiding in both axis, however it is possible to construct a planar waveguide that only guides in one dimension, see Figure 2.11(b).

The use of a planar geometry rather than a channel allows a larger aspect ratio and thus a high surface area to volume ratio. This gives them a thermal management advantage as there is a larger surface for the deposited heat to be extracted through. However, the lack of guiding in one of the axis can impart a brightness penalty on the output as the resonant mode in the unguided axis is dependant on the resonator design and can be susceptible to degradation due to thermal effects.

The ability to guide a resonator mode and pump beam, even if it is in just one axis, allows the overlap to be maintained over longer distances than in non-guiding bulk systems. This is particularly true when small, faster diverging, spot sizes are used. This results in considerably lower threshold powers when compared with bulk lasers, an advantage which very much becomes apparent when low gain cross-section transitions are used [52].

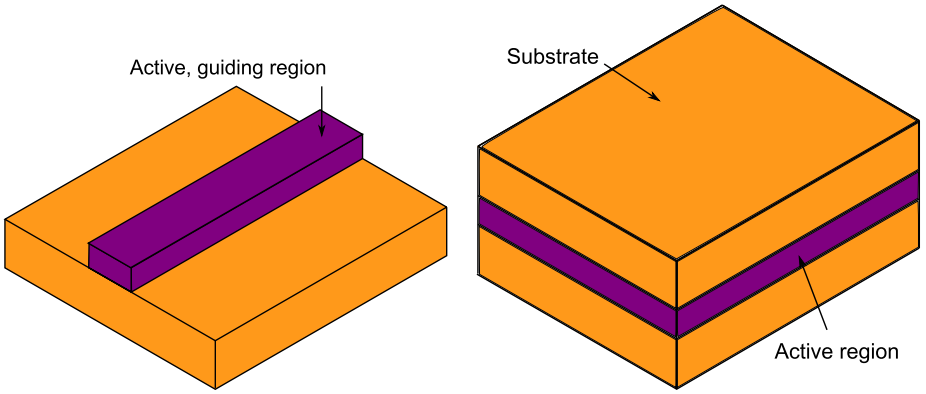

(a) A channel waveguide (b) A double clad planar waveguide

Figure 2.11: A number of different types of waveguide structures can be embedded in slab structures

The excellent thermal management properties of a planar waveguide combined with their typically low thresholds have allowed them to better exploit some laser transitions then other techniques allow. For example the current CW power record for the 946 nm transition in Nd:YAG is held by Ng et al with a double clad planar waveguide [53]. This waveguide was capable of producing 102 W of multimode output compared with more typical power levels of 10s of Watts from traditional solid-sate laser configurations.

2.6.4.5 Thin Disk Lasers

An alternative to reducing the inversion density to limit thermal effects is to instead control the direction of heat flow. In a laser, whilst the absolute temperature can affect the absorption and gain bandwidths, it is the resulting thermal gradients that most often limit performance. In particular it is the thermal gradients normal to the laser mode's propagation direction that are detrimental. For example, if the refractive index change due to a thermal gradient is solely in the direction of the laser mode's propagation the mode will only not experience any lensing effects and will instead undergo a uniform phase shift [54].

To restrict thermal gradients to be collinear with a laser mode the thin disk architecture, see Figure 2.12, can be employed. This consists of a thin disk of gain medium, typically 100's of microns thick, bonded directly to a heat sink. The bonded face also has a HR coating for both the lasing and pump wavelengths, creating an 'active mirror'. The large aperture provided by this active mirror means the pump brightness required is typically less than that needed for a fibre laser [54].

The thickness of the gain medium is often less than the absorption length for the pump light. To increase the efficiency of the laser, unabsorbed pump is passed back through

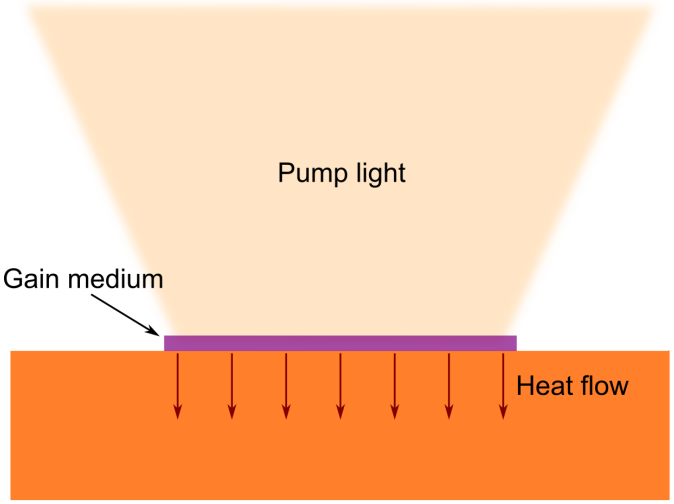

Figure 2.12: A thin disk laser

the thin disk multiple times. These re-imaging optics add to the complexity and cost of the final laser system. For example, Hugel et al use a parabolic mirror to generate 16 pump passes in their 1kW Yb:YAG laser [55].

By increasing the radius of the disk it is possible to increase the incident pump power without increasing the pump density, and thus the temperature rise in the disk. This provides a straightforward power scaling mechanism. However, larger disks become susceptible to gain loss via ASE. This is a particular problem in thin disks as it is possible for the ASE to be total internally reflected at the top of the disk and become trapped within the game medium, extracting gain as it propagates. For this reason the sides of the thin disk are often surrounded by an absorber to remove ASE once it reaches the edge of the disk. To help reduce the parasitic gain loss further thick undoped caps are often placed on top of the thin gain region to reduce the path length of the ASE within the active region [56].

Including an undoped cap has a further advantage. Whilst transverse temperature gradients are reduced by using an extremely thin gain medium, mechanically induced problems can be exacerbated. The higher temperature at the top of the disk caused by the greater pump absorption at this point causes it to expand, producing a bulging effect. At high powers modelling presented in [57] shows this creates greater phase distortions than the temperature gradients present in the disk. By including the undoped cap mechanical rigidity is increased allowing performance to be maintained at higher power levels.

By their nature the single-pass gain of a thin disk is low when compared with rod geometries. Whilst this is not a problem when operating in a CW mode it does have consequences for pulse generation. The length and energy of a laser pulse is directly related to the amount of energy it is possible for the laser mode to extract per pass. If

the single pass gain is low clearly it takes more round trips to extract a given amount of energy, lengthening the pulse and reducing the output's peak power [58].

The low single pass gain offered by the thin gain medium can be partly negated by increasing the dopant concentration. However, as outlined in §2.6.3.6, there is a limit to the amount of dopant that can be used before the adverse effects on the upper state lifetime become more important. This limitation influences the available ions for this architecture as those with more complicated electronic structures are more readily affected by quenching. This has resulted in a particular focus on Yb doped gain media in thin disk architectures [57].

2.6.4.6 Heat Capacity Lasers

Whilst not a different laser architecture as such, the heat capacity laser demonstrates another technique for overcoming the limitations of laser performance, this time at the expense of average output power. A heat capacity laser is run in burst mode, producing a burst of pulses before being allowed to cool [59]. During the laser burst heat is effectively stored within the gain medium and then extracted once lasing is halted. Clearly it is therefore beneficial to use large gain pieces of gain media as this increases the amount of thermal energy that can be stored, for this reason slabs are often used. For example, Rotter et al used Nd:GGG slabs with a clear aperture of 8 cm to produce 16.6 kW of average power in a 0.5 s burst [60].

2.6.4.7 Diode Lasers

All the laser designs described above are optically pumped, if the pump photons are produced by a laser diode the gain medium effectively acts as a brightness enhancer. This increase in brightness comes at an efficiency cost and a slight increase in the complexity of the system. Recent developments in diode manufacturing have now made them appropriate for some applications without any further brightness enhancement.

The output power of a single diode emitter is limited by temperature. The exposed semiconductor material at the facet of the diode can oxidise creating defects. These defects can increase absorption at the facet, both reducing the efficiency of the diode and causing more heating which in turn increases the rate of oxidation. This effect limits the performance of AlGaAs based single emitters to the order of 5 W [61]. The performance of a single emitter is also limited by the maximum heat flux that can be extracted from the semiconductor [62].

As the power output of individual emitters is limited they are often combined to form bars and stacks. These emitter arrays have non-emitting regions within the emitting area, this ratio is known as the 'fill factor'. The higher the fill factor the greater the

inherent brightness of the diode, but this can come at the cost of reliability as thermal crosstalk between the emitter regions limits their performance [63]. The beams produced by these emitter arrays can also be highly asymmetric, particularly in the case of diode bars, with a rapidly diverging diffraction limited fast axis and a multimode slowly diverging slow axis. This asymmetry is a direct consequence of the asymmetric shape of the emitting region and typically requires beam transformation optics to correct and create a symmetric output [64].

By precisely controlling the wavelengths produced by individual emitters within an array it is possible to wavelength combine them into a single fibre. For wavelength combining to be practical the wavelength of each emitter, which is normally dependent on temperature, needs to be controlled. This can be done, for example, by using volume Bragg gratings to provide feedback to each emitter [65] or by making use of external cavities [66]. By making use of an external cavity Huang et el have demonstrated over 2 kW coupled into a fibre with 50 micron core with an NA of 0.15.

2.7 Conclusion

This chapter has introduced the laser resonator and described how they can be constructed by making use of optical gain whilst ensuring a resonator mode reproduces itself after a round trip. Equations were than derived that can predict the performance of a laser and the different modes they can operate in were discussed. The time scales associated with lasing were also presented and compared to those associated with heat flow. The thermal processes were found to be considerably slower than the lasing processes, this provides the foundation for QCW pumping and heat capacity lasers.

The phenomena that can limit the brightness of a laser's output were then discussed and different laser architectures that attempt to overcome these effects presented. End pumped rods and side pumped lasers are most often limited by thermally induced effects, including lensing and stress induced birefringence. However, they are resistant to non linear processes and offer the potential for large quantities of energy storage allowing the production of large pulse energies. Fibre lasers are resilient against thermal effects but are susceptible to non linear processes, limiting the pulse energy they can produce. Thin disk lasers are also resistant to thermal degradation but their thin gain medium make extracting large quantities of energy in a short pulse challenging.

The thermally resistant architectures offer the potential to produce high average power, modern systems can reach multiple kW, but they struggle to produce high peak powers. Those architectures that can produce large pulse energies by contrast cannot dissipate the large thermal load associated with high average powers without degrading the beam quality of the output. Thus producing high peak powers at high repetition rates, and thus high average power, remains a challenge faced by the laser community.

References

[1] A. Einstein, "On the quantum theory of radiation," *Phys. Z*, vol. 18, pp. 121–128, 1917.

[2] O. Svelto, *Principles of Lasers*. New York: Springer, 4th ed., 1998.

[3] C. Webb and J. Jones, *Handbook of Laser Technology and Applications*. Taylor & Francis, 2003.

[4] H. Kogelnik and T. Li, "Laser beams and resonators," *Proceedings of the IEEE*, vol. 54, no. 10, pp. 1312–1329, 1966.

[5] A. Fox and T. Li, "Resonant modes in a maser interferometer," *Bell Syst. Tech. J*, 1961.

[6] A. Bloom, "Gas lasers," *Proceedings of the IEEE*, vol. 54, no. 10, pp. 1262–1276, 1966.

[7] W. Koechner, *Solid State Laser Engineering*. New York: Springer, 6th ed., 2006.

[8] B. K. Venkanna, *Fundamentals of Heat and Mass Transfer*. New Delhei: PHI Learning Private Limited, 2010.

[9] X. Peng, a. Asundi, Y. Chen, and Z. Xiong, "Study of the mechanical properties of Nd:YVO4 crystal by use of laser interferometry and finite-element analysis.," *Applied optics*, vol. 40, pp. 1396–403, Mar. 2001.

[10] P. C. Shardlow, *Enhancement of Self-Organisation and Adaptivity in Laser Systems*. PhD thesis, Imperial College London, 2010.

[11] "Yb:YAG Data Sheet."

[12] "LG-760 Phosphate Laser Glass."

[13] A. Javan, W. R. Bennet Jr., and D. R. Herriott, "Population inversion and continuous optical maser oscillation in a gas discharge containing a He-Ne mixture," *Physical Review Letters*, vol. 6, no. 3, 1961.

[14] A. Owyoung, G. R. Hadley, P. Esherick, R. L. Schmitt, and L. a. Rahn, "Gain switching of a monolithic single-frequency laser-diode-excited Nd:YAG laser.," *Optics letters*, vol. 10, pp. 484–6, Oct. 1985.

[15] F. J. McClung and R. W. Hellwarth, "Giant Optical Pulsations from Ruby," *Journal of Applied Physics*, vol. 33, no. 3, p. 828, 1962.

[16] R. J. Collins and P. Kisliuk, "Control of Population Inversion in Pulsed Optical Masers by Feedback Modulation," *Journal of Applied Physics*, vol. 33, no. 6, p. 2009, 1962.

[17] R. C. Benson and M. R. Mirarchi, "The Spinning Reflector Technique for Ruby Laser Pulse Control," *IEEE Transactions on Military Electronics*, vol. 8, no. 1, pp. 13–21, 1964.

[18] R. Scheps and J. Myers, "Performance of a diode-pumped laser repetitively Q-switched with a mechanical shutter," *Applied optics*, vol. 126, 1994.

[19] N. Fleurot, C. Cavailler, and J. Bourgade, "The Laser Mégajoule (LMJ) Project dedicated to inertial confinement fusion: Development and construction status," *Fusion Engineering and Design*, vol. 74, pp. 147–154, Nov. 2005.

[20] E. Moses, "The National Ignition Facility: status and plans for laser fusion and high-energy-density experimental studies," *Proceedings of the 19th IEEE/IPSS Symposium on Fusion Engineering. 19th SOFE (Cat. No.02CH37231)*, pp. 487–492, 2002.

[21] "QX Laser Glasses Data Sheet," *Kigre Inc.*

[22] W. Koechner, "Thermal Lensing in a Nd:YAG Laser Rod.," *Applied optics*, vol. 9, pp. 2548–53, Nov. 1970.

[23] V. Magni, "Resonators for solid-state lasers with large-volume fundamental mode and high alignment stability.," *Applied optics*, vol. 25, p. 2039, July 1986.

[24] P. R. Yoder, *Opto-Mechanical Systems Design, Third Edition.* Optical Science and Engineering, Taylor & Francis, 2005.

[25] A. Kudryahov and H. Weber, *Laser Resonators: Novel Design and Development.* SPIE Press, 1999.

[26] L. Yan and C. H. Lee, "Thermal effects in end-pumped Nd:phosphate glasses," *Journal of Applied Physics*, vol. 75, no. 3, p. 1286, 1994.

[27] R. Wood, "Laser induced damage thresholds and laser safety levels. Do the units of measurement matter?," *Optics & Laser Technology*, vol. 29, pp. 517–522, Apr. 1998.

[28] G. Agrawal, *Nonlinear Fiber Optics.* Academic Press, 5th ed., 2013.

[29] E. Ippen, "Stimulated Brillouin scattering in optical fibers," *Applied Physics Letters*, vol. 21, no. 11, p. 539, 1972.

[30] G. Agrawal, *Nonlinear Fibre Optics.* Academic Press, 2001.

[31] J. W. Dawson, M. J. Messerly, R. J. Beach, M. Y. Shverdin, E. a. Stappaerts, A. K. Sridharan, P. H. Pax, J. E. Heebner, C. W. Siders, and C. P. J. Barty, "Analysis of the scalability of diffraction-limited fiber lasers and amplifiers to high average power.," *Optics express*, vol. 16, pp. 13240–66, Aug. 2008.

[32] R. H. Stolen, E. P. Ippen, and A. R. Tynes, "Raman Oscillation in Glass Optical Waveguide," *Applied Physics Letters*, vol. 20, pp. 62–64, Jan. 1972.

[33] R. G. Smith, "Optical Power Handling Capacity of Low Loss Optical Fibers as Determined by Stimulated Raman and Brillouin Scattering," *Appl. Opt.*, vol. 11, pp. 2489–2494, Nov. 1972.

[34] G. Fibich and a. L. Gaeta, "Critical power for self-focusing in bulk media and in hollow waveguides.," *Optics letters*, vol. 25, pp. 335–7, Mar. 2000.

[35] W. Marshall, K. Cowles, and H. Hemmati, "Performance of efficient Q-switched diode-laser-pumped Nd: YAG and Ho: YLF lasers for space applications," *The Telecommunications and Data Acquisition Progress Report 42-95*, 1988.

[36] D. L. Dexter and J. H. Schulman, "Theory of Concentration Quenching in Inorganic Phosphors," *The Journal of Chemical Physics*, vol. 22, no. 6, p. 1063, 1954.

[37] H. Danielmeyer, M. Blätte, and P. Balmer, "Fluorescence quenching in Nd: YAG," *Applied physics*, vol. 274, pp. 269–274, 1973.

[38] R. Paschotta, J. Nilsson, P. Barber, J. E. Caplen, A. C. Tropper, and D. C. Hanna, "Lifetime quenching in Yb-doped fibres," *Optics Communications*, vol. 136, no. 5-6, pp. 375–378, 1997.

[39] N. Pavel and T. Taira, "Pump-beam M2 factor approximation for design of diode fiber-coupled end-pumped lasers," *Optical Engineering*, 1999.

[40] W. A. Clarkson, "Thermal effects and their mitigation in end-pumped solid-state lasers," *Journal of Physics D: Applied Physics*, vol. 34, p. 2381, 2001.

[41] W. A. Clarkson, N. S. Felgate, and D. C. Hanna, "Simple method for reducing the depolarization loss resulting from thermally induced birefringence in solid-state lasers," *Optics Letters*, vol. 24, p. 820, June 1999.

[42] R. Wilhelm, M. Frede, and D. Kracht, "Power Scaling of End-Pumped Solid-State Rod Lasers by Longitudinal Dopant Concentration Gradients," *IEEE Journal of Quantum Electronics*, vol. 44, no. 3, pp. 232–244, 2008.

[43] Y. Tzuk, A. Tal, S. Goldring, Y. Glick, E. Lebiush, G. Kaufman, and R. Lavi, "Diamond Cooling of High-Power Diode-Pumped Solid-State Lasers," *IEEE Journal of Quantum Electronics*, vol. 40, pp. 262–269, Mar. 2004.

[44] A. Minassian, B. Thompson, and M. Damzen, "Ultrahigh-efficiency TEM 00 diode-side-pumped Nd:YVO 4 laser," *Applied Physics B: Lasers and Optics*, vol. 76, pp. 341–343, Apr. 2003.

[45] B. J. Comaskey, G. F. Albrecht, R. J. Beach, S. P. Velsko, S. B. Sutton, S. C. Mitchell, C. S. Petty, K. S. Jancaitis, W. J. Benett, B. L. Freitas, and R. W. Solarz, "A One Kilowatt average power diode pumped Nd:YAG folded zigzag slab laser," in *Proc. SPIE 1865* (G. F. Albrecht, R. J. Beach, and S. P. Velsko, eds.), vol. 1865, pp. 9–16, SPIE, Jan. 1993.

[46] J. C. Daly, *Fiber Optics*. CRC Press, 1984.

[47] E. Snitzer, H. Po, F. Hakimi, R. Tumminelli, and B. McCollum, "DOUBLE CLAD, OFFSET CORE Nd FIBER LASER," in *Optical Fiber Sensors*, vol. 2, (New Orleans, LA), p. PD5, Optical Society of America, 1988.

[48] Q. Lou, P. Y. Wang, J. Zhou, T. Li, and Z. Wang, "Development of double-clad fiber lasers," in *Photonics Asia 2002* (D. Fan, K. A. Truesdell, and K. Yasui, eds.), pp. 136–141, International Society for Optics and Photonics, Sept. 2002.

[49] R. Kashyap, *Fiber Bragg Gratings*. Academic Press, 1999.

[50] *Damage threshold of fiber facets - application note*. NKT Photonics, 2012.

[51] D. J. Richardson, J. Nilsson, and W. A. Clarkson, "High power fiber lasers: current status and future perspectives [Invited]," *Journal of the Optical Society of America B*, vol. 27, p. B63, Oct. 2010.

[52] J. I. Mackenzie, "Dielectric Solid-State Planar Waveguide Lasers: A Review," *IEEE Journal of Selected Topics in Quantum Electronics*, vol. 13, no. 3, pp. 626–637, 2007.

[53] S. P. Ng and J. I. Mackenzie, "Power and radiance scaling of a 946 nm Nd:YAG planar waveguide laser," *Laser Physics*, vol. 22, pp. 494–498, Feb. 2012.

[54] A. Giesen, H. Hügel, A. Voss, and K. Wittig, "Scalable concept for diode-pumped high-power solid-state lasers," *Applied Physics B*, vol. 372, pp. 365–372, 1994.

[55] H. Hugel, A. Giesen, M. Larionov, K. Contag, and C. Stewen, "A 1-kW CW thin disc laser," *IEEE Journal of Selected Topics in Quantum Electronics*, vol. 6, no. 4, pp. 650–657, 2000.

[56] D. Kouznetsov, J.-F. Bisson, and K. Ueda, "Scaling laws of disk lasers," *Optical Materials*, vol. 31, pp. 754–759, Mar. 2009.

[57] A. Giesen and J. Speiser, "Fifteen Years of Work on Thin-Disk Lasers: Results and Scaling Laws," *IEEE Journal of Selected Topics in Quantum Electronics*, vol. 13, no. 3, pp. 598–609, 2007.

[58] J. Degnan, "Theory of the optimally coupled Q-switched laser," *Quantum Electronics, IEEE Journal of*, vol. 25, no. 2, pp. 214–220, 1989.

[59] G. F. Albrecht, S. Sutton, E. George, W. Sooy, and W. Krupke, "Solid state heat capacity disk laser," *Laser and Particle Beams*, vol. 16, no. 04, pp. 605–625, 1998.

[60] M. D. Rotter, C. B. Dane, R. D. Gonzales, S. C. Mitchell, C. W. Parks, and R. M. Yamamoto, "The Solid-State Heat-Capactiy Laser," in *Nineteenth Topical Meeting and Tabletop Exhibt*, (Santa Fe), pp. 1–5, 2004.

[61] S. Strohmaier and C. Tillkorn, "High-power, high-brightness direct-diode lasers," *Optics and Photonics*, pp. 24–29, 2010.

[62] X. Liu and W. Zhao, "Technology trend and challenges in high power semiconductor laser packaging," *2009 59th Electronic Components and Technology Conference*, pp. 2106–2113, May 2009.

[63] R. Fehse, H. König, G. Grönninger, C. Lauer, and U. Strauß, "Low fill factor diode laser bars with high brilliance from 808 nm to 1020 nm for fibre coupling," in *High Power Diode Lasers and Systems Conference, 2009. HPD 2009*, vol. 4, pp. 49–50, 2009.

[64] M. Haag, B. Köhler, J. Biesenbach, and T. Brand, "Novel high-brightness fiber coupled diode laser device," in *Proc. SPIE* (M. S. Zediker, ed.), vol. 6456, pp. 64560T–64560T–8, Feb. 2007.

[65] C. Wessling, M. Traub, D. Hoffmann, and R. Poprawe, "Dense wavelength multiplexing for a high power diode laser," in *Proc. of SPIE* (M. S. Zediker, ed.), vol. 6104, pp. 61040O–61040O–8, Feb. 2006.

[66] R. K. R. Huang, B. Chann, J. Burgess, M. Kaiman, R. Overman, J. D. Glenn, P. Tayebati, and B. B. Rd, "Direct diode lasers with comparable beam quality to fiber, CO2, and solid state lasers," in *SPIE LASE*, p. 824102, International Society for Optics and Photonics, 2012.

Chapter 3

Rotating Cavity Laser

3.1 Introduction

This chapter introduces the Rotating Cavity Laser (RCL) concept and presents previously demonstrated laser systems that rely on the same principles. The advantages the RCL enjoys over these techniques are then discussed. The engineering requirements to realise the RCL are then shown followed by a discussion of the unusual thermal and lasing properties of the architecture.

3.2 The Concept

The techniques outlined in §2.6.4 that reduce a laser's susceptibility to thermal effects are based on either averaging the laser mode through any thermal aberrations, by carefully managing the direction of heat flow or by increasing the surface area to pumped volume ratio to improve heat extraction.

Power scaling by increasing the size of the active region is not only limited by the practicalities of having a large gain medium. ASE and nonlinear processes such as SBS are often associated with large pumped volumes or lengths and can limit the performance of a laser system. Controlling the direction of heat flow often requires an increase in size in at least one dimension, making this technique also susceptible to these phenomena.

In this thesis an alternative approach is presented, which takes advantage of the different time scales associated with laser dynamics and heat flow. These differing time scales are already made use of whenever a laser system is run in a quasi-CW mode. In this case lasing and heat flow are separated in time. Simply put the lasing only occurs in the short time window before heat flow occurs. The laser is then turned off and the gain medium allowed to cool before the laser operated again. Clearly, whilst operating in

this regime deleterious thermal phenomena can be avoided it is not possible to operate the laser in a true CW mode. If the laser is pulsed a further constraint is placed on the maximum repetition rate reducing the potential average power.

The advantages given by running in a quasi-CW regime are taken to their extreme in a heat capacity laser, such as that described in [1]. In a heat capacity laser a laser shot is fired and the gain medium is then cooled. By making use of large gain media with large heat capacities considerable pulse energies can be extracted. For example multi-kilowatt heat capacity lasers have been demonstrated [2].

Instead of separating the lasing and thermal processes in time, it also possible to separate them in space. This can be done by introducing motion to the system. By moving both the pump light and laser mode relative to the gain medium the laser mode can be moved into cold material whilst a previously pumped section is allowed to cool. If the pump, laser mode pair are moved at a velocity greater than the time scales associated with heat flow, but slower than those associated with lasing, it is thus possible to avoid detrimental thermal effects whilst maintaining lasing performance.

To achieve this motion the Rotating Cavity Laser is proposed. The RCL consists of a gain medium with a highly reflective coating for both the pump and laser wavelengths on one face. This face is bonded directly to a heat sink in a manner similar to that employed in thin disk lasers. Unlike in a thin disk laser the laser mode is moved through the gain medium. This is achieved with the use of a pair of moving mirrors which act as a rotating periscope, see Figure 3.1. The periscope steers a collinear pump beam and laser mode maintaining the overlap.

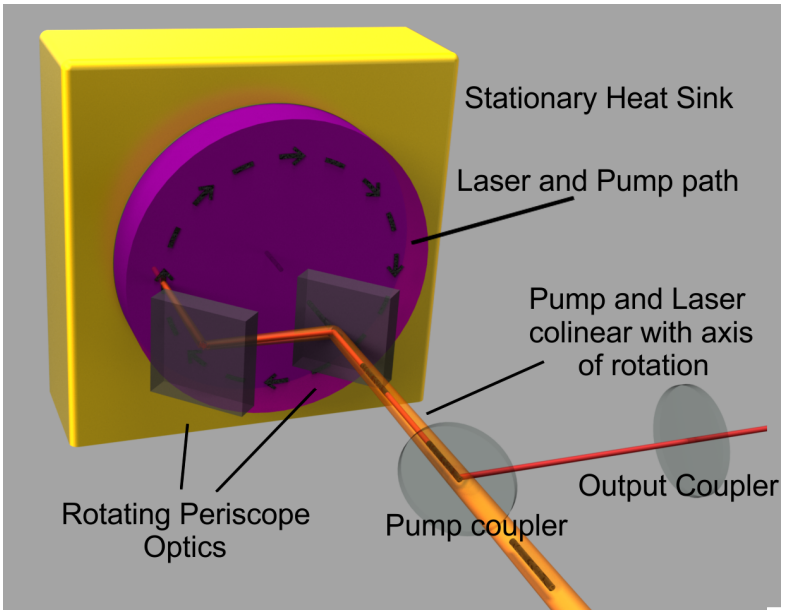

Figure 3.1: The Rotating Cavity Laser

By extracting heat separately from the lasing process the architecture does not rely on restricting temperature gradients to be parallel to the direction of the laser modes propagation. As this constraint is responsible for the requirement that thin disks be typically of the order of 100's of microns thick the gain medium in an RCL can be orders of magnitude thicker [3].

This thicker gain medium has a number of benefits, firstly the gain medium can now be thick enough to absorb the pump light in a simple double pass, removing the need for complicated pump folding schemes like that employed in [4]. This also removes the need to use high dopant levels to compensate for the short interaction length between laser mode and gain medium. This will allow active ions with more complicated electronic structures than are typically used in thin disk lasers to be used as their susceptibility to quenching is no longer a limitation.

Additionally, the mechanical strength afforded by the greater quantity of material provides greater resilience against deformation created by any thermal expansion mismatch between the heat sink and the gain medium. Furthermore, the thicker gain medium allows a smaller pump spot to be used than those associated with thin disk lasers, reducing the amount of gain lost to ASE.

Some of the advantages that stem from the RCL architecture are a result of the thermal load being spread over a much greater volume then that which lases. Thus the problems associated with long interaction lengths are avoided and the minimal nonlinear effects typical of bulk laser system are present.

The end pumped nature of a RCL also give it a number of advantages over zig-zag slab type lasers. Each reflection within a zig-zag slab has an associated loss, which increases the lasing threshold and thus the decreases the overall efficiency of the system. The overlap between the pumped region and the laser mode is also less than that which can be achieved with an end pumped system further reducing the achievable efficiency.

3.3 Examples of Moving Gain Media

The concept of gain medium that is not stationary relative to the laser mode is not a new one. In fact three years after the invention of the ruby laser the He-Ne gas laser was demonstrated by Javan et al [5]. In any gas based laser the excited gas atoms that provide the gain move relative to the laser mode with no detriment to the laser's performance.

In 1966 dye lasers were invented independently by Schäfer and Sorokin [6, 7]. In these original devices the dye was held in a container and pumped with a Q-switched ruby laser. The relative motion between the atoms and laser mode in this case are in principle the same as that in a gas laser.

A dye laser where the dye is not allowed to flow, or were it flows too slowly, will suffer from detrimental thermal effects and absorption losses from the molecular triplet state. Due to this systems have been developed to deliberately flow the dye through the laser mode to prevent the build up of thermal gradients within the laser mode in much the same why as the RCL [8]. However, at high flow rates cavitation can occur between the dye and laser window impeding performance. Whilst flow rates of this order are not required to overcome thermal effects, dye lasers also suffer from losses due to absorption in the molecular triplet state. This can be overcome by high flow rates or through the addition of agents to suppress this deleterious absorption [9].

To overcome the cavitation effects found at the flow rates required to remove triplet state absorption Hecht proposed using a rotating disk of polymethylmethacrylate doped with dye [10]. Hecht achieved pulsed operation of a 4 cm diameter 0.4 cm thick disk at spin rates of an order of 1 kHz [11]. Photobleaching of the relatively small quantity of circulating gain material prevented CW operation.

3.3.1 Solid State Lasers and Motion

The use of moving gain media has not just been restricted to the cases where the gain medium is a fluid. There have been previous demonstrations of functioning lasers with a solid state gain medium that moves relative to the resonator mode. A number of geometries making use of this concept were patented by Byer in 1985 [12]. This patent claims the use of an extension of the zig-zag slab concept to include motion by moving the gain medium.

3.3.1.1 Moving Slab Lasers

A device based on one of the architectures claimed in [12] was demonstrated in 1986 by Basu and Byer [13]. This architecture is known as a 'moving slab laser' and consists of a slab of gain medium that is translated under the pump light, see Figure 3.2, which in this example was provided by a flash lamp.

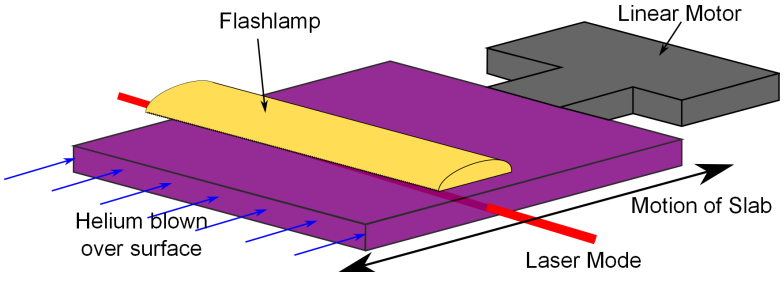

Figure 3.2: A moving slab laser

In the demonstration given in [13] a $16.7 \times 15 \times 0.44$ cm piece of 3.3% doped LHG-5 Nd:glass was pumped with a pair of flash lamps capable of delivering an average power of 7.3 kW. The thermal load handling ability, and in particular the stress fracture limit, of Nd:glass typically limits the performance of resonators based on gain media of this type, see §2.6.3. However by introducing motion Basu and Byer were able to overcome this limit, producing an average output power of 43.8 W for 2.76 kW of input power from the flash lamps at a repetition rate of 30 Hz.

By translating the glass slab 5 cm at 0.5 cm s^{-1} with an acceleration of 147 cm s^{-2} at the turning points the volume the waste heat was deposited over was greatly increased, allowing the observed increase in the allowable pump power. However, the output of this laser was highly multimode. To address this and the authors concerns about the potential consequences of motion on the stability of the output's spatial properties and beam pointing direction an intracavity aperture was used. This aperture also enforced TEM_{00} operation. When running with a single mode output the laser was found to have less than 0.24 mrad of beam steering deviation and a power fluctuation of 5.2%. The system was also Q-switched and found to be able to produce 458 mJ, 50 ns pulses at 2 Hz.

Whilst the power handling ability of the zig-zag slab is increased by introducing motion, the system is complicated by the need to cool a moving object. In this case a flow of helium gas was used to cool both the glass slab and the flash lamps. The flash lamps could not be liquid cooled as a moving seal would have been required between the slab and lamp to contain the liquid and prevent it damaging other components.

A more recent laser design based on the moving slab concept was presented by Stappaers in 2002 [14]. Here a hybrid heat capacity-moving slab laser is proposed to generate power levels of the order of 500 kW. A heat capacity laser's average power is limited by the need to allow it to cool down between pulses to prevent it from over heating. Here the duty period is increased as when the gain medium reaches its maximum allowed temperature the slab is moved, bringing cold material in front of the pump source and allowing the heated material to cool.

3.3.1.2 Rotary Disk Lasers

To simplify the mechanical arrangement of the moving slab laser and to overcome the need to include a turning points in 1990 Basu and Byer proposed the Rotary Disk Laser [15]. This architecture consists of at least one disk of gain medium which are rotated with a fixed laser mode sweeping out a circle on the edge of the disk, see Figure 3.3. This arrangement requires a brighter pump source than the moving slab described above as now for efficient operation the pump spot needs to be matched to the laser mode. This has been made possible by the development of laser diodes.

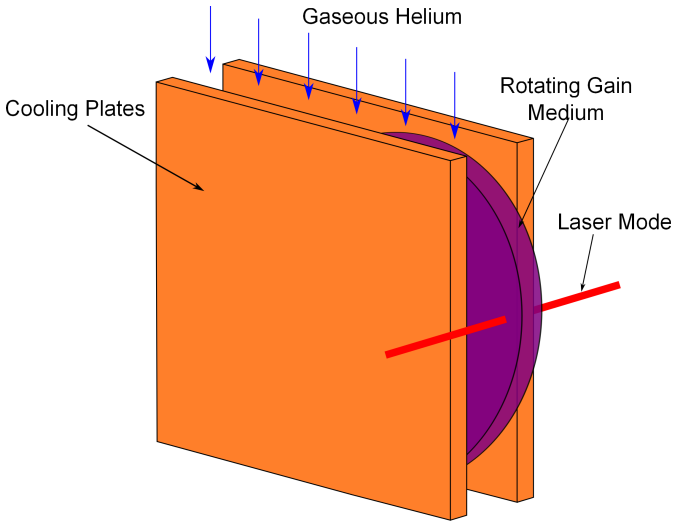

Figure 3.3: A rotating disk laser

The first demonstration of a solid state RDL was conducted by Korn et al in 1991 [16]. The resonator was built around a 50 mm diameter, 5 mm thick, 3.2% wt Nd:phosphate glass disk. The choice of Nd:glass as a gain medium was motivated by the need to overcome it's poor thermal properties and low damage threshold to fully utilise the improved energy storage properties offered by the glass host when compared with a YAG host for pulse generation.

At the time of publication the RDL produced the highest CW output of a diode pumped Nd:glass laser, with a pump limited output of 0.55 W for 2 W of absorbed pump power. At high rotation rates a drop in output power was observed as gain was swept out of the laser mode before it could be extracted via stimulated emission.

The first RDL based on Nd:YAG was demonstrated by Chen et al in 1995 [17], this diode pumped system was capable of producing 1.56 W of output power. This study again included the effect of varying the rotation rate of the gain media and the authors found the resonator's efficiency was reduced by increasing the rotation rate, agreeing with the results in [16].

Further developments of the RDL were published in 2005 with higher power results achieved with Nd:YAG, Nd:Glass and Yb:YAG [18]. The Nd:YAG results presented by Basu in [19] show a single mode output of 31 W for 95 W of 808 nm pump power. This also included the first reported results of the fluctuations created by the moving disk in an RDL, with a pointing stability jitter of 59 μrad and a peak-to-peak power stability of $\sim$35%, see Figure 3.4. Whilst the pointing stability is comparable to other laser systems the power fluctuations are more severe. This paper also includes preliminary results for a Yb:YAG RDL, with 81.9 W reported for 240 W of pump power.

The Nd:glass results presented by Massey et al in [18] are again based on a phosphate glass, with this system able to produce 35 W of multimode output and 13 W in a single

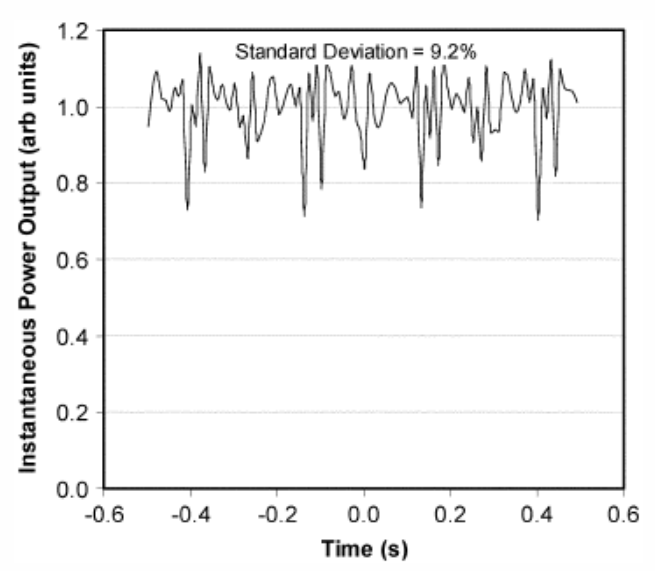

Figure 3.4: The power output of an RDL varies with time, but is cyclic with the rotation period of the disk [19]

mode configuration. The RDL arrangement allows both edge and side pumping and this was explored by Massey. At high rotation rates it was possible to partly compensate for the drop in output power seen at high rotation rates by offsetting the pump beam from the laser mode. In an experiment conducted in Nd:YAG a spatial pump-laser mode separation corresponding to a time delay of a fifth of the upper state lifetime was optimum. This suggests the potential for beam control that makes use of the unusual gain profile provided by a moving gain medium.

Massey also comments that dust accumulation on the Nd:glass disk was responsible for power drop outs over a rotation period, with the system particularly sensitive 'when helium was flowed' suggesting the purge gas transported dust particles into the laser mode, and a limitation created by the need for a gaseous heat sink.

The RDL has also been demonstrated in a pulsed mode by introducing a Q-switch into the laser cavity [20]. This produced 5.9 mJ at 3 kHz from a Nd:YAG disk and was then used to generate both the second and third harmonic. A variety of other wavelengths have also been presented by Basu in [21], including the use of low gain cross section gain media. For example a tunable laser source based on a Er:Yb phosphate glass that could produce 11.1 W of single mode output has been demonstrated. The use of the quasi three level transition in Nd:YAG was also utilised, producing 10 W of 946 nm single mode output, which at the time of publication was the highest reported power of 946 nm in a TEM_{00} mode.

3.3.1.3 Rotating Cylinder Lasers

A further laser architecture based on a moving solid state gain medium was presented in the literature in 1996, the rotating hollow cylinder laser. Here a hollow tube of gain medium, typically much longer than the disks used in a RDL, is rotated whilst being side pumped, see Figure 3.5. Gaseous helium is then blown over all the exposed surfaces of the tube, edge cooling it. This results in a thermal profile more similar to that found in a traditional rod laser [22].

This architecture was developed to take advantage of both the relative inexpense of laser glasses when compared with crystalline media and the high energy storage offered by the high dopant levels it can support. Whilst these goals can both be achieved with moving slabs and the RDL the authors note that the hollow cylinder removes turning points and allows a longer gain medium length. This makes flash lamp pumping practical, which is not the case with a RDL. In a more modern context, this architecture would allow direct pumping from a diode bar, reducing the brightness requirements on the pump source when compared with a RDL.

The example presented in [22] consisted of a cylinder of length 32 cm, an outer diameter of 12.4 cm and a wall thickness of 0.8 cm. This was then pumped from both inside and outside the cylinder by a pair of flash lamps. The glass was cooled by helium, which was consumed at a rate of 5 l an hour. This laser was capable of producing 300 W of average power at a repetition rate of 19 Hz. The repetition rate was limited by the flash lamps cool down period.

3.3.2 Advantages of the Rotating Cavity Laser

The Rotating Cavity Laser architecture has a number of advantages over the moving gain medium systems outlined above. Like the RDL it avoids the tuning points required

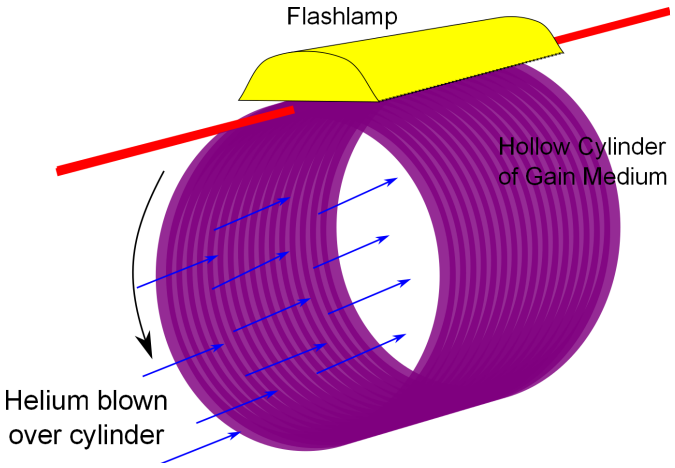

Figure 3.5: A rotating cylinder laser

by the moving slab laser and can be driven by a simple motor as opposed to a linear actuator. Again like the RDL the RCL allows an end pumped geometry to be used increasing the pump - laser mode overlap and thus giving potential for improved beam quality and efficiency. The number of reflections is also reduced when compared to a moving zig-zag slab reducing potential intracavity losses.

A clear advantage the RCL has over other moving gain medium systems is the removal of the need for helium to cool the medium. As the gain medium in a RCL is kept stationary it can be bonded directly to a heat sink in much the same way as a thin disk. This drastically simplifies the heat extraction process as well as removing the potential for the introduction of dust contamination noted by Massey in [18].

Furthermore, unlike a RDL or rotating hollow cylinder the RCL can be used with an anisotropic gain medium such as vanadate. If the intracavity periscope in the RCL is constructed out of suitably coated mirrors it will have no effect on the polarization of the laser mode, instead allowing it to be determined by the stationary gain medium. Thus if a birefringent slab is appropriately cut and mounted its birefringence axis can be used to ensure a RCL operates in a linearly polarized mode.

3.4 Mechanical Requirements

The introduction of moving intracavity parts needs to be done with care to prevent them negatively affecting the performance of the laser. Indeed most opto-mechanical design is focused on preventing components from moving relative to one another. Here the required tolerance on these components is determined, and some techniques that can meet these requirements are outlined.

3.4.1 Required Tolerances

An angular misalignment can prevent any laser modes from being resonant or, if the resonator contains focusing elements, can reduce the overlap between the pumped spot and laser mode. However, as a mode diverges within a resonator angular misalignments can tolerated if any change is small compared to this divergence angle. This is because only a small proportion of the mode will be moved out of the cone previously defined by the laser mode. The divergence angle of the laser mode from its focused spot on the 'thick active mirror' can thus be considered to provide a maximum acceptable variation in beam deflection due to the rotating cavity. If the rotating periscope introduces a deflection an order of magnitude less than this divergence angle its effect on the resonator will therefore be negligible. This angle can be calculated with Equation 2.42 and for a 500 μm beam radius of a 1064 nm laser mode it is 680 μrad. The allowable periscope deflection is thus of the order of 50 μrad.

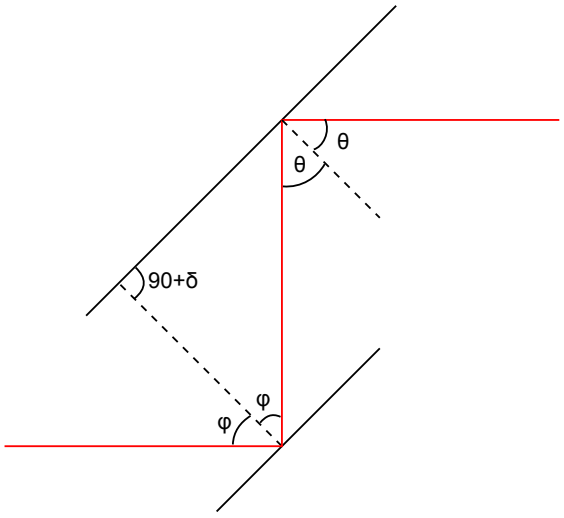

Figure 3.6: Beam deflection due to an imperfect periscope

As the tolerance on beam deflection is known the alignment precision can be determined with straight forward geometric considerations of Figure 3.6. Here δ is the misalignment angle between the two reflecting surfaces and θ and ϕ are the angle of reflection and incidence of the two surfaces. Clearly these two angles are related to one another by the following expression and the deflection angle is thus twice the misalignment angle.

$$\theta = \phi + \delta \tag{3.1}$$

As a double pass is made through the periscope each resonator round trip, the periscope needs to be aligned to the order of 10 μrad. The mechanical arrangement holding the two reflecting surfaces needs to be able to maintain this angle while tolerating different orientations as the periscope is spun, as well as being resilient to any vibration induced by the motor driving the motion. The reflecting surfaces of the periscope will therefore have to be fixed permanently relative to one another.

A key result of the above considerations is that the deflection angle after the imperfect periscope is independent of the initial angle of incidence. It is only a function of the deviation from parallel between the two reflecting surface. This means that the tolerance on the angular positioning of the assembled periscope is only determined by the acceptance angle of any dielectric coatings used, which are typically of the order of 5 degrees. This greatly simplifies the alignment process as the periscope can be assembled as a module and then inserted into the resonator.

3.4.2 Possible Periscope Construction Methods

As stated above the alignment of the two reflecting surfaces that make up the rotating periscope is critical and must be able to tolerate the unusual situation of being rotated. If the required 10 μradalignment can be achieved in a suitably robust manner the major

engineering challenge of a RCL will be overcome as this module can then be inserted into a resonator without any strict tolerances.

3.4.2.1 Silicate Bonding

Space based interferometers have to be able to survive the extreme forces imparted on them at launch and then operate without maintenance for their entire operational lifetimes. The construction methods used to produce these payloads are thus capable of surviving much more inhospitable environments than that of an RCL resonator. Gwo developed, and patented, a technique based on hydroxide-catalysis bonding, often known as silicate bonding, for the construction of Gravity Probe-B [23].

Silicate bonding can occur between two flat surfaces that are capable of supporting silicate like networks. This bonding process results in the formation of covalent bonds between two Si atoms with a bridging O atom. For this to occur two surface -OH groups must first dehydrate, this is described by the following chemical equation.

$$(\text{surface } Si)-OH \; + \; HO-(Si \text{ on surface}) \Leftrightarrow (\text{surface } Si)-O-(Si \text{ on surface}) \; + \; H_2O$$

The activation energy required for this to happen prevents it from occurring at room temperature and thus a catalyst such as KOH or NaOH is required. The water molecules produced by this reaction, and those used to transport the catalyst, eventually diffuse away from the bond into the substrate or air, as this happens the mechanical strength of the bond increases [23].

The LISA space based gravitational wave detector requires an angular tolerance of ± 10 μrads to ensure the two beams forming the interferometer overlap. This is the same level of precision as required by the intra-cavity periscope in an RCL. A prototype of this interferometer was constructed out of a ZERODUR baseplate. Fused silica components were then bonded to this base plate via hydroxide-catalysis bonding. These were moved into place with micropositioners. The time available for adjustment of the blocks position can be controlled by adjusting the pH of the catalyst allowing the alignment to be carried out in-situ and with a diagnostic providing angular information. In this prototype an angular tolerance of 70 μrads was achieved [24].

This technique could thus be used to construct a periscope for an RCL by bonding two blocks with appropriate dielectric coatings onto a small baseplate. As the separation of the two reflecting surfaces is not critical, assuming the resultant beam displacement still traces a circle that will fit on the the gain medium, only one degree of freedom would be required on the alignment micropositioners. This is because it is possible to engineer the silica blocks to remove the need for adjustment of the pitch of the reflecting surfaces relative to the baseplate by ensuring the angle between the base of the reflecting blocks and their reflecting surfaces is matched. This is straightforward to do by manufacturing

them out of a single larger polished silica block. Thus only one block needs rotation adjustment to achieve the desired alignment before the silicate bonding is allowed to set, making the procedure far simpler than that demonstrated to construct the LISA prototype.

3.4.2.2 Rhomboid Prisms

Instead of forming the periscope out of multiple glass blocks it is possible to form one by polishing a single block into a rhomboid prism, see Figure 3.7. This requires both the laser mode and pump beam to enter the close block before undergoing two total internal reflections and then passing through another air-glass interface. Two of the surfaces of the periscope block would thus need appropriate anti-reflection coatings to prevent Fresnel reflection impairing the resonator's performance.

For a rhomboid prism to be a suitable periscope it needs to introduce a beam displacement without producing an angular change in the beams direction. As outlined above these surfaces need to be parallel to within a factor of 4 of the maximum allowed deflection angle, so thus need to be machined to a tolerance of the order of 10 μrad. The polishing of Nd:YAG, Nd:YLF and glass rods to a parallelism of less than 24 μrad has been demonstrated in the literature [25]. Prochnow et al have demonstrated the polishing of BBO and LBO crystals to a greater precision, reporting parallelism of less than 5 μrad with a hand polishing technique [26]. The tolerances required by the RCL are thus possible to achieve with current polishing methods and are available commercially [27].

The internally reflecting surfaces used in this arrangement will also affect the resonator's properties. This is due to the relative phase shift between s and p polarisations that occurs when a beam undergoes total internal reflection. This mechanism provides the functionality behind a Fresnel romb. The phase shift caused by each reflection is given by Equation 3.2 when $n^* = n_2/n_1$ and θ is the angle of incidence [28].

$$\delta\phi = 2\arctan\left(\frac{\cos\theta\sqrt{\sin^2\theta - n^{*2}}}{\sin^2\theta}\right) \tag{3.2}$$

For a BK7 prism with two reflecting surfaces at 45° to the incident light Equation 3.2 predicts a relative phase shift of 38.63° at each reflecting interface. After a pass through the prism the s and p polarisation states will therefore undergo a phase shift of 77.26°. As the prism rotates, so does its fast and slow axis. If there are no polarisation selective elements within the resonator this will have no effect on the laser's performance. However, if a polarised output is desired this rotating prism will have more severe consequences. If light incident on the prism is linearly polarized and aligned to either the prism's fast or slow axis the prism will act as an optical retarder and the polarization

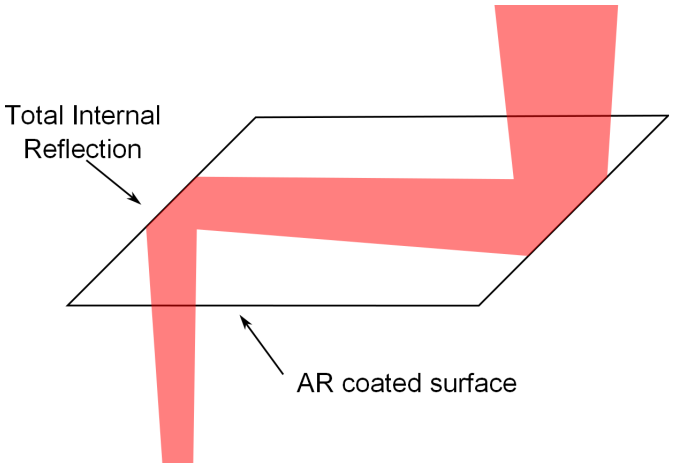

Figure 3.7: A rhomboid prism can be used as a monolithic periscope

state will be unchanged. When incident light is not aligned to either of the prism's axis the relative phase shift will produce an elliptically polarized beam. If the polarisation state of the resonator is enforced by a selective resonator element this varying change in polarisation will create a cyclic cavity loss and thus a variation in laser output power.

3.5 Effect of Motion

The consequences of including moving intracavity parts of the type needed for a RCL are discussed here. Both the expected effects on thermal and lasing processes are considered to determine the rotation rate required for the successful operation of a RCL.

3.5.1 Thermal Properties

3.5.1.1 Predicated Temperature Rise

In a RCL the pumped region of the gain medium does not reach thermal equilibrium. The temperature rise in the adiabatic limit can be approximated by considering the energy flow into the gain medium and assuming a top hat pump profile, this has been done by Basu for the RDL in [15] and is outlined here. The temperature rise due to the heat flow into a volume of gain medium defined by a pump spot can be found with Equation 3.3. Here the energy heating the gain medium has been assumed to come solely from the quantum defect between pump and laser photons. η_{qd} is the quantum defect ($\lambda_{\mathrm{pump}}/\lambda_{\mathrm{laser}}$), C_v is the heat capacity per unit volume (for Nd:YAG this is 2.78 J cm^{-3} K^{-1} [29]), w_p is the radius of the pump beam, E_{pump} is the pump energy that

has entered the spot and l is the length of gain medium the pump interacts with.

$$\Delta T = \frac{E_{\text{pump}}(1-\eta_{\text{qd}})}{C_v \pi w_p^2 l} \tag{3.3}$$

In an RCL and RDL the volume heated is much larger than that used in Equation 3.3 so to account for motion the dwell time of the pump spot needs to be considered. This is simply the time for which a point on the gain medium is exposed to the pump light and can be found with Equation 3.4. Ω is the rotation rate in revolutions per second and r_{rot} is the radius of rotation, see Figure 3.8.

$$\tau = \frac{w_p}{\pi r_{rot}} . \frac{1}{\Omega} \tag{3.4}$$

The heating power in Equation 3.3 can now be modified by this dwell time leaving the resulting temperature rise, which is given by Equation 3.5 where $P_{\text{heat}} = P_{\text{pump}}(1-\eta_{\text{qd}})$.

$$\Delta T = \frac{P_{\text{heat}}}{C_v \pi^2 w_p l r_{rot} \Omega} \tag{3.5}$$

It should be noted that this is the temperature rise experienced by a point after each pass of the pump spot. If the rotation rate is high enough so that a point on the slab is not allowed to cool before it is reheated the absolute temperature rise after a steady state is reached will be higher than this. However, between pump passes the pumped spot will leave the adiabatic regime and heat will flow. If the temperature of the spot becomes uniform when compared to the initial temperature rise there will be no further adverse effect to lasing. This is due to detrimental thermal effects being associated with temperature gradients as opposed to absolute temperature.

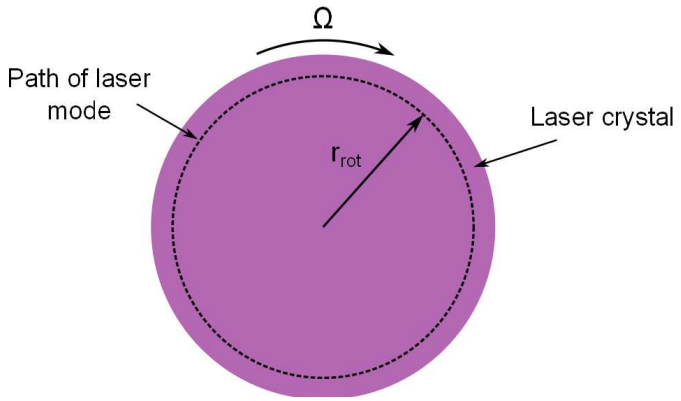

Figure 3.8: The laser mode is rotated around the edge of the laser crystal which is cooled from the back surface.

3.5.1.2 The Adiabatic Limit

To determine whether a RCL will be operating in the adiabatic limit Fourier's Law, Equation 3.6, can be considered. The analysis conducted here could also be applied to the RDL. Here κ the is the material's thermal conductivity, A is the cross-sectional area of the surface conducting the heat, x is the distance between two surfaces of constant, but different, temperature and Δq is the transferred energy.

$$\frac{\Delta q}{\Delta t} = -\kappa A \frac{\Delta T}{\Delta x} \tag{3.6}$$

As radial heat flow is responsible for the majority of deleterious thermal effects in a laser resonator the situation where a cylinder experiences heat flow out of its curved surface will be considered, see Figure 3.9. If the radius of this cylinder is equal to the pump beam and it is as thick as the RCL gain medium this will give a maximum value for the heat flow as clearly a significant proportion of it will be axial in reality.

Substituting Equation 3.5 and Equation 3.4 into Equation 3.6 and expressing the rotation frequency as a velocity, v, gives Equation 3.7.

$$\begin{aligned} \Delta q &= \frac{-2\kappa w_p P_{\text{heat}}}{\Delta x C_v \pi^2 r_{rot}^2 \Omega^2} \\ &= \frac{-8\kappa w_p P_{\text{heat}}}{\Delta x C_v v^2} \end{aligned} \tag{3.7}$$

Considering the heat outflow as a proportion of the heat that is deposited into the pump spot gives the following result by using $q_{\text{in}} = P_{\text{heat}}\tau$.

$$\frac{\Delta q}{q_{\text{in}}} = \frac{-8\kappa}{\Delta x C_v v} \tag{3.8}$$

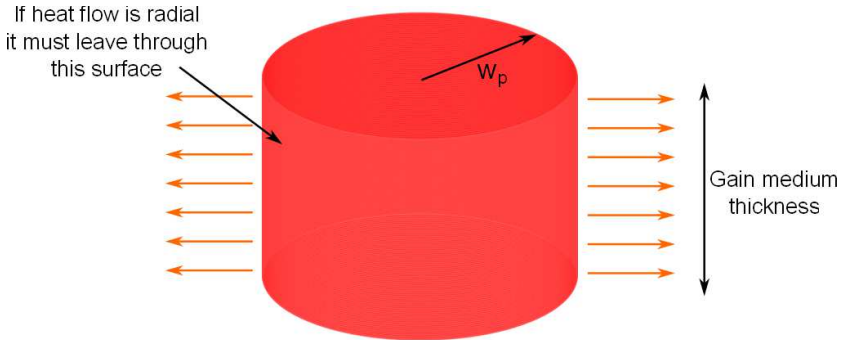

Figure 3.9: If heat flow is assumed to be radial the surface area conduction occurs through can be assumed to be the curved surface of a cylinder defined by the pump radius.

Equation 3.8 is dependent only on the gain medium's physical properties and the velocity of the pump spot. To produce indicative results it is assumed the heat must travel a distance on the order of a beam waist to produce a significant temperature gradient. If this distance is taken to be 1000 μm the heat flow within a pump spot dwell time is given by Figure 3.10. As expected this figure shows that there is a minimum velocity required to counteract detrimental thermal effects and that for higher velocities diminishing returns are realised.

3.5.1.3 Thermal Wedging

The movement of the active spot in the gain medium towards cool material will result in a temperature gradient in the direction of motion. This gradient occurs even when the RCL is operated in the adiabatic limit as it is due to the motion of the pump and signal beams relative to the stationary thermal distribution. This temperature gradient, a sketch of which is given in Figure 3.11, to first order will result in a phase shift across the laser mode, in effect creating a wedge.

As the periscope rotates the direction of the wedge will change relative to the stationary part of the cavity. This is not the case in an RDL style resonator where the wedge direction is constant and can be accounted for by tilting a cavity optic to compensate making this effect unique to the RCL. Here, if wedging is significant, the compensation angle direction is a function of the periscope angle and thus will not be possible to compensate for with a stationary optic.

If the temperature rise is assumed to be a step the angle of this wedge, and hence the angular beam deviation, can be calculated. The path length difference between each side of this temperature step is given by the following equation which assumes the size

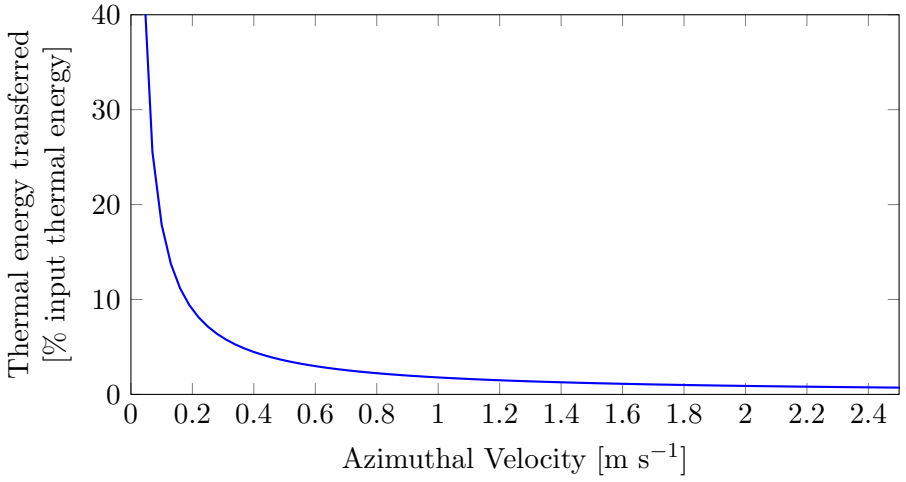

Figure 3.10: Percentage of thermal energy that moves 1000 μm within the pump dwell time in Nd:YAG

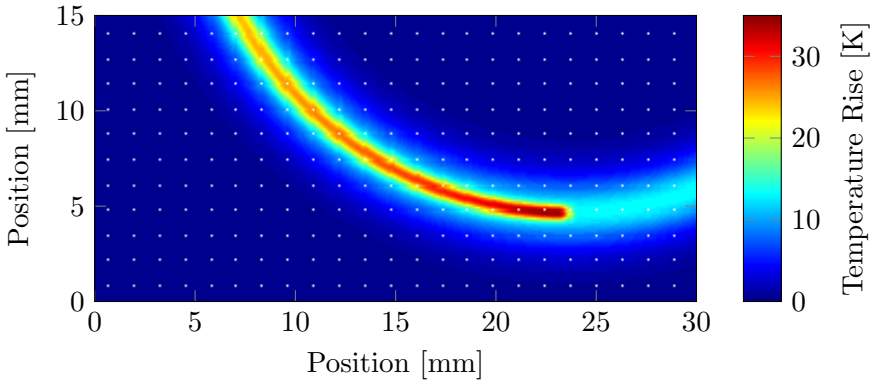

Figure 3.11: Temperature distribution induced by a pump beam moving in a circle.

of the temperature step is given by Equation 3.5. The factor of 2 is included to take into account the double pass through the slab.

$$\Delta l = 2\frac{P_{\text{heat}}}{C_v \pi^2 w_p r_{rot} \Omega}\frac{dn}{dT} \tag{3.9}$$

The wedge angle, α, can then be found with trigonometry, leaving Equation 3.10.

$$\alpha = \frac{\Delta l}{2w_p} \tag{3.10}$$

Through the application of Snell's law and geometric considerations it can be shown that the beam deflection angle from a wedged prism is given by Equation 3.11.

$$\delta\theta \approx (n-1)\alpha \tag{3.11}$$

Figure 3.12 shows the expected deflection a laser mode will experience when passed through a pump spot with a waist of 330 μm within a Nd:YAG crystal under 100 W of heating power. Clearly the wedge deflection can be decreased by increasing the rotation rate.

As stated in §3.4.1 a laser can tolerate misalignments if they are considerably less than the divergence of the laser mode. Ideally this wedge therefore needs to be restricted to the order of 50 μm. Figure 3.13 shows the maximum heating power for a number of pump waists. Whilst the divergence is also a function of the pump waist the maximum heating power is a function of the square of the waist so the 50 μrad tolerance is valid for this range of spot sizes.

By choosing an appropriate pump spot size and rotational velocity it is therefore possible to restrict thermal wedging to an order of magnitude less than the laser mode's divergence angle. The above analysis assumes a step like change in temperature, in

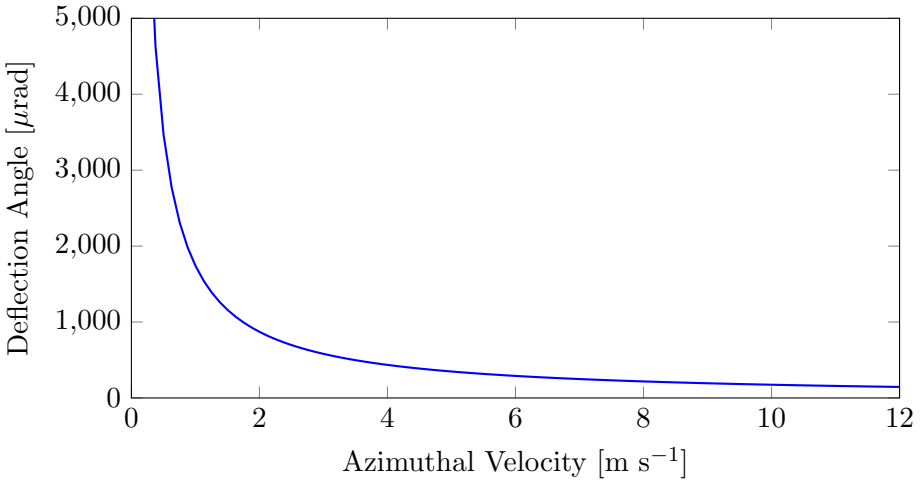

Figure 3.12: Calculated deflection angle under 100 W of heating power in a 6mm thick piece of Nd:YAG with a pump waist of 330 μm.

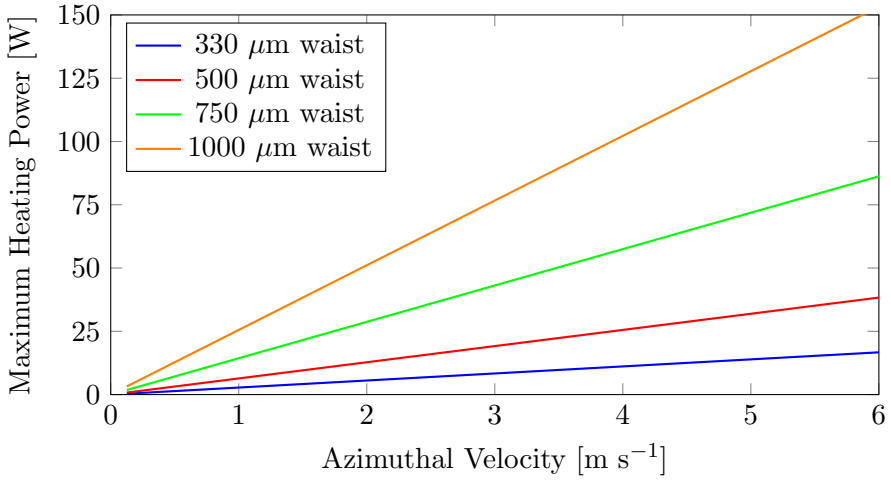

Figure 3.13: The maximum heating power if a wedge angle less than 50 μm is required for a 6mm thick piece of Nd:YAG.

reality this will not be the case and the strength of the wedge will instead be lower. Furthermore the effect of thermal expansion causing the end face to bulge has been ignored. In Nd:YAG the optical path length change due to this effect is small and when calculated by Koechner when considering its influence on the thermal lens it was found to be an order of magnitude less than that caused by the temperature dependence of refractive index [30].

3.5.1.4 Cooldown Time

The time it takes a pumped spot to return to ambient temperature has been calculated for the rod case by Koechner in [31]. In his analysis the assumptions that heat flows uniformly from all of the rods surfaces and the temperature rise is uniform over the

heated volume are made. In the case where there is no thermal impedance between the rod and the cooler medium the temperature change at the centre of the rod is given by Equation 3.12. Here $T(t)$ is the temperature at time t, T_0 is the initial temperature of the centre of the rod, β_n are the roots of the Bessel function of the first kind order 0 and J_1 is the Bessel function of the first kind order 1. τ is w_p^2/α, where α is the thermal diffusivity of the material, 0.046 cm^2 s^{-1} for Nd:YAG at 300 K [32].

$$\frac{T(t)}{T_0} = 2\sum_{n=1}^{\infty} \exp\left(\frac{-\beta_n^2 t}{\tau}\right) \frac{1}{\beta_n J_1(\beta_n)} \tag{3.12}$$

If the rod considered by Koechner is taken to be the heated region inside an infinite slab of gain material an approximation for the cooling time in a RCL can be found. This analysis ignores the face cooled heat sink which typically will have a higher thermal diffusivity than the gain medium, so provides an upper limit on the cooling time, see Figure 3.9.

Figure 3.14 plots the temperature change for the centre of a 500 μm radius spot. If the period of rotation is less than 50 ms, equivalent to a rotation rate of 20 Hz the laser crystal will have been allowed to fully cool before it is pumped again. This corresponds to an azimuthal velocity of 2.5 m s^{-1} if a circle of radius 20 mm is being swept out.

As the rotation rate is increased the temperature profile on the gain medium will tend towards a ring of uniform peak temperature. In the extreme example of the RCL not being allowed to cool at all between periods this profile will be achieved and the thermal properties will become similar to that of a rod laser, with no advantage imparted by operating in the adiabatic limit. Figure 3.14 suggests this regime will occur at rotation speeds of 500 Hz. However, even when the RCL is not allowed to cool it has an advantage over a rod laser, the volume the heat is being dissipated in is larger. The ratio of the

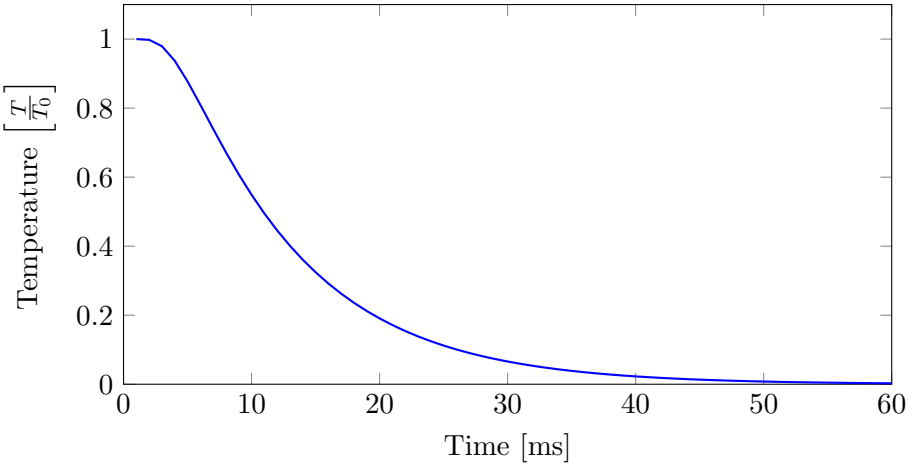

Figure 3.14: The temperature change in the centre of a heated region with a radius of 500 μm

volume of the heated ring compared with the cylinder in a rod geometry is given by the following equation.

$$R = \frac{2r}{w} \tag{3.13}$$

If a pump spot with a 500 μm radius is rotated with a radius of 15 mm the pumped volume is increased by a factor of 60. It will therefore take 60 times the heating power to create a temperature rise in an RCL equal to that found in a rod laser, indicating an increase in pump power by a factor of 60 will be possible. Clearly this scaling factor can be increased by using a larger radius of rotation, a factor of 1000 increase in volume can be achieved with a radius of rotation of 25 cm. This would require an impractically large gain medium. However by using a non-circular beam path, such as a spiral, the pumped volume can be increased without increasing the crystal size, but this would come at the expense of mechanical simplicity.

3.5.2 Lasing Properties

Whilst the overlap between the pump spot and laser mode can be maintained during a rotation period by ensuring they are collinear to one another before they pass through the periscope, the overlap between the laser mode and the available gain will not necessarily be maintained. A solid state laser medium is capable of storing energy and it is therefore possible for energy to be 'left behind' if it is not extracted by the laser mode before the periscope sweeps the mode away from it. This introduces a loss mechanism unique to lasers with moving gain media.

The significance of this new loss mechanism can be found by considering the rate of gain extraction from the gain medium. This can be done by looking at the rate equation for the upper laser level of a 4-level laser, Equation 2.16. By assuming that the population of the second level is zero Equation 3.14 can be found. The population of the ground state can also be assumed to be large compared to its depopulation rate allowing ground state depletion to be ignored letting $W_p n_0$ be rewritten as the constant R_p.

$$\frac{dn_2}{dt} = R_p - n_2\sigma\phi c - \left(\frac{n_2}{\tau_f}\right) \tag{3.14}$$

The effect of motion can be introduced to this rate equation via the coordinate transform $t = \frac{x}{v}$ as used by Massey et al [18]. Here x is the coordinate in the direction of the motion v is the velocity of the overlapping pump spot and laser mode. W_p has been written as a function of x and r, the coordinate perpendicular to the direction of motion.

$$\frac{dn_2}{dx} = \frac{1}{v}\left(R_p(x,r) - n_2\sigma\phi c - \frac{n_2}{\tau_f}\right) \tag{3.15}$$

Previously this coordinate transform has been used to calculate the change in polarized output power as the rotation rate is varied in an RDL. The previously undertaken approach made use of two experimentally determined constants to model the system. Here the coordinate transform is instated used to analytically determine the gain profiles found in a moving gain medium for the first time to the best of our knowledge.

3.5.2.1 At Threshold

The rate of energy extraction will be lowest close to threshold so this 'worst case' will be considered first. This regime can be approximated by setting the photon flux, ϕ, to zero and is described by Equation 3.16.

$$\frac{dn_2}{dx} = \frac{1}{v}\left(R_p(x,r) - \frac{n_2}{\tau_f}\right) \tag{3.16}$$

This equation is of the form

$$\frac{dn_2}{dx} + p(x)n_2 = q(x) \tag{3.17}$$

So can be solved analytically by multiplying by the integrating factor below

$$u(x) = \exp\left(\frac{x}{v\tau_f}\right) \tag{3.18}$$

Which gives

$$n_2 = \frac{1}{v}\exp\left(-\frac{x}{v\tau_f}\right)\int \exp\left(\frac{x}{v\tau_f}\right) R_p(x,r)dx \tag{3.19}$$

This equation can then be solved for any given pump distribution.

Top Hat Pump If the pump beam is assumed to be a top hat distribution of radius w it can be described with

$$R_p(x,r) = \begin{cases} R_p & \text{when} - w < x < w \\ 0 & \text{otherwise} \end{cases} \tag{3.20}$$

If the non-zero part of the pump distribution is considered, Equation 3.19 can be solved to give the following expression, where C is a constant of integration, which describes the inversion distribution within the pumped spot.

$$n_2 = R_p\tau_f + \frac{R_p}{v}\exp\left(\frac{-x}{v\tau_f}\right)C \tag{3.21}$$

If it is assumed that the upper state has a population of zero before it is pumped then $n_2 = 0$ when $x = -w$, with this C can be found as follows.

$$C = -\tau_f \exp\left(\frac{-w}{v\tau_f}\right) \tag{3.22}$$

Combining Equations 3.23 and 3.22 leaves

$$n_2 = R_p\tau_f\left(1 - \exp\left(\frac{-(w+x)}{v\tau_f}\right)\right) \tag{3.23}$$

Equation 3.23 has been plotted in Figure 3.15 for a number of different azimuthal velocities. This figure only includes the inversion distribution within the pumped spot, outside this spot spontaneous emission will deplete the upper state population. Figure 3.15 clearly shows the inversion distribution tending towards a top hat as the azimuthal velocity is reduced. At higher speeds the leading edge of the pump spot moves before fully populated the upper state, creating the observed curves and reducing the amount of inversion.

The total inversion within the pumped spot can be found by integrating Equation 3.23 and is given by Equation 3.24. By setting $v = 0$ the total inversion in the pump spot can also be found for the stationary case.

$$\int_{-w}^{w} n_2 dx = R_p\tau_f\left[2w + vt\left(\exp\left(-2\frac{w}{v\tau_f}\right) - 1\right)\right] \tag{3.24}$$

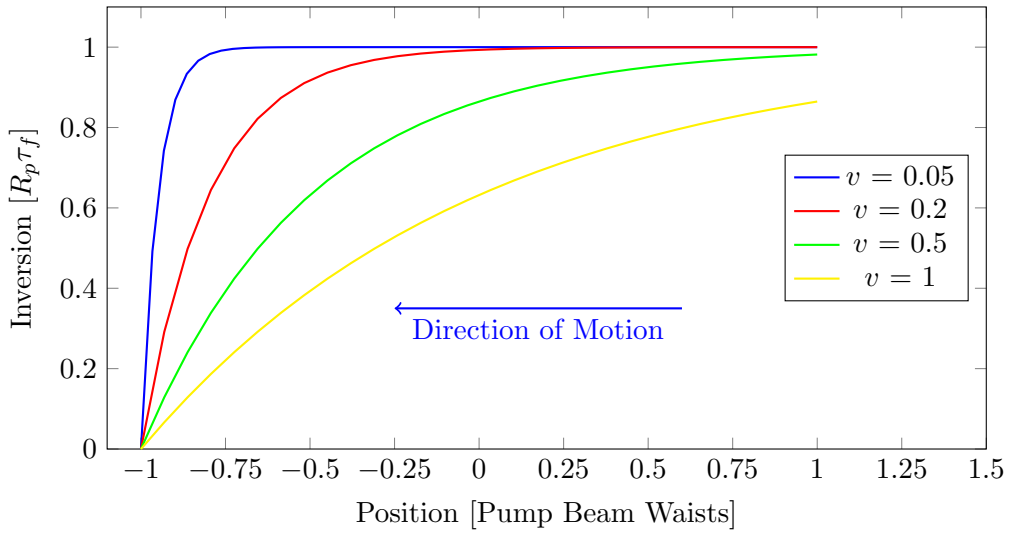

Figure 3.15: The introduction of motion acts to spread out the inversion distribution in the gain, beyond a beam waist spontaneous emission will act to deplete the upper state. v is expressed in beam waists travelled per upper state lifetime.

The minimum amount of inversion that can create lasing is that generated by the threshold pump power. The decrease in inversion within the pumped spot for a given pump power will therefore result in an increase in threshold. With Equation 3.24 it is possible to determine the fraction of the inversion that is present when the periscope is stationary at threshold that is still present under rotation. The reciprocal of this ratio will be the increase in threshold and is given by Equation 3.25 and plotted in Figure 3.16.

$$\Delta P_{\text{threshold}} = 2w\left[2w + vt\left(\exp\left(-2\frac{w}{v\tau_f}\right) - 1\right)\right]^{-1} \tag{3.25}$$

Motion effectively decreases the upper state lifetime which results in an increase in the required pump power at threshold. At azimuthal velocities of the order of a beam waist per upper state life time this increase is significant and may have to be taken into consideration when designing an RCL.

Gaussian Pump The above analysis can be refined by considering Gaussian beams to better describe the laser mode and pump beam. If the the pump beam is Gaussian R_p can be expressed as

$$R_p = R_{\max} e^{-2\frac{x^2}{w_p^2}} \tag{3.26}$$

Using this in Equation 3.19 and solving gives the following expression for the inversion distribution.

$$n_2 = \frac{R_{\max}}{v}\exp\left[\frac{-x}{v\tau_f}\right]\left(C - \frac{w_p}{2}\sqrt{\frac{\pi}{2}}\exp\left[\frac{w_p^2}{8v^2\tau_f^2}\right]\operatorname{erf}\left[\frac{w^2 - 4v\tau_f x}{2\sqrt{2}v\tau_f w}\right]\right) \tag{3.27}$$

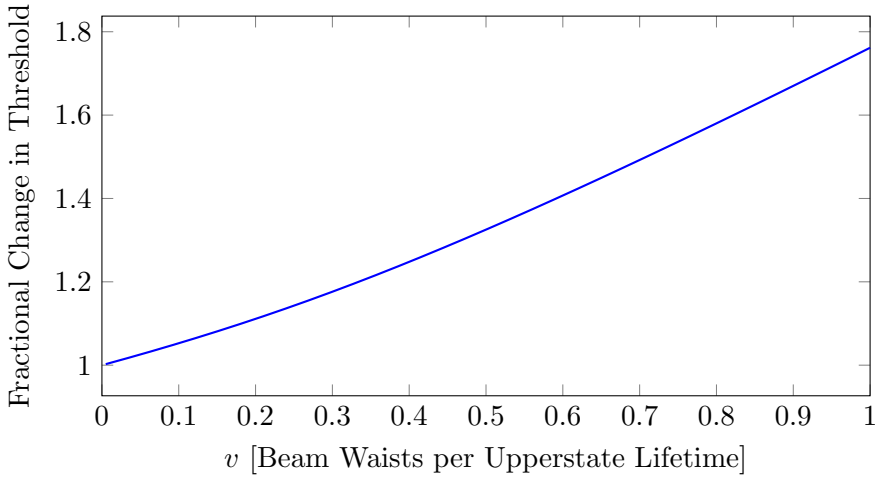

Figure 3.16: The laser threshold increases as the motion of the pump laser mode pair is increased.

Where C is an integration constant and erf is the error function:

$$\mathrm{erf}(x) = \frac{2}{\sqrt{\pi}} \int_0^x e^{-t^2} dt \tag{3.28}$$

As $x \to \pm\infty$ n_2 will tend to 0 as far away from the pumped spot spontaneous emission will deplete the upper state. The integration constant is thus

$$C = \frac{w_p}{2} \sqrt{\frac{\pi}{2}} \exp\left[\frac{w_p^2}{8v^2\tau_f^2}\right] \tag{3.29}$$

Allowing Equation 3.27 to be simplified to Equation 3.30 which makes use of erfc, the complimentary error function which is defined by Equation 3.31.

$$n_2 = \frac{w_p R_{\max}}{2v} \sqrt{\frac{\pi}{2}} \exp\left[\frac{w_p^2}{8v^2\tau_f^2} - \frac{x}{v\tau_f}\right] \mathrm{erfc}\left[\frac{w_p^2 - 4v\tau_f x}{2\sqrt{2}v\tau_f w_p}\right] \tag{3.30}$$

$$\mathrm{erfc}(x) = 1 - \mathrm{erf}(x) \tag{3.31}$$

The motion modified inversion distribution is shown in Figure 3.17. Here the velocity has been expressed in terms of the number of beam waists travelled within an upper state lifetime. As expected the greater the velocity the more spread out the inversion with the distribution tending towards the Gaussian pump shape at slow speeds.

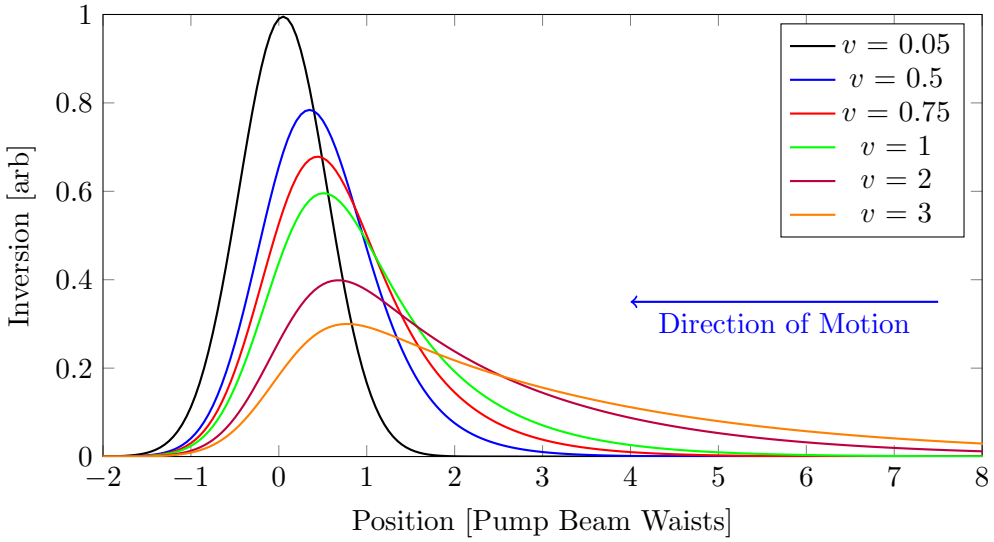

Figure 3.17: The introduction of motion acts to spread out the inversion distribution in the gain. v is expressed in beam waists travelled per upper state lifetime.

The introduction of motion thus effectively modifies the shape of the pump beam which will have consequences for the overlap between it and any resonator modes. The position of the inversion peak relative to the position of the pump also varies as the pump is moved relative to the gain medium. In an RCL configuration the direction of the inversion peak shift will change relative to the stationary part of the resonator as the intracavity periscope rotates. This is in contrast to RDL like resonators, where the direction of the shift will be invariant as the disk rotates. In an RDL it is thus possible to compensate for the change in inversion position by angling a stationary resonator optic. If the RCL is run in a regime where this inversion shift is significant this will not be possible and the alignment between the pump beam and resonator mode will not be optimal.

The location of the peak inversion relative to the centre of the pump beam can be found by considering the differential of Equation 3.27 which is given by Equation 3.32.

$$\frac{dn_2}{dx} = \frac{w_p R_{\max}}{2v^2\tau_f}\sqrt{\frac{\pi}{2}}\exp\left[\frac{w_p^2}{8v^2\tau_f^2} - \frac{x}{v\tau_f}\right]\times \left(\frac{8v^2\tau_f^2}{2v\tau_f w_p\sqrt{2\pi}}\exp\left[\frac{-(w_p^2-4v\tau_f x)^2}{(2\sqrt{2}v\tau_f w_p)^2}\right] - \operatorname{erfc}\left[\frac{w_p^2-4v\tau_f x}{2\sqrt{2}v\tau_f w_p}\right]\right) \tag{3.32}$$

Setting Equation 3.32 to 0 and rearranging leaves

$$0 = \frac{8v^2\tau_f^2}{2v\tau_f w_p\sqrt{2\pi}}\exp\left[\frac{-(w_p^2-4v\tau_f x)^2}{(2\sqrt{2}v\tau_f w_p)^2}\right] - \operatorname{erfc}\left[\frac{w_p^2-4v\tau_f x}{2\sqrt{2}v\tau_f w_p}\right] \tag{3.33}$$

This can then be solved numerically to find the position of peak inversion. It is then also possible to determine the maximum heights of the gain distribution curves. If the resonator mode is constrained to be Gaussian of a certain width, the overlap can be determined by comparing the integral of Equation 3.27 and that of a Gaussian with a maximum given by the peak of the inversion curve.

$$\int_{-\infty}^{\infty} n_2 dx = A\left[-B\operatorname{erf}\left(\frac{-32(v\tau_f)^3x + 8(v\tau_f w_p)^2 - (2\sqrt{2}v\tau_f w_p)^2}{16\sqrt{2}v\tau_f w_p(v\tau_f)^2}\right) - v\tau_f e^{-\frac{x}{v\tau_f}}\operatorname{erfc}\left(\frac{w_p^2-4v\tau_f x}{2\sqrt{2}v\tau_f w_p}\right)\right]_{-\infty}^{\infty} \tag{3.34}$$

Where A and B are as follows

$$A = \frac{w_p R_{\max}}{2v}\sqrt{\frac{\pi}{2}}\exp\left[\frac{w_p^2}{8v^2\tau_f^2}\right] \tag{3.35}$$

$$B = v\tau_f\exp\left[\frac{(2\sqrt{2}v\tau_f w_p)^2 - 16(v\tau_f w_p)^2}{64(v\tau_f)^4}\right] \tag{3.36}$$

The second term within the square brackets in Equation 3.34 is an exponentially modified Gaussian so tends to 0 as $x \to \pm\infty$. The error function $\to \pm 1$ as $x \to \pm\infty$, Equation 3.34 therefore collapses to

$$\int_{-\infty}^{\infty} n_2 dx = 2AB \tag{3.37}$$

Equation 3.37 is the total inversion present in the gain medium and is equivalent to the area under the 'Inversion profile' curve in Figure 3.18. The proportion of inversion within the gain medium seen by a Gaussian resonator mode can be found by considering the area under a Gaussian centred on the peak of the inversion distribution which is also included in Figure 3.18.

As the integral of a Gaussian is given by

$$\int_{-\infty}^{\infty} Ce^{-2\frac{x^2}{w}} dx = C\frac{\sqrt{2\pi}w}{2} \tag{3.38}$$

Where C is some constant. The proportion of inversion within the gain medium seen by a Gaussian resonator mode can now be found by dividing Equation 3.38 by Equation 3.37 leaving

$$n_2^{\text{seen}} = \frac{n_2(X_0)\sqrt{2\pi}w}{4AB} \tag{3.39}$$

Where X_0 is the solution to Equation 3.33. Equation 3.39 is effectively the proportion of the pump light available to a laser mode matched to the stationary inversion profile at threshold, and is the ratio of the two curves in Figure 3.18. If the threshold power is known for the system the increase in threshold power required for a given pump velocity can now be found with the following equation.

$$P_{\text{th}}^{\text{moving}} = \frac{4AB}{Nw\sqrt{2\pi}} P_{\text{th}}^{\text{stationary}} \tag{3.40}$$

Where N has been found by evaluating $n_2(X_0)$ and simplifying, and is given by

$$N = \frac{w_p}{2v}\sqrt{\frac{\pi}{2}} \exp\left[\frac{w_p^2}{8v^2\tau_f^2} - \frac{X_0}{v\tau_f}\right] \text{erfc}\left[\frac{w_p^2 - 4v\tau_f X_0}{2\sqrt{2}v\tau_f w_p}\right] \tag{3.41}$$

The change in resonator threshold as motion is introduced to the system is shown in Figure 3.19. For velocities rates of the order of 10% of a beam waist per upperstate lifetime there is very little change in threshold, in fact the predicted change in threshold is less than 2%. Above a velocity of 0.3 beam waists per upperstate lifetime the change in threshold becomes approximately linear and can be described by Equation 3.42.

$$\Delta P_{\text{threshold}} = 0.81v + 0.87 \tag{3.42}$$

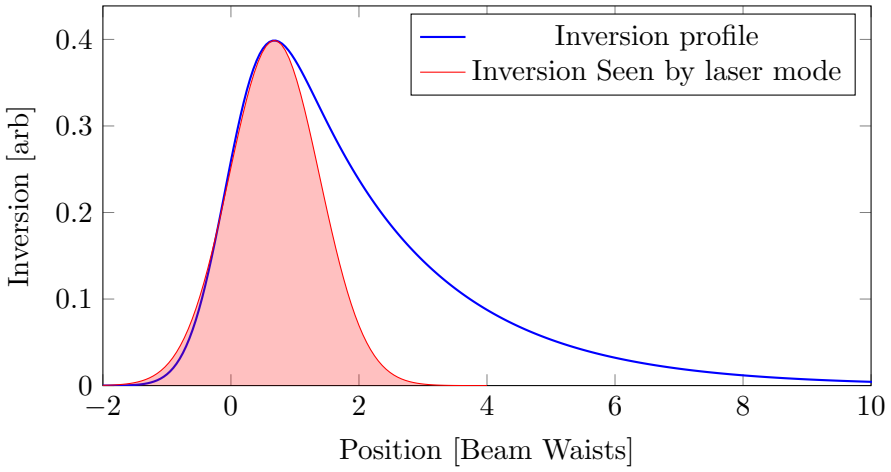

Figure 3.18: The inversion seen by a Gaussian resonator mode matched to the stationary inversion profile can be approximated by a Gaussian under the inversion curve, here v =2.

It should be noted that the constants in Equation 3.42 are artefacts of the use of Gaussian beams and are independent of the laser's properties.

Figure 3.19 also includes the result from the analysis based on top hat beams carried out above. Whilst both approaches show reasonable agreement the Gaussian results indicate there is a regime at low speeds where threshold is not effected by motion. It also indicates a less pronounced increase at higher speeds.

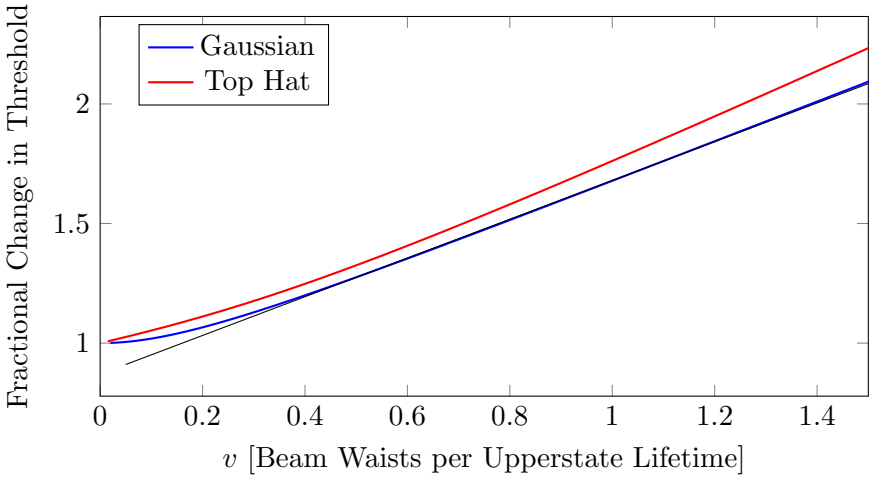

Figure 3.19: The laser threshold increases as the motion of the pump laser mode pair is increased, above $v = 0.3$ this change is approximately linear and is described by Equation 3.42.

3.5.2.2 Above Threshold

Above laser threshold, if the laser is in a steady state, any increase in pump rate will not increase the population of the meta-stable upper state. Instead the intracavity photon flux increases to remove the extra energy via stimulated emission. If the laser is operating in a steady state the output power is by definition constant. The gain within the resonator is thus matched to the resonator loses to maintain a constant circulating power. The population of the metastable level thus does not increase with the pump power, this can be shown mathematically as follows. The amount of gain can be calculated with the following equations, see §2.3.2.

$$g = \frac{g_0(R_p)}{\sigma\phi(R_p)c\tau_f + 1} \tag{3.43}$$

$$= -\frac{\ln(R_{oc}R_l)}{2l} + \alpha \tag{3.44}$$

Gain is directly proportional to the metastable laser level population in a 4 level laser under the assumption that the transition from the lower laser level to the ground state is fast. Equation 3.44 shows that the gain in a resonator is a property of its losses and independent of the pump rate. However, the gain is also a function of the small signal gain, g_0, which is dependent on the pump power, see Equation 3.43. The circulating photon flux must therefore increase to extract the extra energy deposited in the gain medium preventing the population of the meta stable level increasing. Importantly this process occurs 'instantaneously' making it independent of the velocity the laser mode and pump spot make through the gain medium.

This means energy extraction via stimulated emission is unaffected by relative motion between the pump, laser mode and gain medium. The slope efficiency of a RCL will therefore be unchanged by the rotating periscope and only the lasers threshold is modified. Rotation can thus be considered to be a reduction in the upper state lifetime and Equation 2.35 can be written as

$$P_{\text{out}} = \eta\left(P_{\text{in}} - P_{\text{th}}(v)\right) \tag{3.45}$$

$$P_{\text{out}} \approx \eta\left(P_{\text{in}} - P_{\text{th}}^{\text{stationary}}(0.81v + 0.87)\right) \tag{3.46}$$

Figure 3.20 shows the expected change in output power as the velocity is increased for a constant pump power. Clearly there is a maximum velocity an RCL can be operated at before the reduction in power loss created by the increase in threshold becomes unacceptable.

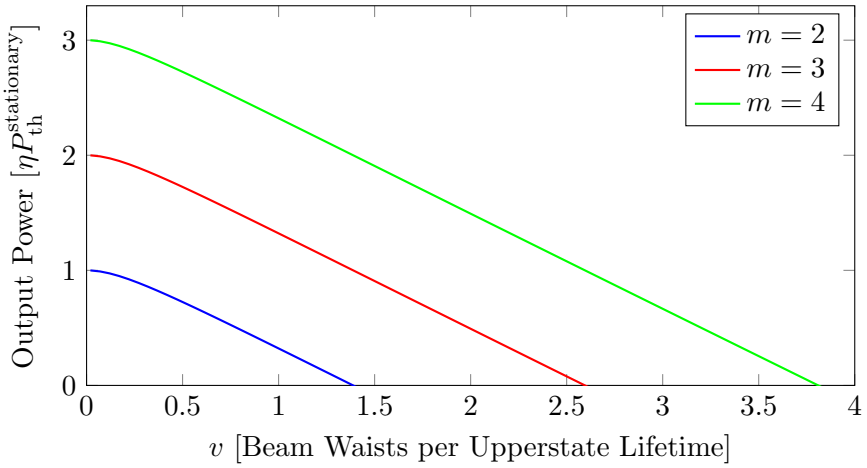

Figure 3.20: As the velocity is increased the output power will be reduced. m is the multiple of the threshold power the laser is pumped with.

3.5.3 Ideal Rotation Speed

To overcome the thermal issues associated with solid state lasers a minimum rotation rate is required. However, the introduction of motion has negative consequences for the lasers threshold.

If it is assumed the temperature of the gain medium at threshold is proportional to the threshold pump power comparing Equations 3.5 and 3.40 gives an indication of how the temperature at laser threshold varies as the velocity is increased. Expressing Equation 3.5 in terms of velocity gives the following expression for the temperature rise in the gain medium after the pump has passed over it at the threshold pump power.

$$\Delta T_{\text{threshold}} = \frac{2P_{\text{heat}}^{\text{threshold}}}{C_v \pi w_p l v} \tag{3.47}$$

$$P_{\text{heat}}^{\text{threshold}}(v) = P_{\text{heat}}^{\text{stationary}} \Delta P_{\text{threshold}}(v) \tag{3.48}$$

Here $P_{\text{heat}}^{\text{stationary}}$ is the heating power inside the gain medium at the threshold pump power when the rotating periscope is kept stationary. $P_{\text{threshold}}^{\text{stationary}}$ is heating power at threshold under rotation which is can be found by considering the change in threshold power induced by the motion, $\Delta P_{\text{threshold}}(v)$.

At velocities greater than 0.3 beam waists per second the change in threshold power is

well approximated by Equation 3.42. Combining Equations 3.47 and 3.48 and substituting this in gives

$$\Delta T_{\text{threshold}}(v) = \frac{2P_{\text{heat}}^{\text{stationary}}(0.81v + 0.87)}{C_v \pi w_p l v} \tag{3.49}$$

$$\rightarrow \frac{1.62P_{\text{heat}}^{\text{stationary}}}{C_v \pi w_p l} \tag{3.50}$$

There is thus a minimum achievable threshold temperature which is determined by properties of the gain medium and the dimensions of the pump beam.

In the adiabatic limit the temperature rise in a laser gain medium is proportional to the pump power. The pump power can be related to the output power of the RCL with Equation 3.46 when $v \gtrsim 0.3$. Substituting this into the form of Equation 3.5 which uses velocity, with the assumption that any heating is the result of the quantum defect, gives an expression for the expected temperature rise within an RCL.

$$\Delta T = \frac{2(1-\eta_{qd})}{C_v \pi w_p l v}\left(\frac{P_{\text{out}}}{\eta} + P_{\text{heat}}^{\text{stationary}}(0.81v + 0.87)\right) \tag{3.51}$$

$$= \frac{(1-\eta_{qd})}{C_v \pi w_p l}\left(2\frac{P_{\text{out}}}{\eta v} + \frac{1.74P_{\text{heat}}^{\text{stationary}}}{v} + 1.62P_{\text{heat}}^{\text{stationary}}\right) \tag{3.52}$$

If v is sufficiently large the temperature rise can be thus be kept constant as P_{out} is increased. As discussed in §2.6.3.1 the properties of a laser resonator are thermally dependent, which leads to systems having an operating window. The introduction of motion gives a method independent of the pump power to control the thermal lens strength and thus increase the size of the operating window.

However, not only this will require an increase in P_{in} to counterbalance the increase in threshold, which soon becomes impractical for real world systems, there are limits on v. Figure 3.20 shows that for a given pump power there is a maximum allowable v. When designing a RCL a balance must therefore be struck between between this increase and threshold and reducing the temperature rise, with different rotation rates appropriate for different levels of pump power.

Furthermore, at extreme values of v the circular nature of the pump path cannot be ignored. If material has not been allowed to fully cool the absolute temperature will be increased further on the next pump pass, this should not have severe consequences for the laser mode as the temperature distribution will be dominated by the new pump pass. However, eventually no cooling will be able to occur between pump passes and a ring of uniform temperature will develop in the gain medium. The RCL will no longer be able to take advantage of operating in the adiabatic limit and will have a temperature profile similar to that of a traditional solid state laser gain medium. The RCL will still

maintain the advantage of the larger heated volume, allowing a performance increase over an equivalent non-moving system even in this extreme regime.

3.6 Conclusion

Whilst a number of laser architectures have been previously demonstrated that make use of relative motion between the pump beam, laser mode and the gain medium, there have been no demonstrations of a system where this occurs whilst the gain medium is kept stationary. These previous systems have been able to demonstrate competitive performance with contemporary systems, but the engineering challenge of cooling a moving piece of gain media has prevented their wide spread adoption. This chapter has introduced a new laser architecture that makes use of relative motion, but without this obstacle.

The RCL overcomes this hurdle by instead moving the laser mode and pump beam through a stationary, and conventionally heat sunk, piece of gain medium. This new strategy leverages recent developments in pump sources, namely laser diodes. Unlike previous moving gain media lasers the RCL requires the pump and laser mode to be collinear as they pass through the rotating components and then into the gain medium. The rotating prism forms an aperture not present in previous designs and precludes the use of flashlamps. However, this brightness constraint is less than that faced by a fibre laser and modern diodes are capable of producing the brightness required to deliver considerable powers whilst satisfying the constraint this aperture applies, see §2.6.4.7.

This chapter then went on to discuss the required mechanical tolerances to implement this strategy and found that they where achievable with modern manufacturing techniques. The consequences of relative motion between a gain medium and laser mode was then discussed. The effect on temperature was found to be large, which is of benefit to laser operation. The lasing properties were also found to change under the influence of rotation, these changes manifest as an increase in laser threshold. The reduction in temperature was found to be more sensitive than that for threshold providing a window where successful operation of a RCL can occur. Furthermore, the ability to change the rotation rate of the intra-cavity periscope will give control over the thermal lens strength allowing the window of operation of an RCL to be larger than that of many traditional solid state lasers.

The analysis conducted in this chapter indicated that azimuthal velocities of the order of 1 m s^{-1} are required to significantly reduce the temperature rise in Nd:YAG. If a circle of radius 20 mm is being swept out this corresponds to a rotation rate of the order of 8 Hz, or 500 RPM. A 1× CD-ROM spins with an azimuthal velocity of between 1.2 m s^{-1} and **1**.4 m s^{-1} (a 12× disk spins 12 times faster when reading the outer edge) within an optical system whilst maintaining a precision alignment [33]. If the periscope

in the RCL is built as a rugged unit both its alignment requirements and spin rates are less than that of a CD. While the periscope is heavier than a CD a number of consumer products reliably rotate components faster than 500 RPM for extended periods of time in more hostile environments than the RCL. Washing machines spin uneven loads at rates of the order of 1000 RPM and components within a car engine function over a wide temperature range for years even though they revolve at thousands of RPM. The moving components in an RCL should therefore have no consequences for the longevity of the laser system.

References

[1] G. F. Albrecht, S. Sutton, E. George, W. Sooy, and W. Krupke, "Solid state heat capacity disk laser," *Laser and Particle Beams*, vol. 16, no. 04, pp. 605–625, 1998.

[2] M. Eichhorn, "High-efficiency multi-kilowatt Er3+:YAG solid-state heat-capacity laser.," *Optics letters*, vol. 36, pp. 1245–7, Apr. 2011.

[3] A. Giesen and J. Speiser, "Fifteen Years of Work on Thin-Disk Lasers: Results and Scaling Laws," *IEEE Journal of Selected Topics in Quantum Electronics*, vol. 13, no. 3, pp. 598–609, 2007.

[4] H. Hugel, A. Giesen, M. Larionov, K. Contag, and C. Stewen, "A 1-kW CW thin disc laser," *IEEE Journal of Selected Topics in Quantum Electronics*, vol. 6, no. 4, pp. 650–657, 2000.

[5] A. Javan, W. R. Bennet Jr., and D. R. Herriott, "Population inversion and continuous optical maser oscillation in a gas discharge containing a He-Ne mixture," *Physical Review Letters*, vol. 6, no. 3, 1961.

[6] F. P. Schafer, "Organic Dye Solution Laser," *Applied Physics Letters*, vol. 9, no. 8, p. 306, 1966.

[7] P. Sorokin and J. Lankard, "Stimulated emission observed from an organic dye, chloro-aluminum phthalocyanine," *IBM Journal of Research and ...*, no. March, pp. 162–163, 1966.

[8] M. Boiteux and O. de Witte, "A transverse flow repetitive dye laser," *Applied optics*, vol. 9, pp. 514–5, Feb. 1970.

[9] O. G. Peterson, S. A. Tuccio, and B. B. Snavely, "CW operation of an organic dye solution laser," *Applied Physics Letters*, vol. 17, no. 6, p. 245, 1970.

[10] D. Hecht, W. Bond, R. Pantell, and H. Puthoff, "Rotating plastic disk dye laser," *Quantum Electronics, IEEE Journal of*, vol. 7, p. 271, June 1971.

[11] D. Hecht, W. Bond, R. Pantell, and H. Puthoff, "Dye lasers with ultrafast transverse flow," *IEEE Journal of Quantum Electronics*, vol. 8, no. 1, pp. 15–19, 1972.

[12] R. Byer, "High power solid state laser," *US Patent 4,555,786*, 1985.

[13] S. Basu and R. L. Byer, "40-W average power, 30-Hz moving-slab Nd:glass laser.," *Optics letters*, vol. 11, pp. 617–9, Oct. 1986.

[14] E. Stappaerts, "Hybrid Heat capacity-moving slab laser concept," Tech. Rep. April, Lawrence Livermore National Laboratory (LLNL), Livermore, CA, 2002.

[15] S. Basu and R. L. Byer, "Diode-pumped moving-disc laser: a new configuration for high average power generation," *Optical and Quantum Electronics*, vol. 22, pp. S33–S37, July 1990.

[16] J. Korn, T. H. Jeys, and T. Fan, "Continuous-wave operation of a diode-pumped rotating Nd:glass disk laser.," *Optics letters*, vol. 16, pp. 1741–3, Nov. 1991.

[17] Y. Chen and V. Kushawaha, "Rotating-disk diode-pumped continuous-wave Nd: YAG laser," *Applied Physics B: Lasers and Optics*, vol. 61, no. 5, pp. 525–528, 1995.

[18] S. M. Massey, J. B. McKay, T. H. Russell, A. H. Paxton, H. C. Miller, and S. Basu, "Diode-pumped Nd:YAG and Nd:glass spinning-disk lasers," *Journal of the Optical Society of America B*, vol. 22, no. 5, p. 1003, 2005.

[19] S. Basu, "Nd-YAG and Yb-YAG rotary disk lasers," *IEEE Journal of Quantum Electronics*, vol. 11, no. 3, pp. 626–630, 2005.

[20] S. Basu and B. Norton, "High-power Q-switched rotary disk lasers," in *Proceedings of SPIE*, 2006.

[21] S. Basu, "Rotary Disk Lasers in the UV, the Visible and the Infrared," in *Proceedings of SPIE*, 2008.

[22] F. Zhou, G. Huang, and S. Gu, "A high average power rotating hollow cylinder Nd: glass laser," *Applied Physics B*, vol. 591, pp. 585–591, 1996.

[23] D.-h. Gwo, "Ultra-precision bonding for cryogenic fused-silica optics," *Proc. SPIE*, vol. 3435, no. July, 1998.

[24] E. J. Elliffe, J. Bogenstahl, a. Deshpande, J. Hough, C. Killow, S. Reid, D. Robertson, S. Rowan, H. Ward, and G. Cagnoli, "Hydroxide-catalysis bonding for stable optical systems for space," *Classical and Quantum Gravity*, vol. 22, pp. S257–S267, May 2005.

[25] S. Chatterjee, "Simple technique for polishing laser rods," *Optical Engineering*, vol. 42, p. 1076, Apr. 2003.

[26] E. Prochnow and D. Edwards, "The precision hand polishing of BBO and LBO," *Applied optics*, pp. 8130–8131, 1998.

[27] "Precision Glass and Optics Rhomboid Prisms." http://www.pgo.com/precision-optics#rhomboid-prisms. Accesed: 11/6/14.

[28] D. F. Vanderwerf, *Applied Prismatic and Reflective Optics*. Washington: SPIE, 2010.

[29] Fan and T.Y., "Heat generation in Nd:YAG and Yb:YAG," *IEEE Journal of Quantum Electronics*, vol. 29, pp. 1457–1459, June 1993.

[30] W. Koechner, "Thermal Lensing in a Nd:YAG Laser Rod.," *Applied optics*, vol. 9, pp. 2548–53, Nov. 1970.

[31] W. Koechner, "Transient thermal profile in optically pumped laser rods," *Journal of Applied Physics*, vol. 44, no. 7, p. 3162, 1973.

[32] W. Koechner, *Solid State Laser Engineering*. New York: Springer, 6th ed., 2006.

[33] "ISO/IEC 10149:1989, EN 30149:1991 Information technology. Data interchange on read-only 120 mm optical data disks (CD-ROM)," 1990.

Chapter 4

Lasing with Intracavity Motion

4.1 Introduction

Having introduced the concept of the RCL in the previous chapter, this chapter describes the first working RCL prototypes. The first system was designed to operate at slow rotation rates, operating with a maximum azimuthal velocity of 40 RPM, equivalent to 0.065 m s^{-1}. This introduced a movement of 5% of a beam waist within a lifetime. This was to demonstrate the lasing processes would not be impeded by the introduction of motion. A second prototype is then described which could operate with velocities of multiple beam waists per lifetime. Particular attention is paid to the repercussions of introducing moving components into these resonators. The effect on pointing and power stability is described as well as the change in laser threshold as the rotation frequency is varied. This is then compared with the theoretical predictions made in §3.5.2.1.

The unusual pointing properties of an RCL were found to have consequences for measuring beam quality. Two different measurement techniques for measuring the M^2 of the RCL are presented which attempted to account for this pointing instability. One of these was limited by the exposure time of a CCD and the other diagnostic made use of the periodicity of the RCL's output to reconstruct beam profiles from a series of readings synchronised to the rotation of the intracavity periscope. This allowed the evolution of the RCL's output beam profile to be determined over a rotation of the periscope.

4.2 Low Speed Demonstration

To test the RCL technique and confirm that any detrimental effects introduced by the intracavity moving parts did not out weigh the beneficial thermal properties predicted in §3.5.1, a laser resonator was built around a BK7 rhomboid prism. This prism had a 13 mm square clear aperture and introduced a beam displacement of 15 mm. The prism

was mounted inside a bearing with the centre of one of the prism's apertures positioned over the axis of rotation. The bearing and prism module was then attached to an electric motor via a drive belt. This could then be used to spin the prism and thus move any laser mode aligned to the axis of rotation.

4.2.1 Resonator Design

The gain medium used in this resonator was a 1% doped, 35 mm diameter, 6 mm thick Nd:YAG ceramic slab. The slab had a AR coating on its front face for 808 nm and 1064 nm and the back face was HR coated at both 1064 nm and 808 nm. The back face also had a layer of silver deposited to act as a bonding layer. A 125 μm thick layer of indium foil was placed between the slab and a gold plated copper heat sink. This was then compressed to adhere the slab to the heat sink.

Figure 4.1 shows a schematic of the resonator. The distance between the curved mirror and output coupler was 140 mm and the total cavity length was 330 mm. The pump telescope created a pump waist of 300 μm at the back of the slab. The ray transfer matrix that describes a round trip of this resonator, which can then be used to calculate the laser mode size in the gain medium, is as follows.

$$\begin{pmatrix} 1 & 0 \\ -\frac{1}{f_{th}} & 1 \end{pmatrix} \begin{pmatrix} 1 & d_1 \\ 0 & 1 \end{pmatrix} \begin{pmatrix} 1 & 0 \\ -\frac{2}{R} & 1 \end{pmatrix} \begin{pmatrix} 1 & 2d_2 \\ 0 & 1 \end{pmatrix} \begin{pmatrix} 1 & 0 \\ -\frac{2}{R} & 1 \end{pmatrix} \begin{pmatrix} 1 & d_1 \\ 0 & 1 \end{pmatrix} \begin{pmatrix} 1 & 0 \\ -\frac{1}{f_{th}} & 1 \end{pmatrix} \tag{4.1}$$

Here d_1 is the distance between the curved mirror and the gain medium, d_2 is the distance between the curved mirror and the output coupler, R is the radius of curvature of the mirror and f_{th} is the thermally dependent lens inside the Nd:YAG. These distances include the optical path lengths through both the rhomboid prism and the Nd:YAG which are found be dividing the geometric path distance by the refractive index of the material. The air dielectric interfaces can be ignored in this case as the incident laser mode is collimated as they are within a Rayleigh length of a beam waist.

With this ray transfer matrix it is possible to find the beam waist as the thermal lens strength varies. Koechner shows that the thermal lens strength due to the temperature dependence of the refractive index in a rod geometry is given by Equation 4.2 in [1]. This equation is derived by considering the temperature profile in an edge cooled rod and comparing the resulting refractive index profile with a lens. The assumption that all heat flow is radial is made and it is assumed that contributions from factors other than the temperature dependence of the refractive index are small. Here K is the thermal conductivity of the gain medium, P_{th} is the heating power, A is the cross section of the pump beam and $\frac{dn}{dT}$ is the temperature dependence of the refractive index.

$$f_{th} = \frac{KA}{P_{th}} \left(\frac{1}{2} \frac{dn}{dT} \right)^{-1} \tag{4.2}$$

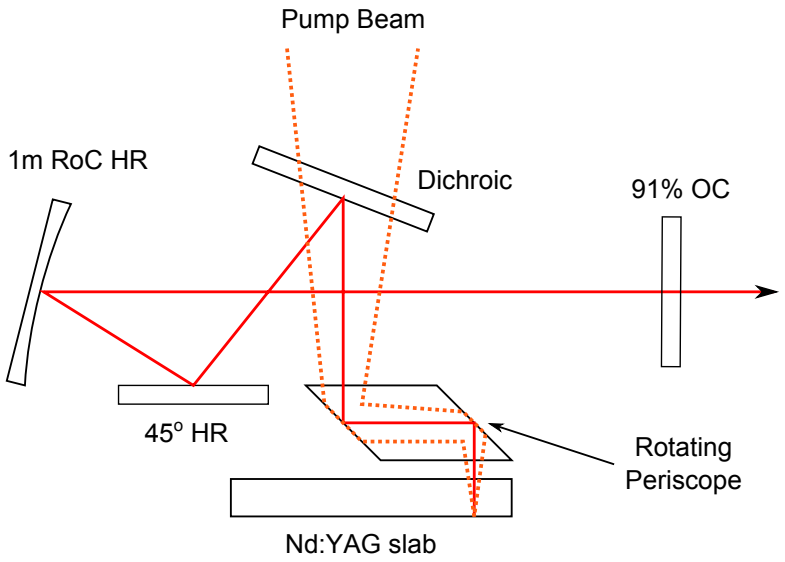

Figure 4.1: Schematic of the first RCL prototype.

Whilst the RCL gain medium is not a traditional laser rod, if the laser spot is kept far enough from the edge of the gain medium for edge effects to be ignored, the disk of gain medium can be treated as a an infinitely wide rod. However the back face cooling of the gain medium will help encourage axial heat flow at the expense of radial flow. This can be expected to produce less serve radial temperature distribution and thus a weaker thermal lens. Furthermore, Equation 4.2 ignores contributions to the thermal lens from stress induced refractive index changes and end face bulging, however this have been shown to be small when compared to the lensing due to the temperature dependence of refractive index [2]. Equation 4.2 therefore gives an indication of the expected thermal lens strength experienced by a stationary RCL.

It should be noted this equation ignores the contribution to the thermal lens created by induced stress and end face bulging, however these are typically smaller than the contribution from the refractive index. In a Nd:YAG rod the temperature dependence of the refractive index is responsible for 73% of the lensing effects [2].

Using the ray transfer matrix and Equation 4.2 it is possible to predict how the resonator TEM_{00} mode will change under different pump conditions, including the position of the stability zones described by Magni in [3] and discussed in §2.6.3.1. This is plotted in Figure 4.2 for this resonator design. As the thermal lens is taken to be at one of the end mirrors only one stability zone exists for this resonator.

4.2.2 Performance

Figure 4.2 indicates the resonator will become unstable when the order of 1 W of heat is deposited into the Nd:YAG slab. When the rhomboid prism was held stationary

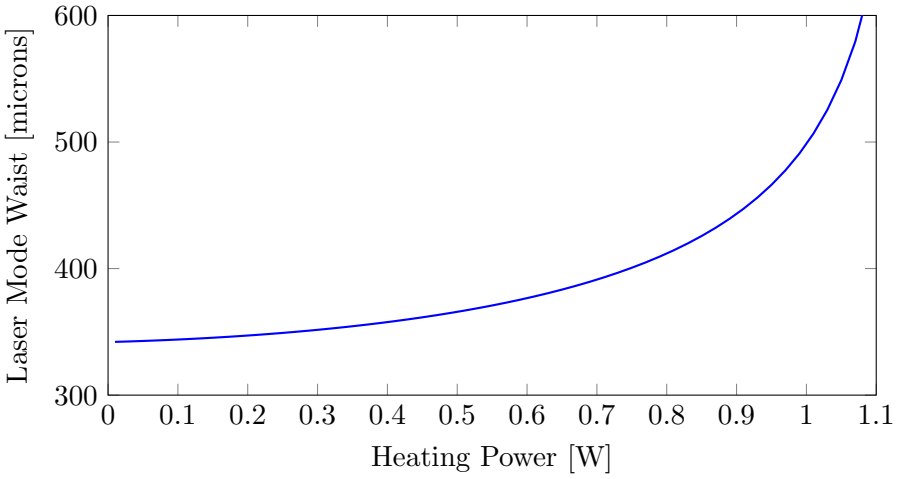

Figure 4.2: Resonator mode radius in the slab as a function of heating power.

Figure 4.3 gives the output of the resonator. It shows the slope efficiency reducing to a level where the output power no longer increases as the pump power is increased. The sudden change in slope efficiency under 5.75 W of pump power is suggestive that this is not due to the temperature dependence of the emission cross section, which in Nd:YAG is linear with temperature between 15 °C and 250 °C [4]. However, the behaviour of the laser is consistent with the resonator becoming unstable as the thermal lens strengthens [5]. Furthermore, 5.75 W of pump power results in approximately 1.4 W of quantum defect heating. This level of heating is consistent with the theoretical prediction of the resonator's behaviour shown in Figure 4.2 when the change from the rod like geometry is considered.

Figure 4.4 shows the output power of the resonator for a number of different rotation speeds. By introducing motion the RCL was able to operate at power levels considerably higher than that of the stationary case. At an azimuthal velocity of 0.063 m s^{-1}, equivalent to 40 RPM, the laser remained stable under 32 W of absorbed pump light which would create 7.7 W of quantum defect heating.

By increasing the speed of rotation Figure 4.4 clearly shows it was possible to delay the onset of thermal roll over by increasing the rotation rate. If the drop in slope efficiency at the top of the power curves is caused by the thermal lens reducing the overlap between the pump and laser mode and eventually driving the resonator unstable, then this indicates the strength of the thermal lens can be reduced by introducing motion to a laser system, as predicted in §3.

4.2.3 Consequences of Rotation

The moving components inside the laser resonator were expected to have some repercussions on the output of the laser. For example, if the movement introduces changes in

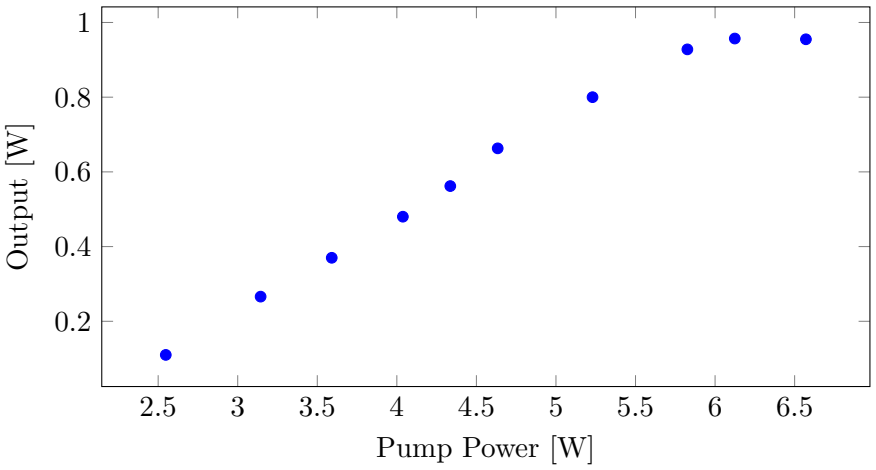

Figure 4.3: Resonator output when the rhomboid prism was held stationary.

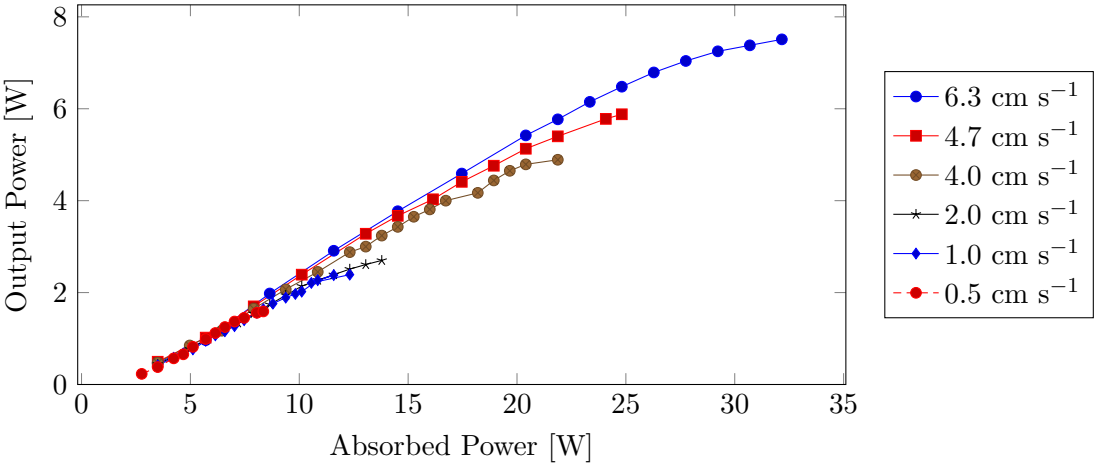

Figure 4.4: Power output of the initial prototype at a number of rotation speeds.

the cavity length the spectral properties of the resonator will change as different longitudinal modes come into and out of existence. Whilst for many applications this will have minimal consequences other effects may be more severe. Angular changes in alignment of the order of the beam divergence will create changes in the the spatial and power characteristics of the output beam as the resonator alignment evolves over a rotation. Variations in the gain medium's properties will also manifest in the output as different parts of the slab are sampled over a rotation.

4.2.3.1 Threshold

The maximum rotation rate of the periscope in this system was 40 RPM, this produced an azimuthal velocity of 0.062 m s^{-1} for the pump spot and laser mode. This corresponds to a movement of 0.048 beam waists within a upper state lifetime. While §3.5.2.1 predicts a change in threshold as motion is introduced, at these speeds this change is expected to be negligible. In fact the threshold is only expected to change by 0.5%. Figure 4.4

shows consistent values for threshold over this range of rotational speeds, agreeing with theory.

4.2.3.2 Power Stability

Figure 4.5 shows the power variation when the RCL is operating in the stationary regime. This was done by operating the laser with the periscope still before moving it a step to interrogate the next point on the Nd:YAG slab. The rhomboid prism was rotated 10° each step and the output power generated by 4.23 W of absorbed pump recorded. The power varied over the points investigated with a standard deviation of 5.9%. The changes in output power seen here can be attributed to alignment of the resonator and changes in the properties of the slab. It should also be noted that if the pump is not collinear with the laser mode on entry to the rhomboid prism the position of the pump spot can change relative to the laser mode over a rotation.

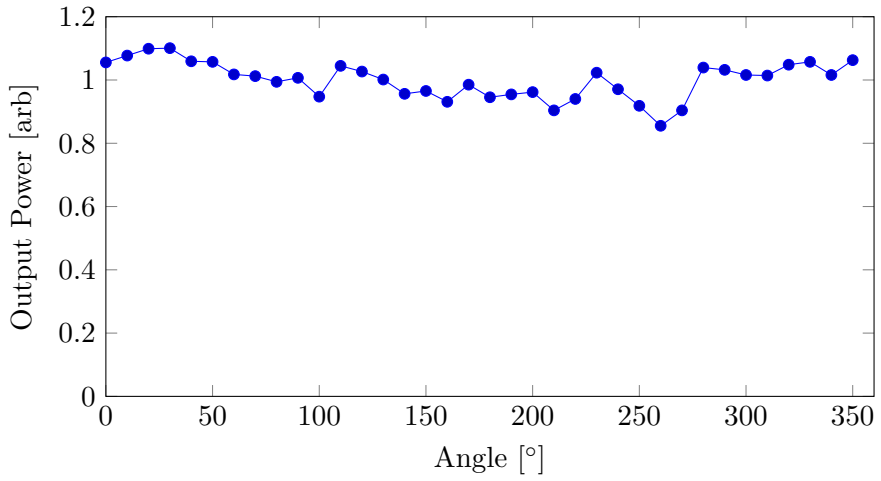

Figure 4.5: Normalised laser output for a stationary RCL.

When the RCL is operated in a rotating regime the periodicity of the power output becomes apparent. Figure 4.6 gives the variation in power output when the rhomboid prism is rotated with a period of 1.5s, equivalent to an azimuthal velocity of 0.06 m s^{-1}. With the rhomboid prism now moving the standard deviation of the output reduced to 3.1%. The difference in variation in power output between the two cases is likely being caused by detrimental thermal effects more adversely effecting some areas of the slab than others. The larger power variation seen in the stationary case suggests there is some variation in the temperature response of the gain medium.

When the periscope is moving the thermal load each 'laser spot' was under is drastically reduced compared to the stationary case. When stationary the gain medium was allowed to increase in temperature until a steady temperature distribution is reached. This stable temperature profile is dependent on the materials properties at that location as well as the distance the spot is from the edge of the Nd:YAG disk and the quality of the thermal

interface. Under rotation these features become less significant, however at higher power levels they could again manifest.

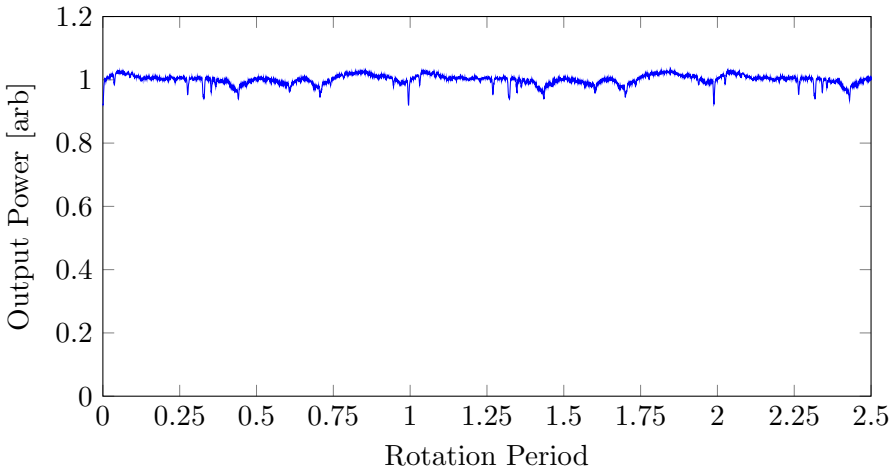

Figure 4.6: Normalised laser output for a rotating RCL.

4.2.3.3 Pointing Stability

The intracavity motion may not be restricted to influencing just the output power of the resonator, and may have consequences for the pointing stability as well. As the resonator has a plane output coupler the output beam must be normal to it for the mode to be stable within the cavity. Any angular variation within the resonator will therefore manifest as a change in position on this optic. This can be measured by re-imaging the output coupler onto a CCD.

By positioning the beam on a CCD Figure 4.7 was produced when the periscope was rotating with a period of 2.26 s, equivalent to 0.04 m s^{-1}, and the laser was pumped with 2.2 W of absorbed power. To test for ellipticity in the beam's path a sine wave of the form given by the following equation was fitted to both data sets. Here $d(t)$ is the beam displacement at time t, B and ϕ are constants to account for the starting position of the laser mode and A is the amplitude of the motion.

$$d(t) = A \sin\left(\frac{2\pi t}{T} + \phi\right) + B \tag{4.3}$$

The beam moved with an amplitude of 107 μm in the horizontal direction, shown in Figure 4.7(a), and 110 μm in the vertical direction, Figure 4.7(b). The similarity between these amplitudes shows motion of the beam on the output coupler is indeed circular. Furthermore there is a $\frac{1}{2}\pi$ phase shift between the two sine waves, as expected for circular

motion. The period of both fitted sine waves is 2.26 s, matching that of the periscope, again as expected.

The lack of ellipticity in the motion of the output beam means that the variation in angle within the resonator is varying at a constant rate with rotation. This suggests the angle is not being induced by a variation in flatness or parallelism of the Nd:YAG disk.

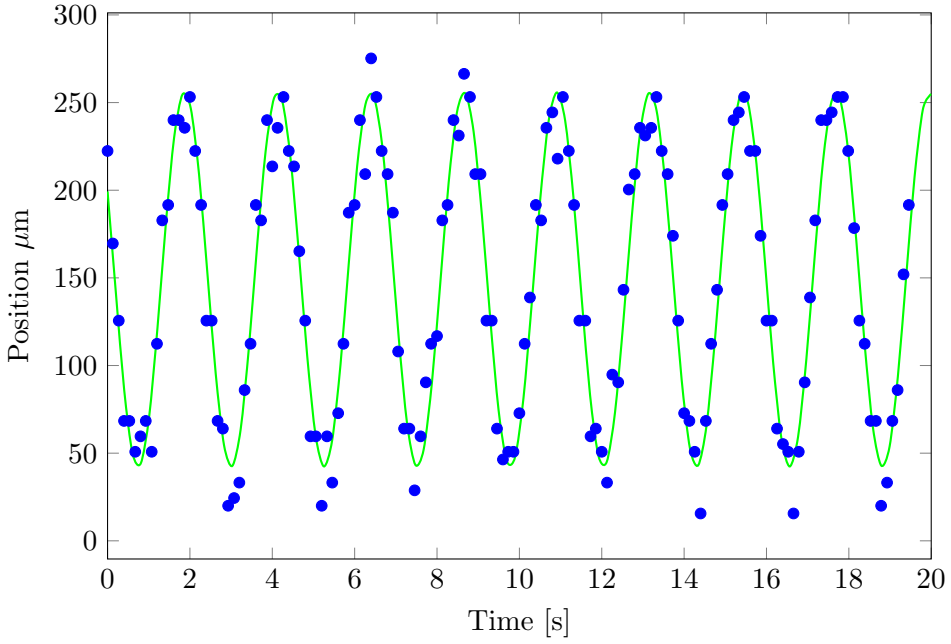

(a) Horizontal motion

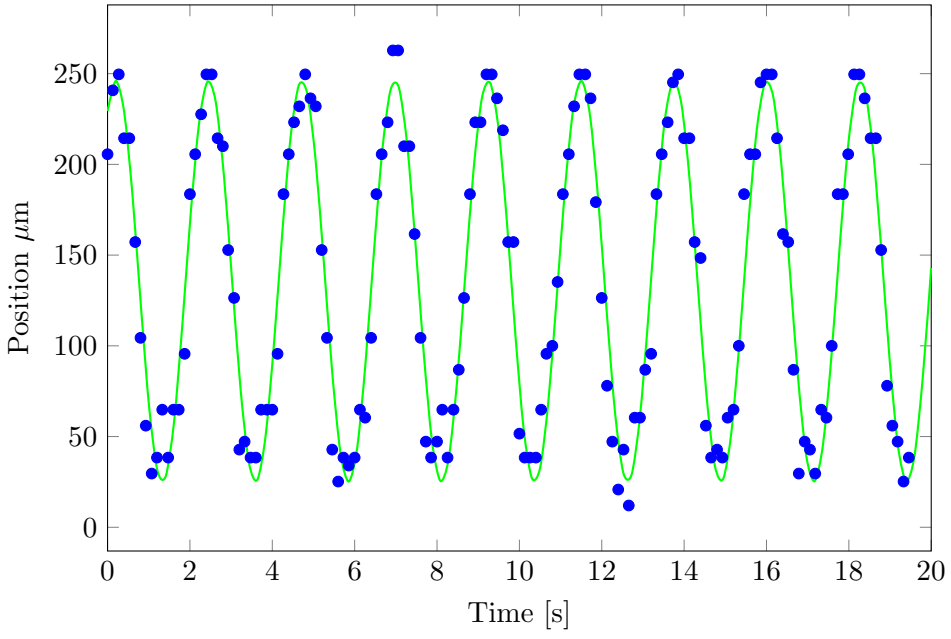

(b) Vertical motion

Figure 4.7: The position of the laser mode on the output coupler varied as the periscope rotated.

If the angle variation induced by the periscope is of the order of 0.5 milliradians, an order of magnitude greater than the predicted required tolerance in §3.4.1, the pump beam will be moved in a circle with an eccentricity on the order of microns. This is two orders of magnitude less than the pump waist, thus the pump spot can be thought to be stationary in the frame of the moving laser mode. This constrains the laser mode to a single point on the Nd:YAG in this frame of reference. The intracavity path of the laser mode is thus that shown in Figure 4.8.

As there is only one curved surface inside this resonator that can provide the mapping of an angular variation to a translation, it is possible to calculate the angular deviation through straightforward geometric considerations of Figure 4.8. On this figure A is the distance between the curved mirror and the periscope once the angle introduced by the periscope is taken into account. Application of the law of cosines gives this distance which can then be used with the sine rule to calculate θ, the angle introduced by the imperfect periscope. With the small angle approximation this gives the following equation, where δ is the displacement on the output coupler created by the imperfect periscope and ϕ is the angle between the curved mirror and the unperturbed laser mode, see Figure 4.8.

$$\theta = \delta \frac{\sin(\phi)}{\sqrt{\delta^2 + x^2 - 2x\delta\cos(\phi)}} \tag{4.4}$$

In this resonator the periscope was positioned 160 mm from the curved mirror and the angle of incidence was approximately 10°. Taking δ to be 50 μm as found in Figure 4.7 leads to an angular variation of ≈300 microradians. This is of the order of the manufactures quoted tolerance for the BK7 rhomboid prism.

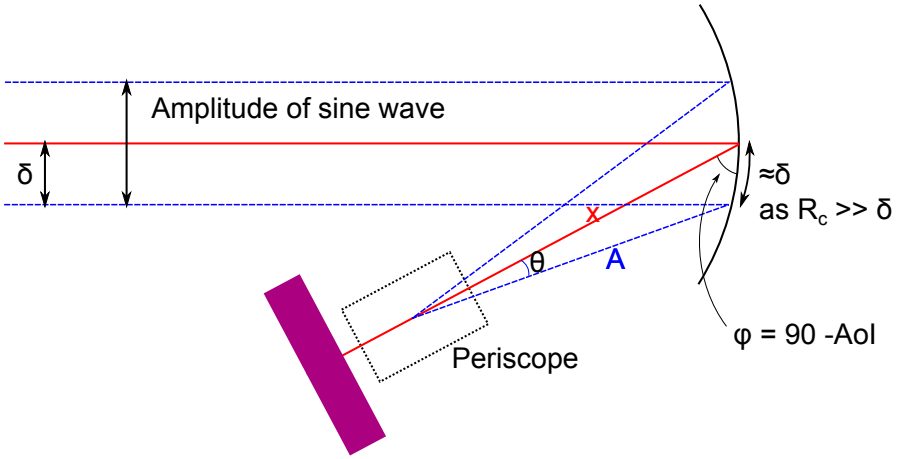

Figure 4.8: The curved mirror maps the variation in angle induced by the imperfect periscope into a translation on the output coupler.

4.2.3.4 Polarisation

The presence of a rotating intracavity rhomboid also has consequences for the output polarisation of the laser as discussed in §3.4.2.2. When a Brewster window is inserted into the RCL resonator laser action no longer occurs over a complete rotation, see Figure 4.9. This is due to the relative phase shift between s and p polarisations that occurs when the beam undergoes total internal reflection inside the rhomboid prism.

After a pass through the rhomboid prism the s and p polarisation states will therefore undergo a phase shift of 77.26°. When incident linearly polarized light is not aligned to either of the rhomboid prism's axes, the relative phase shift will produce an elliptically polarized beam. This creates a depolarization loss when this new polarisation state is incident on the intracavity Brewster window. The loss due to Brewster window is at a minimum when the prism's fast or slow axis is aligned to the incident polarization. This occurs four times within a rotation period and matches the behaviour observed in Figure 4.9.

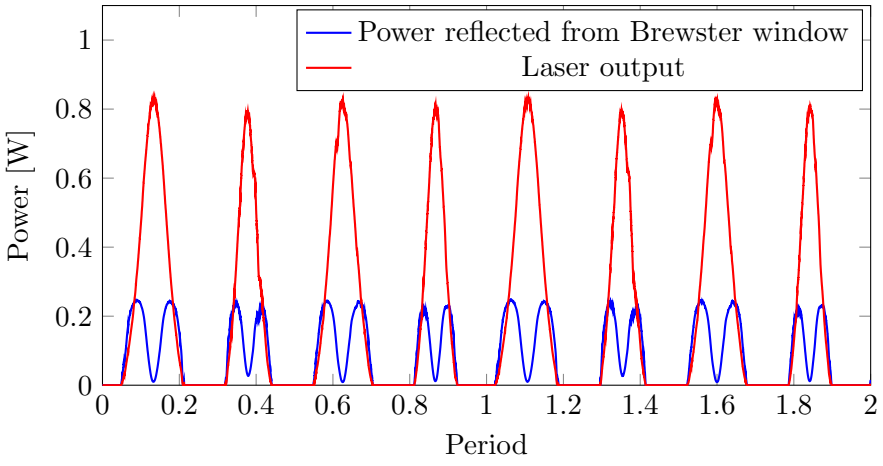

Figure 4.9: Laser behaviour with an intracavity Brewster window.

This behaviour, which prevents the operation of the laser in a polarized mode, could be prevented by replacing the rhomboid prism with a pair of mirrors. An alternative solution is presented in §7.2.

4.3 High Speed Demonstration

The mechanical arrangement supporting the periscope was modified to allow operation at higher azimuthal velocities. This was done by replacing both the bearing supporting the periscope and the electric motor. By operating at higher velocities the regime where threshold is modified by rotation was able to be explored as well as allowing the further drop in temperature associated with higher velocities to be exploited.

4.3.1 Laser Threshold

In §3.5.2 a discussion was presented predicting the consequence the new loss mechanism created by the relative motion between the gain medium and laser mode has on the threshold power. To test this the resonator was changed to include a second focusing intracavity optic. This was done to maintain the 330 μm, TEM_{00} waist whilst allowing a longer resonator arm into which the new mechanical assembly could be placed. By using a resonator with a spot size of 330 μm, and the relatively low threshold power associated with it, it was hoped detrimental thermal effects would be kept at a minimum allowing the effect of rotation to dominate any change in threshold.

The threshold power for this resonator, at a number of different rotation speeds, was found with an IR viewer. Figure 4.10 shows the predicted change in threshold from both the top hat and Gaussian analysis with experimentally determined values.

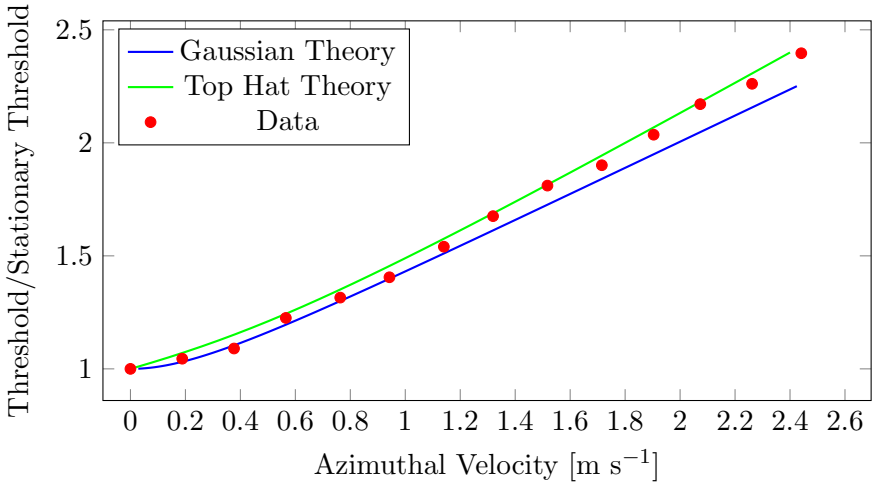

Figure 4.10: Measured change in laser threshold as the pump and laser mode velocity is increased and the theoretical prediction.

The data shows good agreement with both models. At low azimuthal velocities the Gaussian analysis correctly predicts the smaller changes observed in the threshold power, see Figure 4.11. At faster rotation rates, and higher threshold powers, this model underestimates the change in laser threshold and the top hat approach gives a better indication to the increase in threshold. However, at higher azimuthal velocities it is not known if the threshold pump power will continue to increase faster than both models predict. In reality the pump beam was relay imaged from a multimode fibre, creating a super Gaussian profile in the gain medium. The actual behaviour of laser threshold found in this experiment would this be expected to be in between that calculated for a top hot and Gaussian pump profile, which is what was found.

At higher pump powers thermal effects may also be acting to increase threshold. For example, even if the pump laser mode pair is swept fast enough to avoid operating in the regime where heat is moving through the laser mode, a temperature profile matched to the pump beam profile will still exist. The focusing effect of this lens can result in a change in overlap between the pump spot and laser mode, potentially increasing threshold. The addition of thermal effects can thus explain the increase in threshold over what the Gaussian model presented in §3.5.2 suggests.

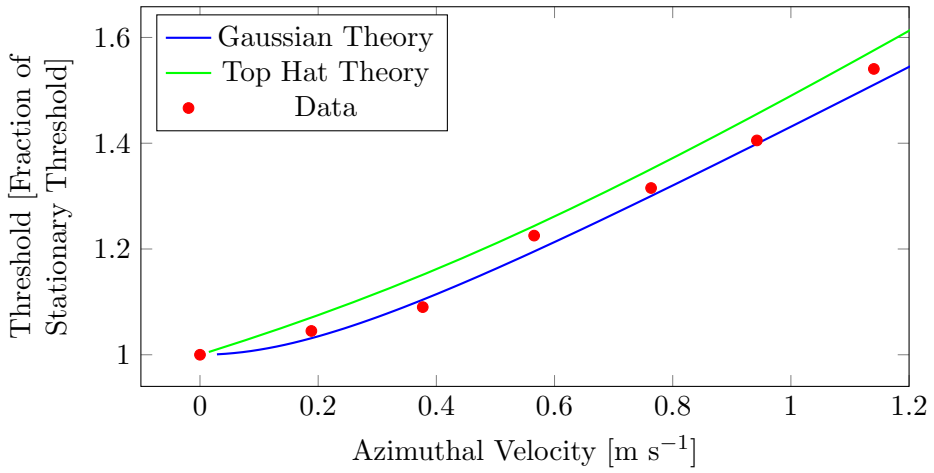

Figure 4.11: Measured change in laser threshold as the pump and laser mode velocity is increased and the theoretical prediction.

4.3.2 Resonator Design

Introducing a second focusing intracavity mirror to the resonator, see Figure 4.12, can improve the resonator's resilience to the thermal lens. The laser's window of operation can then be increased. The new optic can be included in the ray transfer matrix, RTM, analysis of the resonator, resulting in Equation 4.5.

$$\begin{pmatrix} 1 & 0 \\ -\frac{1}{f_{th}} & 1 \end{pmatrix} \begin{pmatrix} 1 & d_1 \\ 0 & 1 \end{pmatrix} \begin{pmatrix} 1 & 0 \\ -\frac{2}{R_1} & 1 \end{pmatrix} \begin{pmatrix} 1 & d_2 \\ 0 & 1 \end{pmatrix} \begin{pmatrix} 1 & 0 \\ -\frac{2}{R_2} & 1 \end{pmatrix} \begin{pmatrix} 1 & 2d_3 \\ 0 & 1 \end{pmatrix} \begin{pmatrix} 1 & 0 \\ -\frac{2}{R_2} & 1 \end{pmatrix} \begin{pmatrix} 1 & d_2 \\ 0 & 1 \end{pmatrix} \begin{pmatrix} 1 & 0 \\ -\frac{2}{R_1} & 1 \end{pmatrix} \begin{pmatrix} 1 & d_1 \\ 0 & 1 \end{pmatrix} \begin{pmatrix} 1 & 0 \\ -\frac{1}{f_{th}} & 1 \end{pmatrix} \tag{4.5}$$

By again making use of Equation 4.2 the resonator mode's behaviour with a varying thermal lens can be modelled. Figure 4.13 shows the stability region for this resonator is approximately a factor of 3.5 times that of the resonator used previously. Furthermore, this resonator was matched to a lager pump spot which contributes to a reduction in thermal lens strength for a given pump power.

Furthermore, the resonator mode was designed to allow Q-switched operation. A Q-switched laser pulse has a peak intensity far greater than that found when a laser is operated in a CW mode. These high peak powers can cause damage to optical coatings if care is not take to ensure the beam size on intracavity optics is large enough to prevent the optical intensity surpassing the damage threshold of the optic.

The pump beam was focused through a telescope constructed out of a 60 mm and a 300 mm lens to deliver a waist of 500 μm within the Nd:YAG slab by magnifying the 200 μm diameter core diode delivery fibre. A 74% reflective plane mirror provided the output coupling.

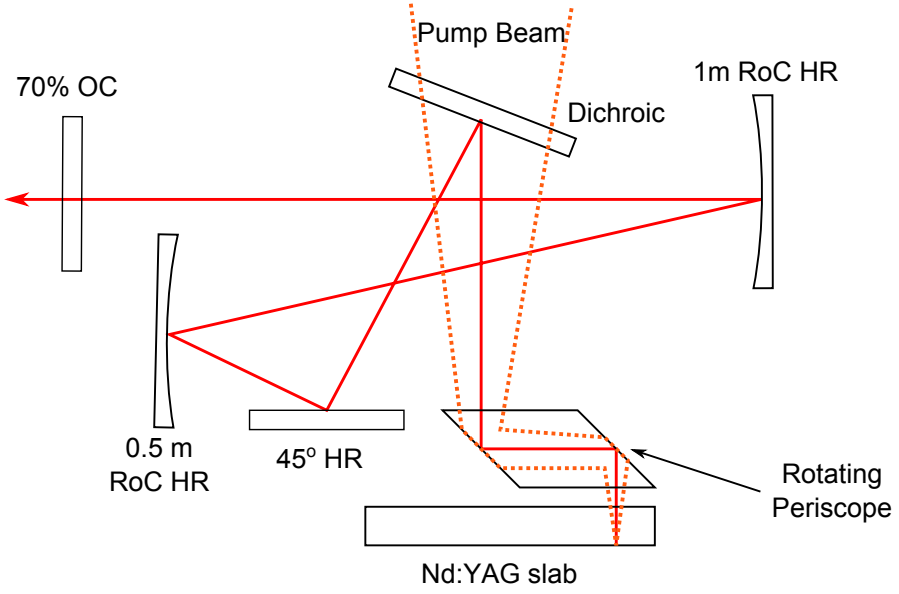

Figure 4.12: This resonator had a larger operating window than the previous design. The distance between the slab and 0.5 m mirror was 235 mm, the curved mirrors were separated by 100 mm and the OC was 200 mm from the 1 m mirror.

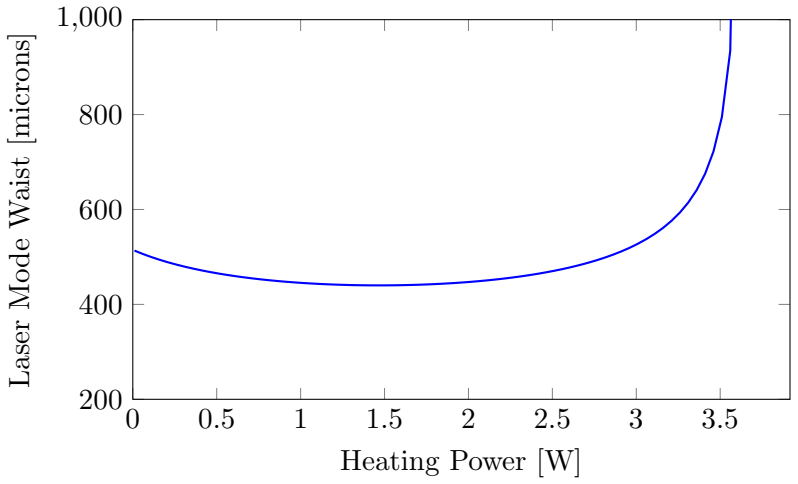

Figure 4.13: Resonator mode radius in the slab as a function of heating power.

4.3.3 Results

4.3.3.1 Performance

When the periscope was held stationary the laser's performance was severely impeded. Laser threshold was achieved with 11.7 W of pump power and the resonator went unstable under 13.5 W after producing a maximum output of 180 mW. Figure 4.13 indicates that in a rod like geometry the resonator would become unstable under a heating power of 3.5 W. If the heating power is taken to be caused by the quantum defect the heating power triggering roll over is thus 3.24 W, showing good agreement with Figure 4.13.

Figure 4.14 shows the lasers output when the periscope was rotating. After the introduction of motion the resonator was no longer severely thermally limited. Instead it could be operated in a regime where the power output was limited by the available pump light. When the periscope was rotated at 2 Hz, which produced an azimuthal velocity of 0.19 m s^{-1}, the slope efficiency was 33%. However increasing the rotation frequency to 5 Hz, equivalent to 0.47 m s^{-1}, caused the slope efficiency to increase to 40%.

Equation 2.35 shows that a laser's slope efficiency is only dependent on the resonator's losses, and efficiency factors describing the the proportion of pump energy that enters the gain medium's upper laser level. Clearly the overlap between the laser mode and pump beam therefore effects the slope efficiency of a laser. By changing the temperature profile by changing the rotation rate the properties of the thermal lens must also change. Thus there are ramifications for the laser mode size which has consequences for the overlap. As the quantum efficiency is constant above room temperature in Nd:YAG this is the only slope efficiency affecting factor that the rotation rate can modify [6].

In §3.5.2.2 a reduction in output power as the azimuthal velocity is increased when the laser is operated above threshold is predicted. This is due to the increase in the required

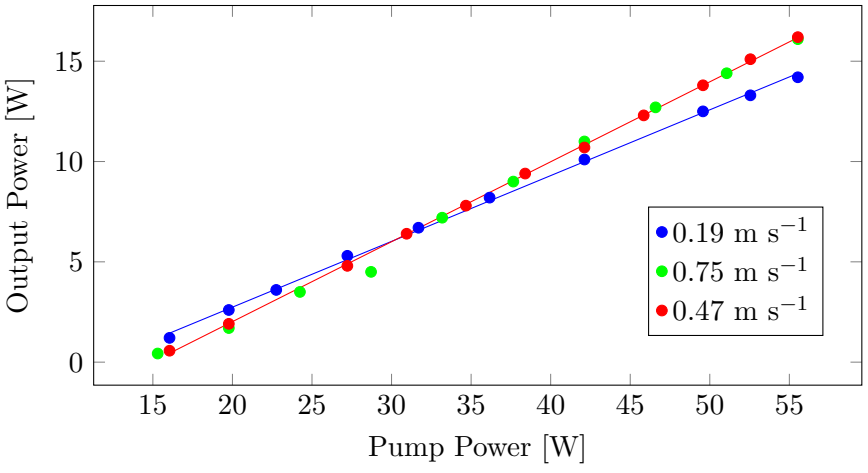

Figure 4.14: The slope efficiency, and thus the output power, could be improved by increasing the azimuthal velocity.

threshold power. Figure 4.15 shows how the resonator's output behaved under 51 W of pump power as the rotation rate was increased.

The stationary threshold was 11.7 W and Equation 3.42 predicts that at an azimuthal velocity of 1.8 m s^{-1}, which corresponds to a movement of 1.4 beam waists per lifetime, it will increase by a factor of two. Looking at Figure 4.14 this is clearly not the case. Under the required threshold power for this resonator performance is already being curtailed by thermal effects, indeed this power level is over three times that required to render the resonator unstable in the stationary case. In this resonator the threshold is lowered by the reduction in thermal effects created by the motion and this dominates over the increase in threshold created by gain being swept out of the pump spot. This is a clear example of the negative consequences of rotation being dominated by the advantageous thermal properties.

Figure 4.15 does show that there is a optimum rotation rate for a given operating power as discussed in §3.5.3. Below an azimuthal velocity of 0.5 m s^{-1} negative thermal effects are still significant enough to limit lasing performance. Above 0.6 m s^{-1} the losses induced by motion imped performance and further reduction in thermal effects are not significant enough to out way them. To maintain the peak output the azimuthal velocity needs to be between 0.5 and 0.6 m s^{-1}. For a periscope sweeping out a radius of 15 mm this corresponds to a rotational rate of 5.3 to 6.4 Hz which is readily achievable.

4.3.3.2 Q Switching

To generate pulses from this laser an AOM operating in a shear mode was placed inside the resonator. The entry and exit faces of the Q-switch were anti-reflection coated at 1

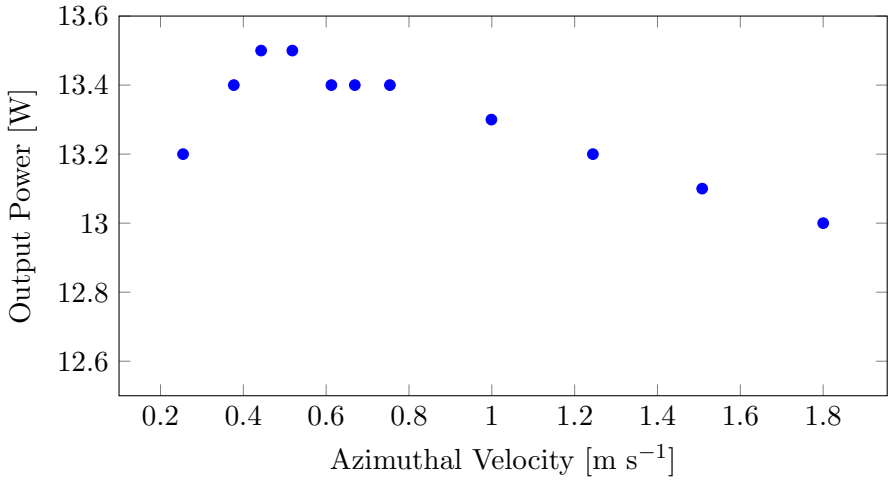

Figure 4.15: Increasing the rotation rate caused a drop in output power as expected.

μm. This type of Q-switch was chosen as it is polarisation independent so does not need the resonator to be run in a polarized mode making them unaffected by the rotating rhomboid prism's polarization properties, see §4.2.3.4.

Figure 4.16 shows the pulsed output of the RCL under 57 W of pump power and an azimuthal velocity of 0.59 m s^{-1}. The maximum pulse energy occurs for a repetition' rate of between 0.8 and 1 kHz, as expected for a Nd:YAG based laser [1]. Below these repetition rates the pulse energy is not expected to change. The small decrease in pulse energy seen in Figure 4.16 could be due to an increase in thermal load due to upconversion processes having a greater effect in the low inversion extraction regime. The stored energy is therefore not being swept out of the laser mode fast enough to change the time it takes the upper state to reach its maximum electron density.

The pointing instability induced by the periscope paired with the presence of a intracavity aperture in the form of the Q-switch has consequences for pulse to pulse stability of the output. By recording every pulse and determining their energy content Figure 4.17 was produced. The pulse energy varied with a standard deviation of 5.9% over a rotation period. This is approximately twice that for the CW resonator described in §4.2.3.2.

Figure 4.17 also shows how the pulse timing varied with respect to the electronic trigger sent to the AOM. As the laser mode moved over the acoustical standing wave within the AOM the time delay for the loss seen by the laser mode changed. If the available gain changed over a rotation period, either due to a variation in the properties of the slab or changes in the resonator alignment, the number of round trips required for lasing to occur would also have changed. This would also have contributed to the timing jitter.

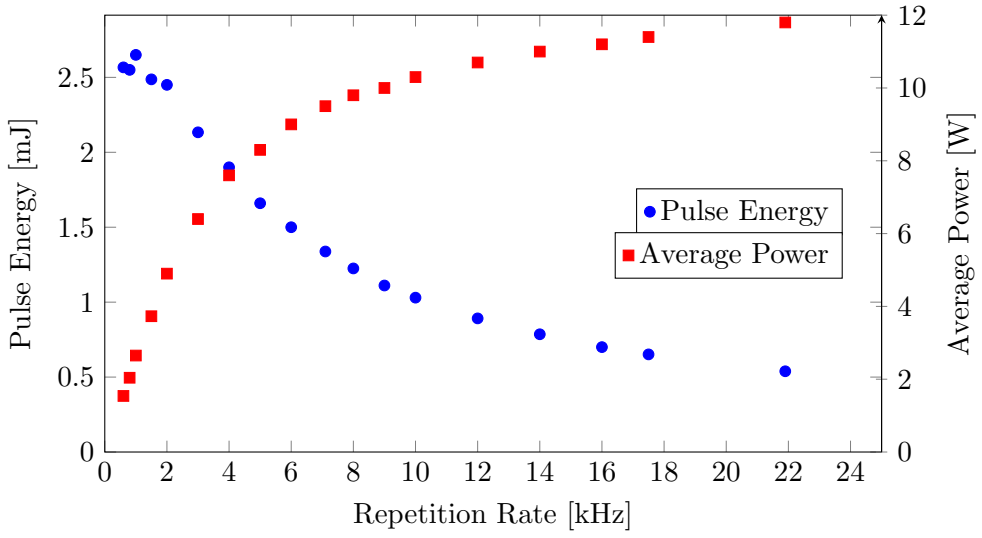

Figure 4.16: Pulsed performance of the RCL.

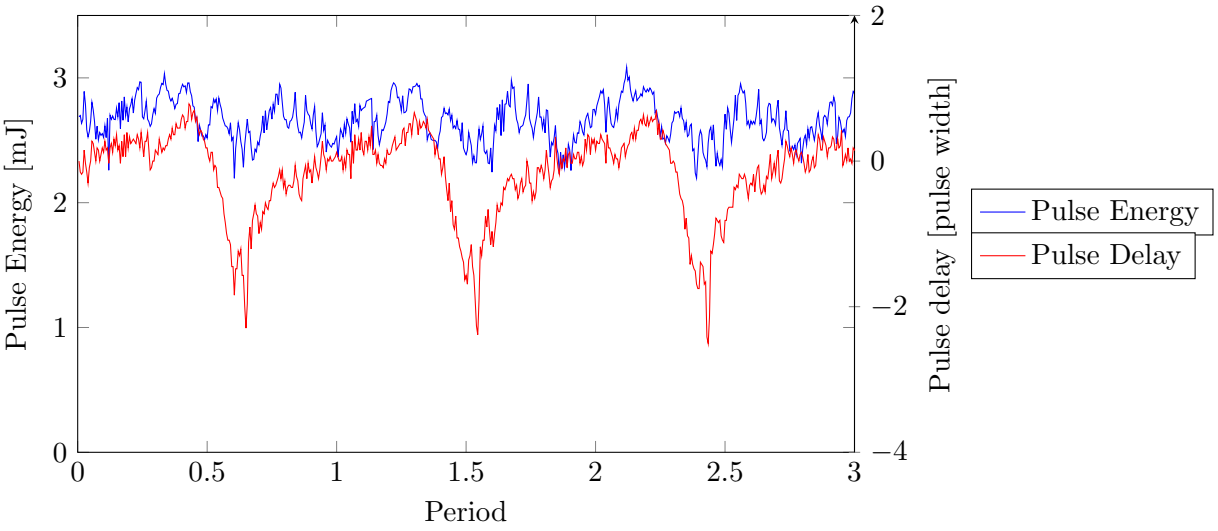

Figure 4.17: Power stability and timing jitter.

4.3.3.3 Beam Quality

The cyclic pointing instability introduced by the imperfect rotating periscope has consequences for measuring the M^2 of the RCL's output. A number of different techniques can be used to measure the M^2 of a laser as defined in [7]. All of these techniques require an accurate measurement of the beam waist through a focus. These measurements can then be fitted to Equation 2.40 where z_R is now as follows

$$z_R = \frac{\pi w_0^2}{M^2 \lambda} \tag{4.6}$$

Equation 4.6 modifies the Rayleigh range to account for none TEM_{00} laser modes. With this it is straightforward to determine the M^2 [7].

In the case of a RCL the rotating rhomboid prism, if it is imperfect, has a steering effect on the resonator mode. If the RCL also has a plane output coupler this results in a translation of the mode on the output coupler and after a full rotation of the rhomboid prism the output will have traced out a circle. As a laser mode must propagate normal to a plane end mirror this results in the output having a constant output angle but a varying output position. If the output coupler is curved this will either manifest as a change in the laser mode's angle as it leaves the resonator or make the resonator multimode.

For the case with a plane output coupler, when the moving beam is incident on a lens the focus will be the only point where the beam will appear to be stationary. Away from focus the moving beam will appear to form a cone and if a profiler with a exposure time of the same order as the rotation rate is used it will measure the cross section of this cone rather than the beam waist itself, see Figure 4.18.

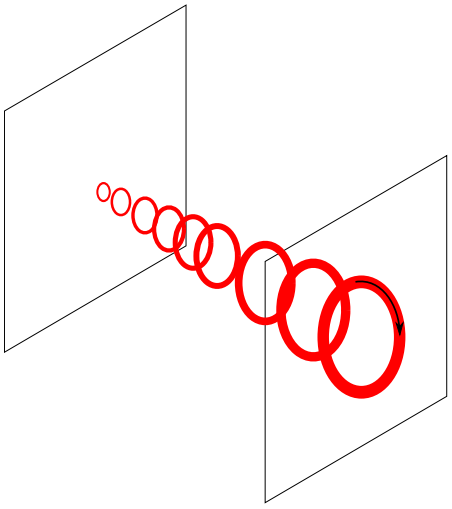

Figure 4.18: The cyclic pointing instability introduced by the rhomboid prism effectively smears the beam on a detector away from focus. In this figure the effect has been exaggerated for clarity, it is expected that the radius swept out will be less than a beam waist.

The non-zero amount of time required to take a beam waist measurement could therefore result in an artificially high M^2 measurement. It should be noted that the pointing stability is also an important consideration when determining the usefulness of a laser source, but while pointing stability can be corrected with an active steering mirror brightness is conserved. It is therefore useful to find the M^2 independently of the pointing instability.

To prevent the time the measurements take adversely effecting the M^2 the technique described in [8] was employed. Here the laser mode is simultaneously imaged in the near and far field allowing an approximate M^2 to be determined after a 'single shot', this was done with the optical arrangement shown in Figure 4.19.

The near field is relay imaged with a telescope, making it straightforward to determine the original beam waist, w_0, with the measurement of the near field beam, w_{nf}.

$$w_0 = \frac{f_1}{f_2} w_{\mathrm{nf}} \tag{4.7}$$

By considering the Fourier transforming property of a lens, Day and Stubenrauch have shown that the beam waist, w_{ff}, a focal length, f_3 away from a lens is related to the divergence angle, θ by Equation 4.8 [9]. This result does not depend on the beam being collimated on entry to the lens.

$$w_{\mathrm{ff}} = \theta f_3 \tag{4.8}$$

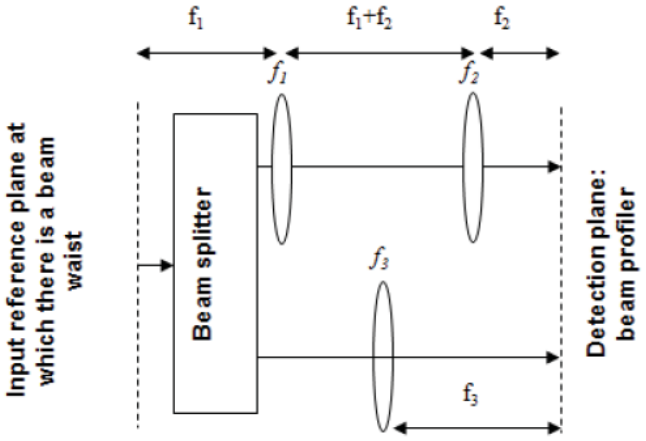

Figure 4.19: Optical arrangement to image the near and far field of a laser mode, taken from [8]

Combinging Equations 2.43, 4.7 and 4.8 gives following equation which allows the M^2 to be calculated from readily measurable variables.

$$M^2 = \frac{\pi}{\lambda}\frac{f_1}{f_2 f_3} w_{\mathrm{nf}} w_{\mathrm{ff}} \tag{4.9}$$

Figure 4.20 shows the change in M^2 as the rotation rate is changed under 51 W of pumping. This produced an average output power of 13.1 W over the range of azimuthal velocities used. The beam waists where calculated from images taken by the CCD over a 20 ms exposure time. As expected the reduction in thermal load associated with the introduction of motion causes the M^2 to drop from 2.8 at a velocity of 0.24 m s^{-1} to 1.3 when the rhomboid prism is moved at 0.71 m s^{-1}. However increasing the rotation rate further caused the measured M^2 to rise.

Figure 4.20 also contains M^2 readings taken with the CCD exposure time set to record a fixed proportion of a rotation period. With these measurements of a beam waist the behaviour of the measured M^2 as the rotation rate is varied is different. The minimum reported M^2 was higher, at 1.7, and the rise in M^2 with rotation rate was not present. This is consistent with the pointing instability artificially increasing the M^2 when 40% of a rotation period was sampled. When sampling a smaller section of a rotation period, by using a shorter exposure time, the measured M^2 was lower for moderate azimuthal velocities. Furthermore is not known if the 20 ms exposure time is influencing the M^2 measurement even at slower azimuthal velocities. An alternative approach is therefore required to accurately determine the M^2 of a RCL.

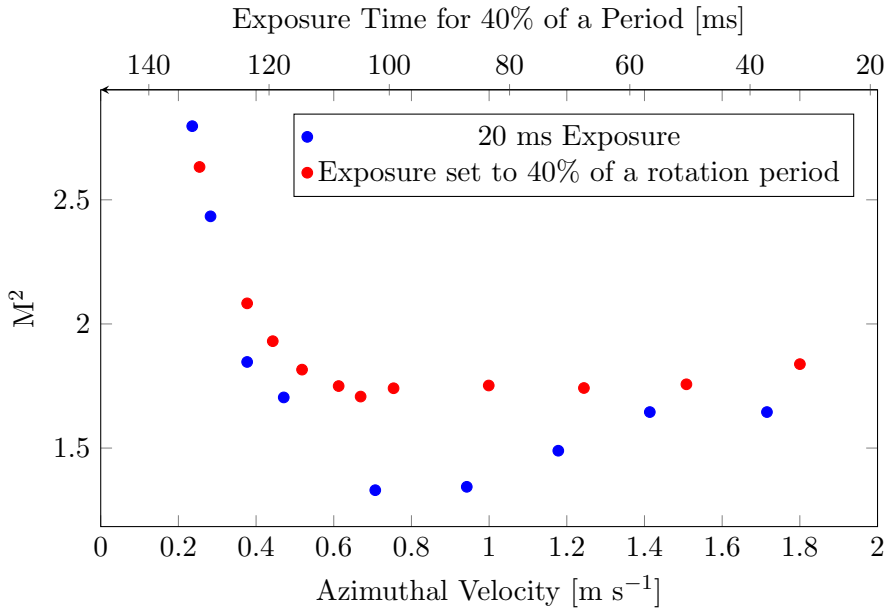

Figure 4.20: The M^2 of the RCL operating under 51 W of pump power, the exposure time of the CCD affected the result.

4.4 Measuring Beam Quality

The beam quality measurements taken in §4.3.3.3 were affected by the finite exposure time of the CCD. This effectively increased the measured beam waist further away from focus and gives the impression of a more rapidly diverging beam. Furthermore, any fluctuation in beam quality over a rotation period due to changes in alignment and any variations in the slab would be masked by the averaging effect of the detector. To determine if the M^2 varies over a period, and to solve the beam smearing problem, a system was constructed that could profile sections of a rotation period.

A number of different strategies exist for measuring a laser beam waist, ideally the second moment width is calculated to determine the width as specified in [7]. However, a common approximation makes use of a moving knife edge. This technique scans a moving hard aperture in front of a power meter which then measures the cumulative integral of the laser mode. If the beam is near Gaussian the beam waist can then be extracted by fitting the error function to these measurements [10].

Both the moving knife edge and CCD used to measure the beam waist in 4.3.3.3 sample the beam profile over an exposure time, in the case of the knife edge this time is determined by the speed the edge moves. A CCD chip requires a period of time to capture an image, typically of the order of 100ms. If this exposure time is set too short vertical blooming artefacts can occur which can then impact the accuracy of any beam waist measurement of that image [11]. Neither approach can thus resolve the motion embedded within the pointing stability of an RCL's output.

To achieve the desired temporal resolution of the waist measurement an approach that made use of the cyclic nature of the RCL output was used. This system reconstructed a beam profile from the measurement of multiple rotation periods. This arrangement consisted of a knife edge on motorised x stage placed on a motorised rail to give motion in the beam propagation axis, see Figure 4.21.

A photodiode was attached to an oscilloscope which was triggered by a reed switch and magnet connected to the rotating assembly. The magnet was attached to the rhomboid prism in such a way as to close the reed switch, and thereby trigger the oscilloscope, when the rhomboid prism was orientated at a particular angle. This ensured that each power trace generated by the photodiode was synchronised to the laser mode's position on the slab.

The knife edge was stepped through the laser mode and a trace of the transmitted power taken at each position. The recording of these traces was triggered by the reed switch, synchronising them all to the rhomboid prism's position. Each power trace could then be separated into an arbitrary number of bins, with each bin representing a segment of the rhomboid prism's rotation, see Figure 4.22.

Each bin was then averaged and combined with the corresponding bins from each knife edge position to create individual knife edge profiles for each segment of the rotation period, see Figure 4.23. The beam waist could then be determined for each slice by fitting the error function to the knife edge profiles.

By plotting the change in beam waist for each slice as the knife edge was moved through the focus and then fitting the result to Equation 2.40 the M^2 could be calculated as normal, see Figure 4.24. This procedure was repeated for each segment of a rotation period, generating individual M^2 readings for each slice.

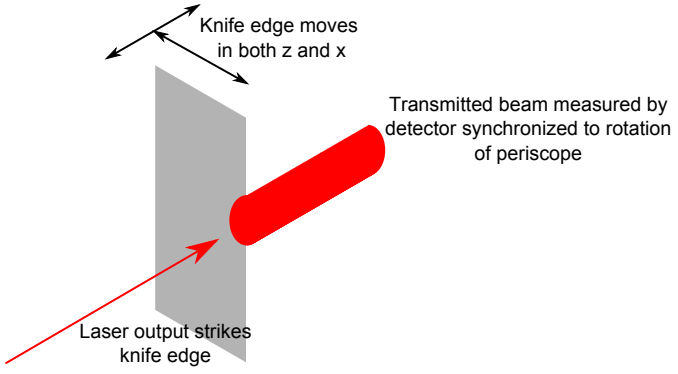

Figure 4.21: Sections of a rotation period could be profiled with a custom scanning knife edge detector.

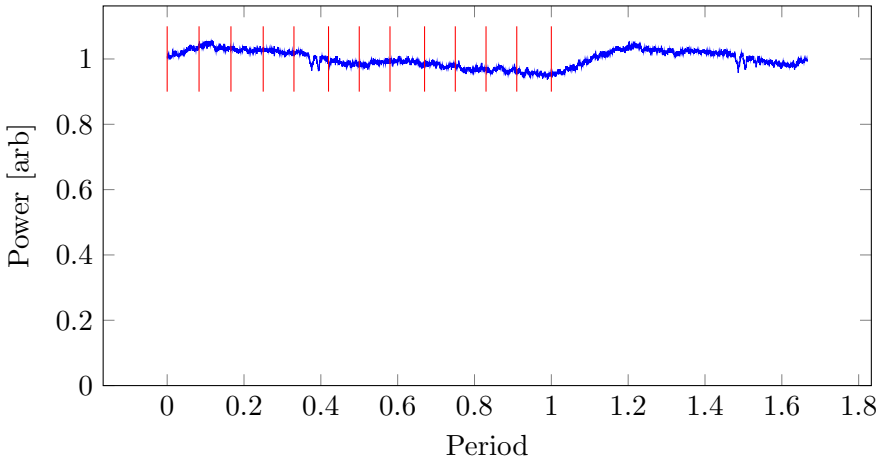

Figure 4.22: Recorded power trace when knife edge is approximately in the centre of the beam. The red lines show the segments the power trace is divided into, each one is analysed separately.

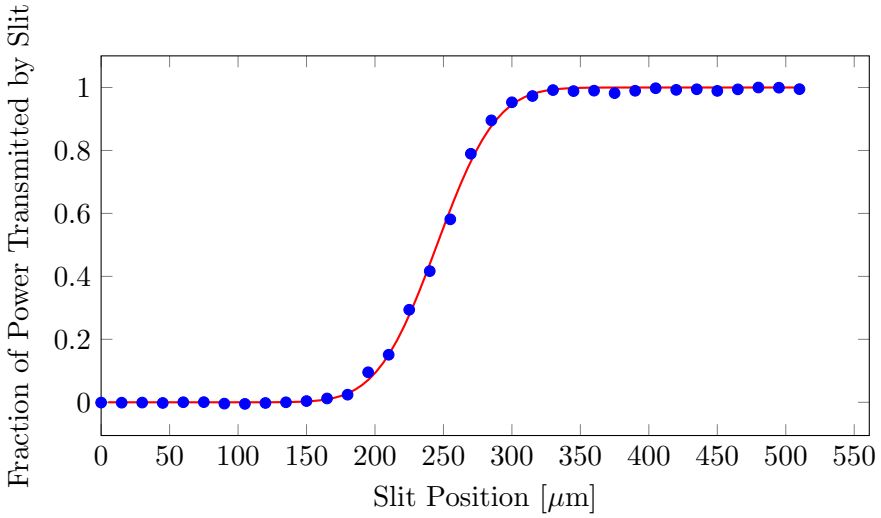

Figure 4.23: Each segment then has a knife edge plot generated for it, and is fitted to the error function, shown here in red.

Each M^2 measurement was then displayed on a polar plot where position represents the position of the start of each power segment on the slab. An example of this is shown in Figure 4.25 which also has the average M^2 displayed as a red circle.

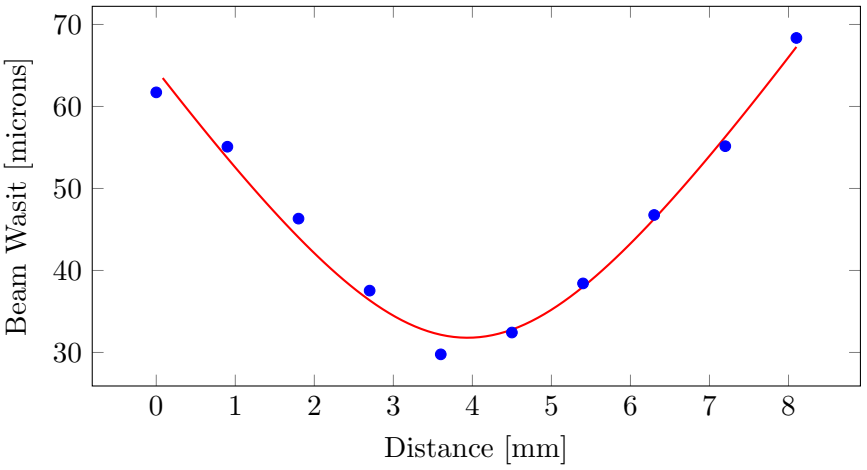

Figure 4.24: Measured beam waist through a focus with a curve fitted to find the M^2.

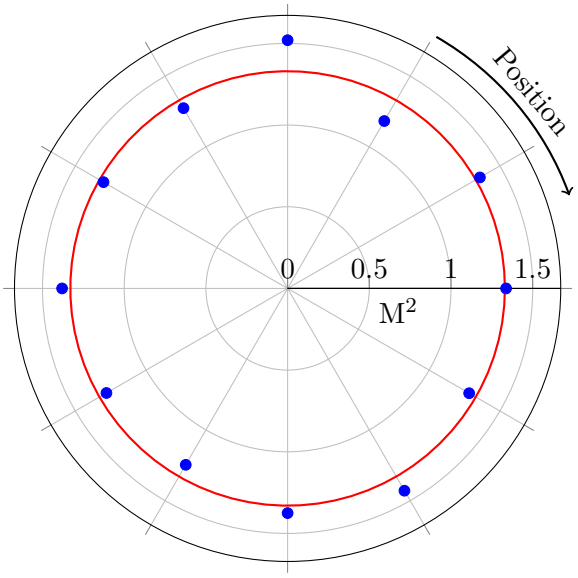

Figure 4.25: The position on the polar plot represents the segment for M^2 has been calculated for.

4.5 Conclusion

In this chapter results from both a low and high speed RCL were presented. The low speed demonstration showed that the presence of intracavity moving parts did not prevent lasing action. However, the intracavity rotating periscope was found to effect both the stability of the laser's power output and its pointing stability. Both these effects were cyclic and could be mapped to the orientation of the periscope.

The power variation over a rotation of the periscope was found to be greater when the RCL was run with the periscope paused to interrogate each position, suggesting there is some temperature dependant effect in the Nd:YAG slab that is not uniform over its

surface. When the periscope was rotating the power varied with a standard deviation of 3.1%, a factor of two improvement on the stationary case.

The pointing instability was calculated to be caused by an angular variation on the order of the tolerance on the intracavity periscope. This suggests that an improvement in the engineering of this component could reduce this. The use of a rhomboid prism as a rotating periscope was also found to have the expected consequences on the polarisation of the laser's output.

Whilst the moving parts did effect the output of the laser their effect on deleterious thermal phenomena was more marked. The introduction of an azimuthal velocity of 0.063 m s^{-1} increased the operating window of the laser from an output of 0 to 1.5 W to 0 to 7 W.

Replacing the moving parts allowed the regime were laser threshold is affected by rotation to be explored. With this new mechanical arrangement the theory presented in §3.5.2.1 was verified. Again the introduction of motion allowed an increase in output power, with 16 W generated from a pump limited end pumped Nd:YAG laser. An AOM was also inserted into the laser and motion was found not to significantly influence the build up time for lasing.

A technique for characterising the beam quality of an RCL which takes into account the pointing instability induced by the rotating periscope was then described. This was done after the exposure times of standard measurement techniques were found to be too slow to resolve any change in beam quality over a rotation cycle. This strategy made use of the periodicity of the RCL's output and reconstructed the beam profile from a number of readings synchronised to the rotation of the periscope.

References

[1] W. Koechner, *Solid State Laser Engineering*. New York: Springer, 6th ed., 2006.

[2] W. Koechner, "Thermal Lensing in a Nd:YAG Laser Rod.," *Applied optics*, vol. 9, pp. 2548–53, Nov. 1970.

[3] V. Magni, "Resonators for solid-state lasers with large-volume fundamental mode and high alignment stability.," *Applied optics*, vol. 25, p. 2039, July 1986.

[4] Y. Sato and T. Taira, "Temperature dependencies of stimulated emission cross section for Nd-doped solid-state laser materials," *Optical Materials Express*, vol. 2, no. 8, pp. 514–522, 2012.

[5] W. Xie, W. Hu, J. Xu, and F. Zhou, "Dynamical thermal lensing of high-power solid-state lasers," *Optical Engineering*, vol. 42, p. 1439, May 2003.

[6] D. Devor and L. DeShazer, "Evidence of Nd: YAG quantum efficiency dependence on nonequivalent crystal field effects," *Optics Communications*, vol. 46, no. 2, pp. 97–102, 1983.

[7] ISO, "Lasers and laser-related equipment. Test methods for laser beam widths, divergence angles and beam propagation ratios. Stigmatic and simple astigmatic beams," BS EN ISO 11146-1:2005, International Organization for Standardization, 2005.

[8] S. P. Ng and J. I. Mackenzie, "Planar waveguide laser optimization and characterization employing real-time beam quality measurement," *IEEE JOURNAL OF QUANTUM ELECTRONICS*, vol. 49, no. 2, pp. 146–153, 2013.

[9] G. W. Day and C. F. Stubenrauch, "Laser far-field beam-profile measurements by the focal plane technique," in *NBS Technical Note 1001*, National Bureau of Standards (U.S.), 1978.

[10] G. Veshapidze, M. L. Trachy, M. H. Shah, and B. D. DePaola, "Reducing the uncertainty in laser beam size measurement with a scanning edge method.," *Applied optics*, vol. 45, pp. 8197–9, Nov. 2006.

[11] Spiricon, "BeamGage User Guide," 2011.

Chapter 5

High Power Developments of the Rotating Cavity Laser

5.1 Introduction

In this chapter the capabilities of the RCL are further explored. The resonator described in §4.3 was pump limited, here results produced with a more powerful pump source are presented. The rhomboid prisms used previously were also replaced with larger versions to compensate for the more rapidly divergent pump light.

Findings from when the system was configured as an amplifier are then discussed. They revealed the gain medium mounting procedure had adversely affected the the stability of the RCLs performance over a rotation cycle. A description of a new crystal mounting procedure that made use of an ultrasonic soldering iron and an oxygen free environment to enhance the uniformity of the thermal interface then follows. This includes a brief introduction to the soldering process to justify the approach taken. Evidence that protective metallic layers are needed to protect the dielectric reflective layers from the indium solder used to form the bond is also included.

Experimental data suggesting the thermal wedge proposed in §3.5.1.3 is more significant than predicted follows. FEA analysis of the temperature profile of the RCL was then conducted to try and determine the source of this larger wedge.

5.2 High Power Results

To further explore the capabilities of the RCl the 60 W pump diode used previously was replaced by a 400 W, 808 nm diode. The diode was fibre coupled into a 0.22 NA, 600 μm diameter delivery fibre. This was then used to drive the telescopic resonator

shown in Figure 5.1 after being passed through a fused silica rhomboid prism. This prism introduced a beam displacement of 20 mm and had a clear aperture of 19 mm. The Nd:YAG ceramic was also replaced with a larger sample, in this case the ceramic was 6 mm thick with a diameter of 50 mm.

Telescopic resonators were developed by Sarkies and allow stable operation of large TEM_{00} modes [1]. The large TEM_{00} mode was required to match the pump spot in the ceramic. The pump beam from this diode was more rapidly divergent than the source used previously, the M^2 was approximately 260 as opposed to 75. The apertures imposed by the periscope thus limited the minimum achievable pump spot radius to 500 μm.

The behaviour of the TEM_{00} mode under a laser rod like thermal lens is shown in Figure 5.2. The pump delivery fibre was reimaged onto the slab to produce a 700 μm waist to match this mode. The predicted stability window is similar to that predicted for the resonator shown in Figure 4.12 which was pump limited under 60 W of available pump power.

5.2.1 Performance

Again the point of thermal rollover could be influenced by the rotation rate of the rhomboid prism. Under an azimuthal velocity of 1.51 m s^{-1}, equivalent to a rotation of 12 Hz, the output power started to roll over under a pump power of approximately 260 W, here an output of 92 W was produced, see Figure 5.3. By increasing the azimuthal velocity to 2.64 m s^{-1}, 21 Hz, this rollover was removed. The output power was then increased to 121 W under 352 W of pump power.

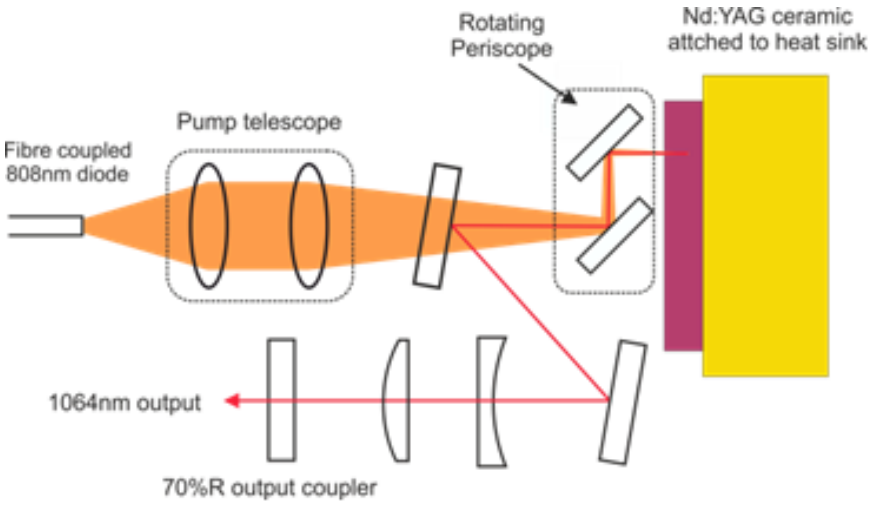

Figure 5.1: Telescopic resonator driven by the 400 W diode, the positive lens was 300 mm from the Nd:YAG slab.

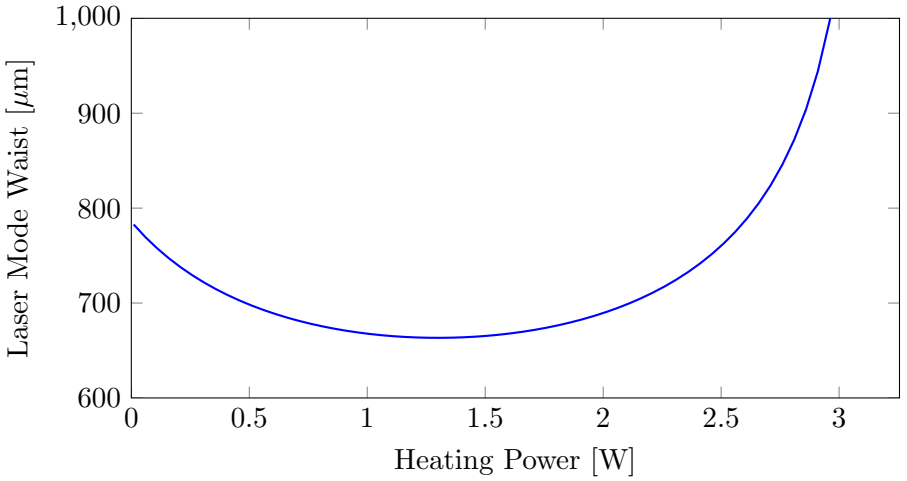

Figure 5.2: Resonator mode waist in the slab as a function of heating power

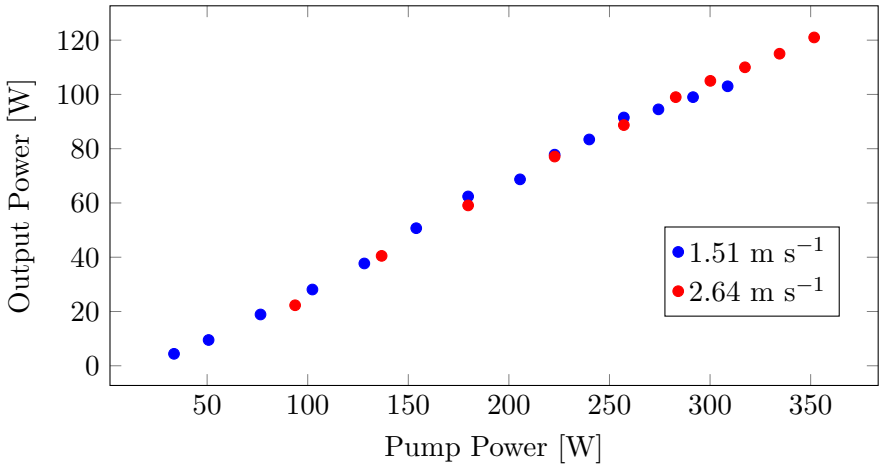

Figure 5.3: Output power from the resonator

Ignoring the points after thermal rollover the 1.51 m s^{-1} output had a slope efficiency of 39% and the output when the rhomboid prism was introducing a azimuthal velocity of 2.64 m s^{-1} had a slope of 38%. These values are consistent with the slope efficiencies produced by the resonator described in §4.3, however they are less than the values predicted by the equation derived in §2.3.2 which are of the order of 60% (the exact value is dependant on the assumed intracavity losses).

These slope efficiencies are comparable with other Nd:YAG systems working in the 100 W regime. Frede et al report 114 W of output for 400 W of pump power from a resonator which includes two composite Nd:YAG rods designed to spread the pump absorption over the length of each rod [2]. This compares favourably with the 121 W for 352 W achieved out of a single gain medium in an RCL.

100 W power levels have also been achieved previously with ceramic Nd:YAG. 110 W have been reported by Lu et al from a 105 mm long ceramic which mode use of a 'virtual pump source' scheme [3]. This resonator had a slope efficiency of 41% which is again

comparable with the RCL. The authors also achieved similar results with a single crystal Nd:YAG.

High power Nd:YAG lasers often do not reach their theoretical efficiency limits. This is due to a combination of factors including the brightness mismatch between the pump and laser mode and thermal effects reducing performance at these high power levels.

The power output was again cyclic, Figure 5.4 shows the variation in output power over two and a half periods whilst 72 W was being produced. The data was taken at this power level to avoid risking damage to diagnostic components. The output power varied with a standard deviation of 2.8% over a rotation period. This is consistent with the result from the initial RCL prototype, see §4.2.3.2, indicating that the instability in the power output is independent of the power level the RCL is operated at.

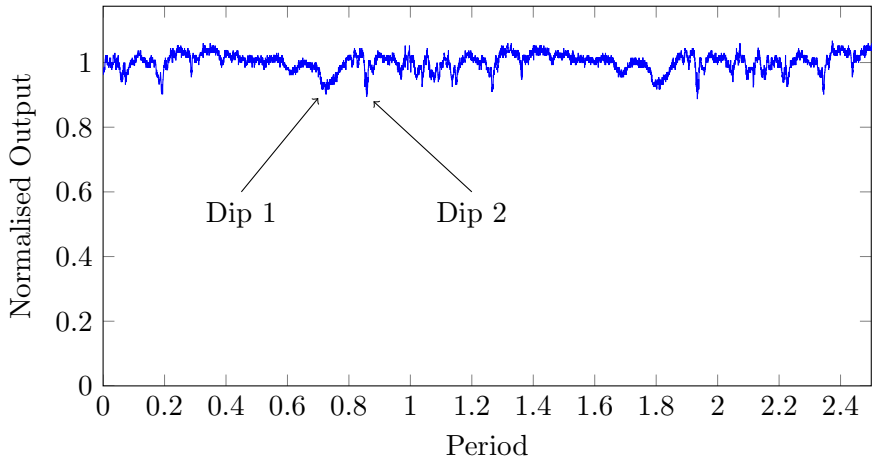

Figure 5.4: The output power of the RCL producing 72 W over a number of rotation periods.

Figure 5.4 shows there is structure in the variation in power output which repeats every rotation. Some features exist over a longer proportion of a period than others. For example, the feature labelled 'Dip 1' exists over 12% of a period whereas 'Dip 2' exists for 1.5%. As the periscope sweeps out a radius of 20 mm these features correspond to 15 mm and 2 mm across the surface of the slab respectively.

The finer structure is thus of the order of a beam diameter indicating that it is being caused by a feature on the slab. This could be dust contamination or an area where the Nd:YAG does not perform as well due to damage to its surface or variations in the optical coatings.

The 15 mm long path the larger feature occurs over makes it unlikely to be a property of the slab. Instead these artefacts could be being caused by the imperfect periscope misaligning the resonator enough at this point in a rotation cycle to impede lasing performance.

5.2.2 Beam Quality

At low power, 6.3 W of output, the average M^2 of the resonator was 1.1. As the pump power was increased the M^2 also increased, see Figure 5.5. Under 94 W of pump power the resonator produced 23 W of output with an average M^2 of 1.71. Here there was 22.6 W of heating due to the quantum defect between pump and laser photons. Figure 4.13 shows that this resonator with a laser rod would be expected to go unstable under 3 W of heating power. The RCL offers a marked improvement in performance over this case.

With rotation the pumped spot is nominally operating within the adiabatic limit with regard to heat flow, see §3.5.1.2. The adiabatic temperature profile seen by the laser mode is determined by the pump profile. Under high pump powers there can still therefore be a significant thermal lens present. The increase in M^2 with pump power could therefore be due to the variation in strength of the thermal lens changing the overlap between the pump and laser mode allowing higher order resonator modes to exist rather than due to thermal aberrations. The sensitivity of the beam quality to the ratio of the pump and laser mode waist in end pumped systems is well known and for cases when the laser mode is larger than the pump is partly the result of greater spherical aberrations generated by the thermal lens away from its centre [4].

It should also be noted that as the pump power was increased the resonator required realignment to maintain the stability of the output power. The misalignment associated with an increase in pump power evolved over a number of seconds after the pump was increased. This is strongly suggestive of a thermal wedge like artefact changing the alignment properties of the resonator. This may also be acting to degrade the beam quality at higher powers.

Figure 5.6 shows the behaviour of the M^2 over a rotation of the periscope. At output powers of less than 51 W the beam quality showed very little variation over a rotation

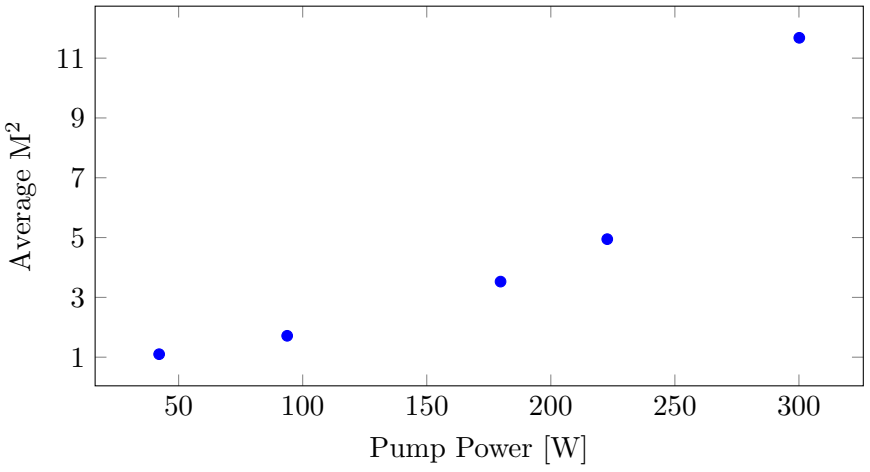

Figure 5.5: The M^2 of the output increased with the applied pump power.

cycle. Above this the beam quality varied after a rotation period and with an output power of 100 W the beam quality not only became very poor but fluctuated heavily, this has been plotted separately in Figure 5.7 for clarity.

The beam profiler measures the beam quality in the plane of the optical bench. The thermal profile present in the RCL will contain an azimuthal and radial component with respect to the motion of the periscope. The M^2 measurement will therefore sample values made up of different contributions of these components over a rotation period. When generating less than 51 W the uniformity of the M^2 see Figure 5.6, indicates any difference in magnitude of the aberrating effect of the azimuthal and radial component of the thermal profile is negligible. However, at high power the beam quality traces an ellipse on Figure 5.6 and 5.7.

The orientation of the ellipses in Figures 5.6 and 5.7 show that the highest M^2 occurred where the beam profiler's axis aligned with the azimuthal axis of the periscope. This is consistent with the unusual azimuthal thermal profile acting to decrease the beam quality at high power but the M^2 had increased to 3.5 before the ellipses manifested. It is therefore likely there other factors causing the M^2 to rise. These could be related to resonator stability or another resonator component could be being heated by either the laser mode or pump light creating a further misalignment. §4.2.3.2 also indicated that there is a variation in the thermal handling properties of the slab that could manifest at higher pump powers and act to add to the variation observed in beam quality.

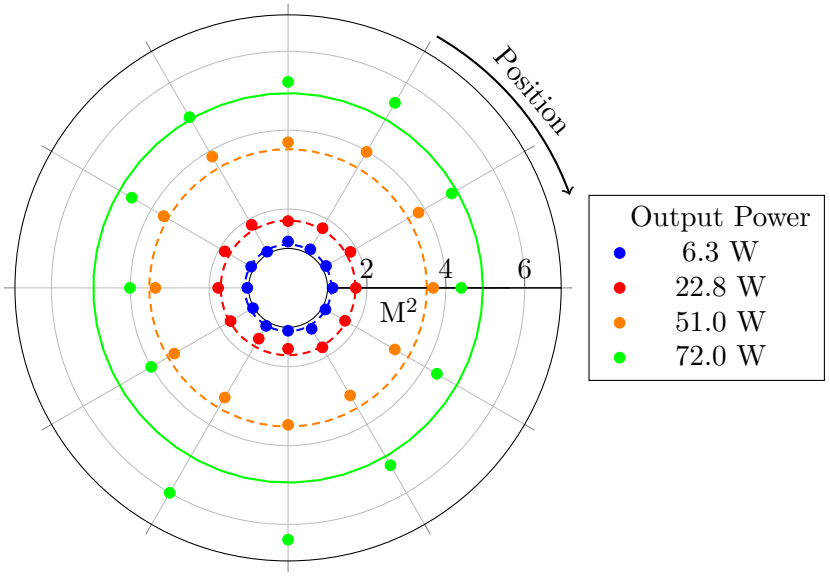

Figure 5.6: The M^2 of the output remained stable at lower powers, the solid lines represent the average M^2.

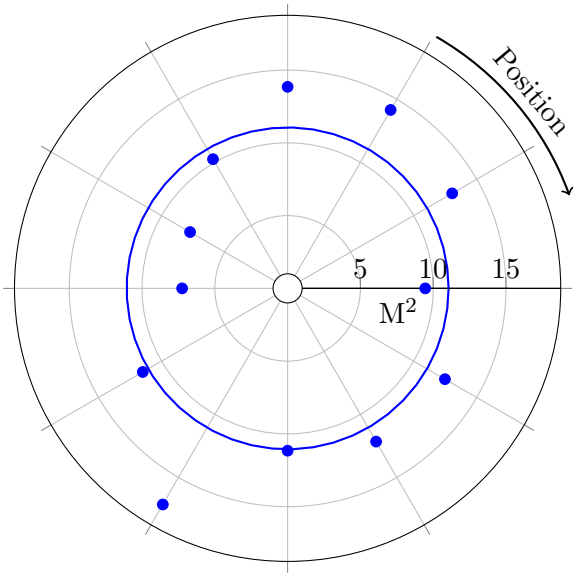

Figure 5.7: At higher power levels the M^2 become unstable around a cycle, here data is shown for a 99.8 W output.

5.3 Preliminary Amplifier Findings

The RCL gain medium and rotating periscope were reconfigured into an amplifier by removing the output coupler. A seed 0.5 W 1064 nm beam that was matched to the pump spot size of 750 μm was then passed through the periscope. This seed beam was aligned so it passed through the pump beam, but was incident on the HR surface at the back of the Nd:YAG slab at small angle away from normal. The reflected beam could then be separated with a knife edge mirror post amplification.

It was expected that the power of the returned beam would be insensitive to the rotating rhomboid prism angle if the seed was aligned such that its overlap with the pumped region was unchanged over a rotation cycle. Initially after the amplifier pump was turned on this was the case, however the power of the amplified beam dropped and became more unstable over time, see Figure 5.8.

Furthermore, it was found that by rotating the Nd:YAG slab 90° relative to the optical bench, whilst leaving the rest of the resonator unchanged, it was possible to move the position of the point of the large power decrease, as illustrated by Figure 5.9. The magnitude of the reduction in amplification is thus a property of the mounted slab. Unlike a traditional solid state laser, the RCL samples many points of the gain medium, making uniformity key. In other architectures the gain medium, or laser mode, is often moved until the path that gives optimal performance is found. These results suggest there is a non-uniformity present in the gain medium which is leading to a reduction in the systems performance. To help determine the nature of this non-uniformity the time scale of the power drop was considered.

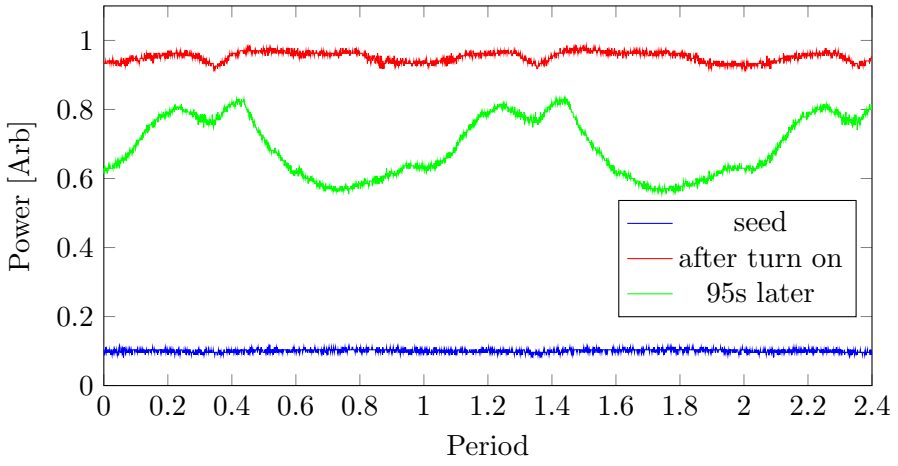

Figure 5.8: The output power from the amplifier under 115 W of pump. The output power reduced and the modulation depth increased after the system was switched on.

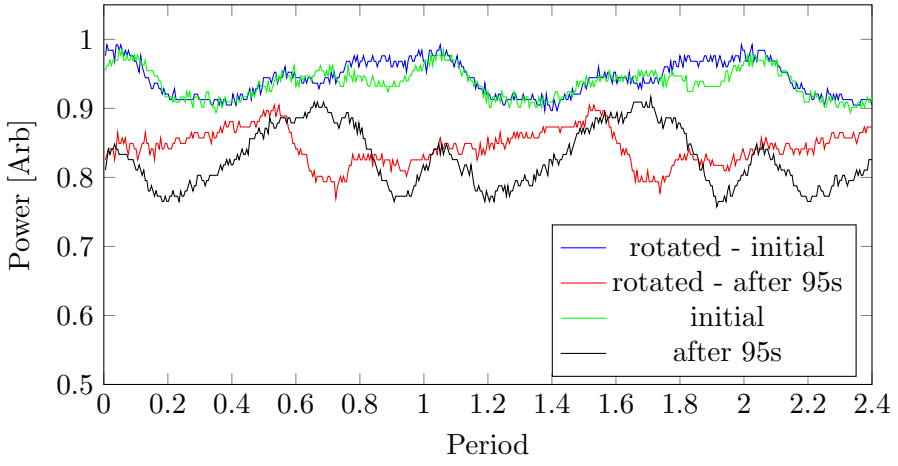

Figure 5.9: Rotating the Nd:YAG slab 90° relative to the optical bench indicated the artefact creating the power drop was a feature of the Nd:YAG.

The temporal aspect of the drop in amplification is shown in Figure 5.10. The power drop occurs over 10s of seconds. This time scale is strongly indicative that the mechanism causing it is related to the thermal properties of the system as it is similar to that required for the moving pump spot to reach a steady temperature. Furthermore, Figure 5.11 shows that proportion the gain drops is directly proportional to the pump power and thus the temperature rise.

The small signal gain coefficient is given by Equation 2.23 which includes the emission cross-section σ. Sato and Taura show that this cross section has a temperature dependence and between 15 °C and 250 °C varies with the following relation where T is the temperature in °C and $T_0 = 20$ °C [5].

$$\sigma(T) = \sigma(T_0)(1.042 - (2.1 \times 10^{-3})T) \tag{5.1}$$

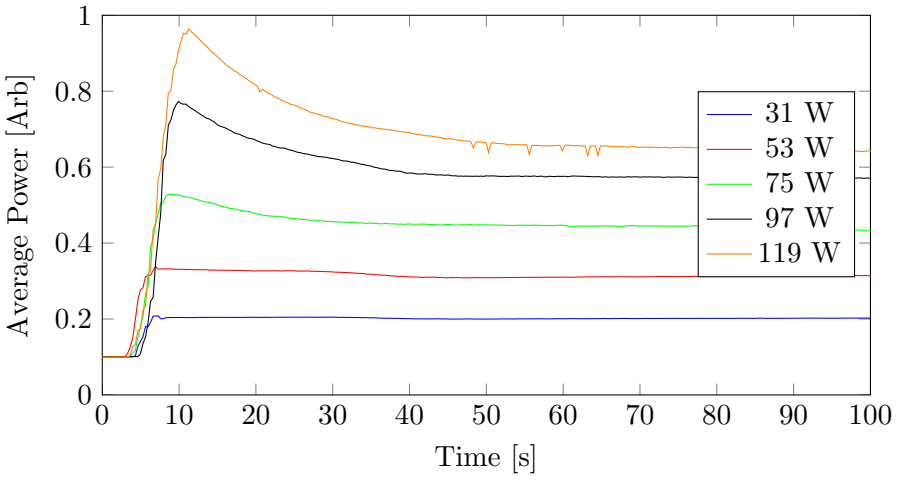

Figure 5.10: The drop in amplification occurs over 10s of seconds and is related to the incident pump power. The spikes seen on the 119 W trace are due to the oscilloscope recording the data miss triggering.

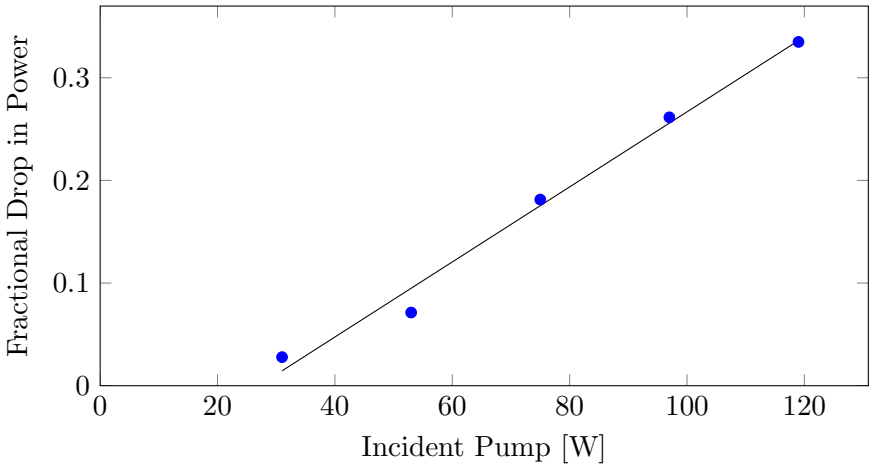

Figure 5.11: The proportion the amplification drops is directly proportional to the pump power

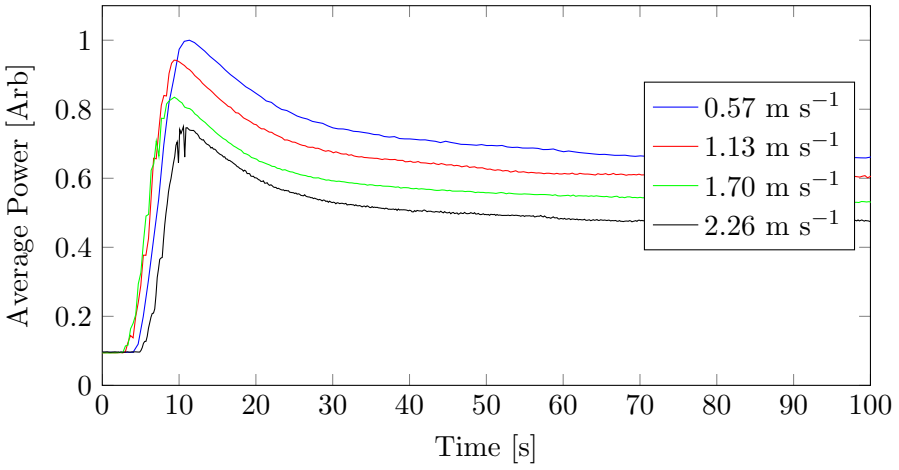

Figure 5.12: The size of the power drop and the maximum amplification is a function of the rotational velocity

Furthermore Fan in [6] shows that the thermal load in Nd:YAG without laser action is higher than that due to the quantum defect alone. He found a heating effect of 40% of the pump power due to non-radiative decay paths from dead sites within the gain medium. The expected drop in gain from the temperature rise after a pass of the pump can be calculated for Nd:YAG using Equation 5.1 to modify Equation 2.23 and thus Equation 2.22. This has been plotted in Figure 5.13.

Gain drops of the order seen above would require a temperature increase in the region of 80 K. If the first 1 mm of the Nd:YAG is considered, which is where 65% of the pump light is absorbed, Equation 3.5 predicts a temperature rise of 15 K after one pump pass if an azimuthal velocity of 1 m s^{-1} is assumed. The reduction in emission cross-section at 1064 nm due to the increase in temperature will therefore be contributing to the observed reduction in gain as the Nd:YAG heats up, however the large increase in temperature needed to explain the total reduction suggest there is another, currently unknown, mechanism. This mechanism could be an increase in thermal load beyond that predicted by Fan and could be linked to the use of a ceramic gain medium.

There was a strong dependence on the azimuthal velocity for the magnitude of the drop in amplification as well as the maximum returned power. Figure 5.12 gives the temporal behaviour of the returned beam under 119 W of pumping at different rotational rates. The amplification drop is most significant at slower speeds, where the temperature increase would be expected to be highest, this is consistent with the results shown above. At lower speeds the the signal beam still experiences more amplification than at higher speeds. In this regime energy extraction is low as the signal beam is of low power compared to the pump and the system is thus operating in the small signal gain regime. Stimulated emission is therefore not dominating the energy extraction process, allowing the rotation rate to have an impact on the amount of available gain as the signal beam is swept away from the stored energy, see §3.5.2.1.

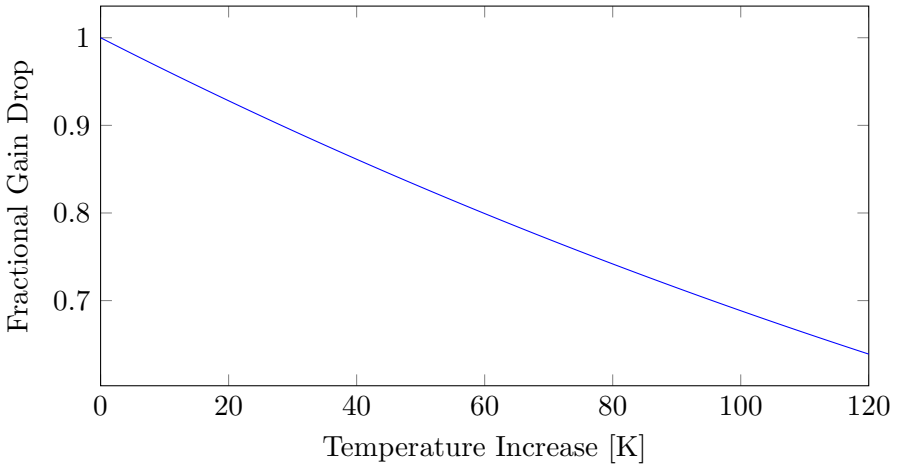

Figure 5.13: Predicted small signal gain drop as the Nd:YAG heats up.

The amount the power drops is not uniform over the periscope rotation cycle. This suggests the temperature of the slab under pumping is also not constant over a rotation period and instead is also a function of position on the slab; Figure 5.9 supports this. It was therefore postulated that these effects could be consequences of a poor, non-uniform thermal interface between the slab and the heat sink. The method of creating this bond, and any consequences it would have for the dielectric mirror, was therefore reconsidered. A discussion of the current thermal interface and an alternative follows.

5.4 Gain Medium Coatings

The gain's dependence on the thermal properties of the gain medium found in the amplifier suggested there could be a problem with the metal dielectric interface on the back surface of the slab. It has been reported that particular care has to be taken when interfacing thin disks with indium due to its tendency to migrate when exposed to a thermal gradient [7, 8].

5.4.1 Current Coatings

The ceramics used in the experiments detailed in §4 had a metallic silver layer deposited directly onto the HR dielectric structure. This layer was designed to act as a broadband reflector to reflect any non-normal incident fluorescence away from the interface and as a surface to solder onto when mounting onto a heat sink. It was decided to inspect this silver coating to see if there were any visible defects due to the indium. Figure 5.14 shows this surface after it was removed from the indium.

Previously a thermocouple had been applied to the side of the slab with thermally conducting paste to monitor the temperature of the slab. The dark discolouration visible in Figure 5.14, as well as some liquid residue, is thought to be the result of this paste seeping into gaps between the indium and the slab. The silver has also visibly tarnished indicating it has been exposed to air. This suggests there were voids between the indium and the slab and thus the effectiveness of the heat sinking was not uniform over the entire slab. These air pockets will have created zones within the heat sink where heat flow is impeded, producing nonuniformites in the thermal properties of the interface between the gain medium and its heat sink.

A varying thermal contact between the slab and heat sink means the temperature reached by different regions of the slab also varied. Figure 5.8 shows that the reduction in gain once the slab has warmed up is not uniform over a rotation period, the poor quality of the heat sinking may therefore be responsible for some of the gain variation seen as the rhomboid prism rotates.

Figure 5.14: Slab removed from heatsink showing evidence of tarnishing, in the act of removing the slab from the heat sink the right hand side of the metallic coating was damaged

As the process of removing the slab from the heat sink could have damaged the silver layer the coating on an unused ceramic was also inspected. Figure 5.15 shows a microscope image taken of the unused slab. Small holes are clearly visible over the entirety of this layer, there were also two larger defects on the slab's silver layer one of which is near the centre of this image.

The smaller holes are characteristic of a thin film and are the result of oxidation during and after the deposition process. These holes allow the indium to come into direct contact with the dielectric potentially damaging them.

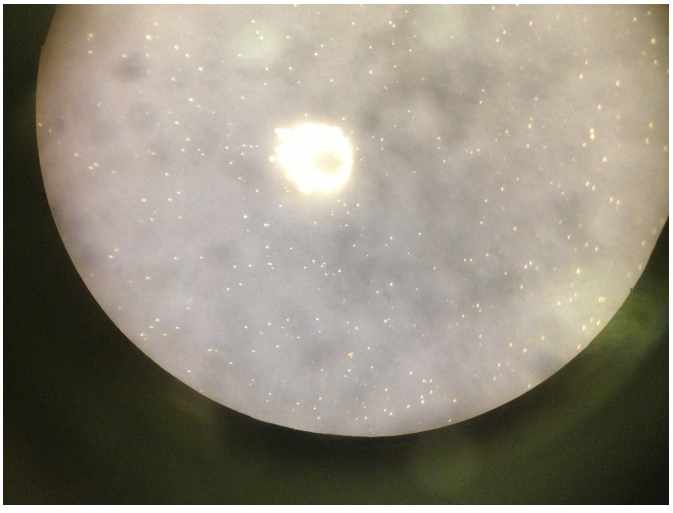

Figure 5.15: Microscope image of the silver coating of an unused ceramic

5.4.2 Reflectivity

The visible defects in the slabs metallic coating created concerns for the integrity of the dielectric layer. It was therefore decided to map the reflectivity of the ceramic at 1064 nm. Any variation in its optical properties could explain the high frequency structure seen in the RCL's output in the experiments described in §4.

The reflectivity was mapped with the experiment shown in Figure 5.16. Here a 1064 nm probe beam, with a beam radius of 600 μm at the ceramic's back face, was incident on the slab at a shallow angle. The reflected power was then measured with a photodiode and compared with the incident power. The incident power was determined by a second photodiode reading a pick off beam. The slab was mounted on a x-y translation stage allowing it to be moved relative to the probe beam. A raster scan of a section of the slab could then be produced.

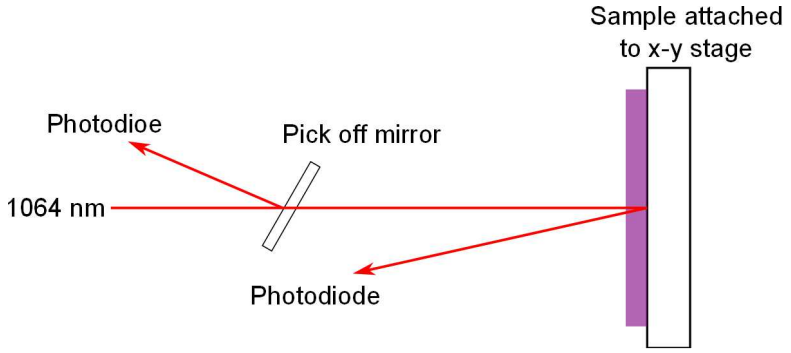

Figure 5.16: Optical setup to determine slab uniformity

Figures 5.17 and 5.18 show a map of the variation in reflectivity across a ceramic that had been bonded to a heat sink with indium foil and one that had not been mounted. A 20 mm by 20 mm area was mapped with a pitch of 1 mm. The map of the unmounted slab, Figure 5.17, shows a map varying within the uncertainty of the measurement. Figure 5.18 on the other hand shows sharp features in the reflectivity of the mounted slab. The optical coatings have thus either been disturbed by the act of bonding the ceramic to the heat sink or by localised heating during operation showing the current bonding procedure was inadequate.

The global slopes seen in the reflectivity maps are due to nearing the edge of the ceramic. If the laser mode is passed over the large dips in reflectivity seen in Figure 5.18 a corresponding drop in output power would be expected. The power output of the RCL includes fine structure that repeats itself over a cycle, see Figure 5.4, the size of these structures in the reflectivity map is of the same order as the fine structure and could therefore be responsible for them.

An alternative to compressing the silver coated Nd:YAG slab onto an indium sheet is therefore required to mount the ceramic. The current procedure has resulted in a

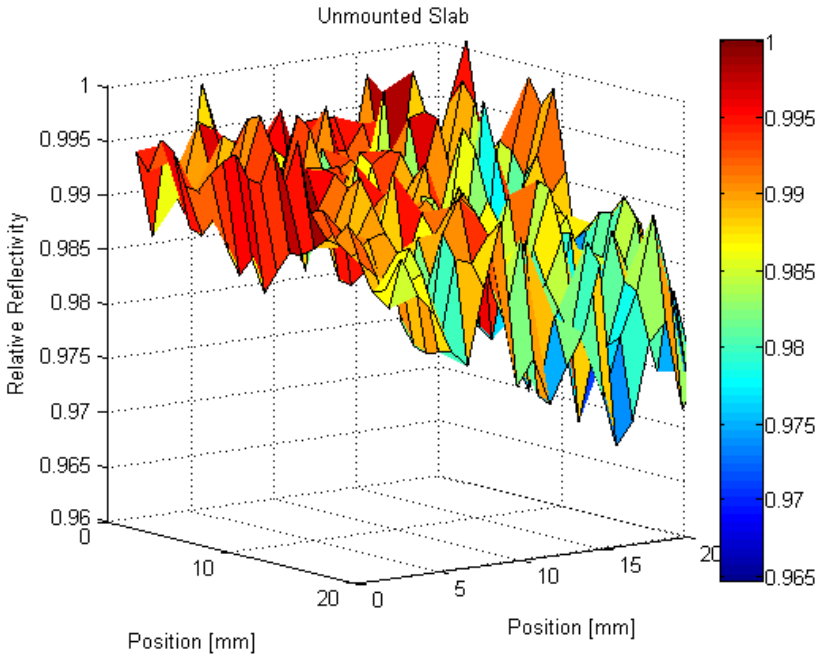

Figure 5.17: Reflectivity map of the Nd:YAG ceramic before it had been bonded to a heat sink with indium

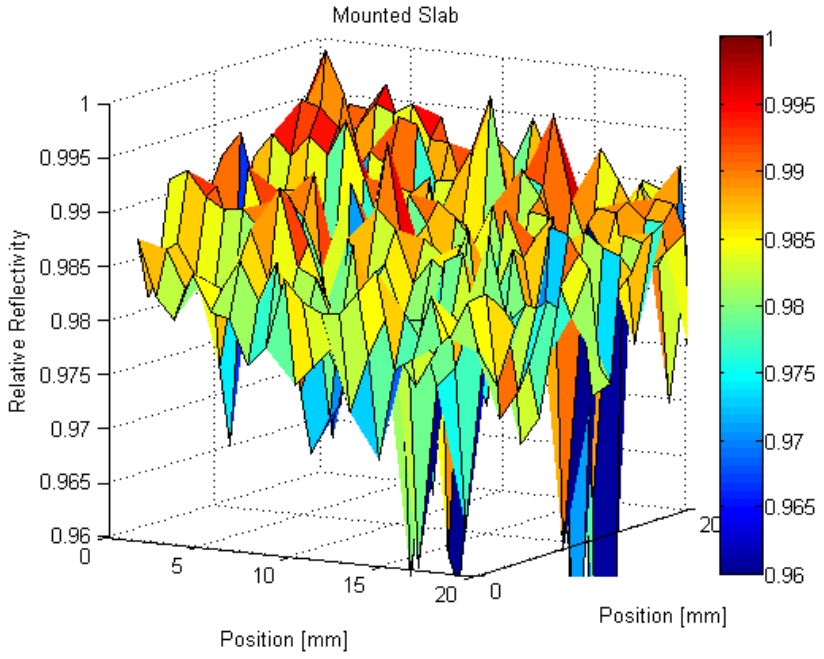

Figure 5.18: Reflectivity map of the Nd:YAG ceramic after it had been bonded to a heat sink with indium

questionable thermal interface and could have damaged the dielectric coating. The development of this new method is described below.

5.5 Investigating alternative coating structures

If a laser crystal is to be actively cooled it needs to be interfaced with a cooling mechanism. This could be in the form of a water jacket which allows coolant to pass directly over the surface of the gain medium, or it can be bonded to a heat sink. Heat sinks are typically made of high conductivity materials such as aluminium or copper. Diamond with its extremely high thermal conductivity is also sometimes used and has the further advantage of a wide transparency window.

In rod and slab type geometries the heat is typically extracted through surfaces that do not interact with either the pump beam or the laser mode, see §2.6.4. In these cases the bonding of the gain medium to the heat sink is straightforward and can be achieved with a thin layer of wax or a malleable metal such as indium or one of its alloys. These act to fill in any gaps between the heat sink and gain medium improving the thermal contact. They also provide strain relief for any stresses created by the thermal expansion mismatch between the gain medium and the heat sink material.

When the heat flux is removed through an optically active surface, such as in a thin disk or the RCL, more constraints are placed on the bond. Not only does the joining method now need to provide adhesion, transfer a large heat flux, and provide strain relief, it must also not interact with the dielectric layers either during the joining process or after. A popular method of producing the mechanical join between the gain medium and the heat sink is to solder them together.

5.5.1 Soldering

Traditional soldering makes use of a solder agent to join two surfaces together and is common technique for bonding surfaces. The mechanisms behind the formation of a successful join are described in [9] and the key points when considering the soldering of optical components are summarized here.

For the join to be successful the solder must be able to 'wet' on both the materials being joined. Wetting describes how a liquid behaves when introduced to a dry surface, if it demonstrates a high degree of wetting the liquid will flow over the surface and produce a thin film. If it does not wet the liquid will ball up to avoid contact with the surface. In the case of soldering if the solder does not wet to the substrate it will not be possible to produce a thin, uniform layer of solder over the substrates. This limits the formation

of solder-substrate bonds and prevents the formation of a high quality bond, if a bond forms at all.

This wetting behaviour can be explained by considering the surface tension forces on the liquid drop, see Figure 5.19. This can be described by Young's equation:

$$\gamma_{SL} + \gamma_{LV} \cos\theta_c = \gamma_{SV} \tag{5.2}$$

Where γ_{SL}, γ_{LV} and γ_{SV} are the tensional forces between the solid and the liquid, liquid and the surrounding vapour, and the solid and the vapour respectively; $\cos\theta_c$ is the contact angle formed when the forces are in equilibrium. The lower θ_c the more the liquid drop spreads and the greater the 'wetting' performance of the liquid solid pair.

By considering Equation 5.2 it is clear the wetting performance of a liquid can be improved by either increasing γ_{SV} or by decreasing γ_{LV} and γ_{SL}. γ_{LV} and γ_{SL} are both fixed for a given liquid substrate combination and temperature (γ_{LV} can also be affected by pressure) and are most easily manipulated by controlling the solder composition. These tensional forces arise from a systems predisposition to exist in the lowest energetic state possible. Atoms at the surface of a material can have unsaturated bonds, giving them a higher potential energy then those inside the material. A fluid will therefore arrange itself into a sphere to minimise its surface area if no other forces are acting on it.

Whilst a solid does not have a surface tension as such, it does have a surface energy. The surface energy of a solid, and thus γ_{SV}, can be changed by introducing particles to the surface to partially saturate any available bonds. The degree of saturation that occurs depends on the properties of the two materials. For example, if an oxide layer is present on the surface of the solid the surface energy will be low. This makes γ_{SV} low and it is therefore unlikely that a liquid will wet to the surface. The presence of other containments such as dust or an oil film will also reduce the surface energy and impair the wetting performance.

The need for a surface to have a high surface energy for soldering to be successful limits the materials that can be soldered. For example, glasses and plastics typically have very

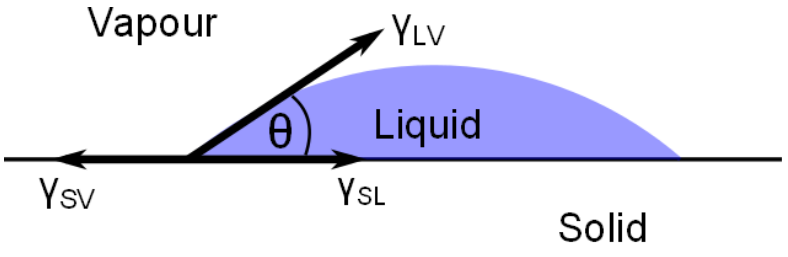

Figure 5.19: Surface tension forces experienced by a liquid on a solid surface.

stable surfaces so have low surface energy. Metals such as aluminium have a oxide layer that make traditional soldering impractical. To improve wetting performance a flux is often used. A flux acts to clean the solid surface, remove any oxide present, and prevent it reforming during the soldering process.

Care must be taken to choose an appropriate flux, it must be chemically active enough to remove any oxides present on the substrate, or in the solder, but once soldering is complete any residual flux needs to be easy to remove or inert within the join. When soldering relatively large optical components cleaning of the join after soldering is not practical as the majority of the soldered area is not accessible. When using an indium based solder this can lead to a problem when bonding an optical component with a dielectric coating. To work the flux must be capable of removing indium oxide from the solder, but as the dielectric stack is formed out of layers of oxides, any residual flux has the potential to reduce the performance and uniformity of the dielectric. A fluxless approach is therefore preferable.

5.5.1.1 Soldering to Non-Metals

Indium The low surface energy of most non-metals makes them challenging to solder to. Indium has the unusual property that it can adhere, and wet, to glass and other non-metals. However, for this to happen the indium needs to be 99.99995% pure [10]. Indium of this purity can be used without flux for both non-metals and metals. When soldering a substrate with a thin film the indium will penetrate the film and bond directly with the glass [11]. Whilst this leads to a mechanically very strong bond, clearly if the thin films form a dielectric stack this indium ingress will have consequences for its optical qualities.

Importantly, pure indium cannot be used to solder to a thin film of silver as it will be absorbed by the indium. This can be prevented by using a In95Ag5 alloy at the expense of fluxless wetting performance [11]. Gold on the other hand provides an ideal surface for indium soldering. On contact with indium, the two materials undergo an oxidation reaction to form $AuIn_2$ which is extremely stable and prevents further oxidation within the indium [12].

Ultrasonic Soldering Instead of chemically removing oxides it is possible to clean a surface mechanically. This can be done by applying an abrasive to the surface and polishing the oxide surface off. A more controlled method makes use of a soldering iron with a tip driven by an ultrasonic transducer. Cavitation created by this transducer acts to break down the surface removing any oxide present. This can be so effective it is possible to use an ultrasonic soldering iron to tin aluminium in air [13].

As well as allowing soldering to 'unsolderable' metals ultrasonic soldering irons can also trigger wetting on ceramics and glasses. Introducing ultrasonic waves into the liquid solder also removes any air trapped inside it, improving the uniformity and strength of a bond. The liquid solder is also forced into any defects on the substrate surface, again improving the properties of the join.

With an ultrasonic soldering iron it is possible to tin dielectric coated glass with InSn solder without the use of flux, see Figure 5.20(a). However, the soldering iron tip scratched the glass surface and the dielectric layers were damaged by the ultrasonic processing; discolouration is visible in Figure 5.20(b). This method is therefore not appropriate for applying solder to an optical surface.

5.5.2 New Coating Structure

The coating structure used on a RCL gain medium most have the following properties. It most be a high performance, uniform, mirror at both pump and signal wavelengths, handle a large heat flux and be suitable to be bonded to a heat sink. Importantly, any bonding process used must not adversely effect the other properties of the coating structure. Damage to the optical coating could be caused by requiring ultrasonic tinning directly to the dielectric surface as described above, through indium ingress or through reactions with excess flux.

After communicating with the ceramic manufacturer, Baikowski Japan, who recommend using a stack made up of the dielectric then chromium and gold stack, undoped YAG ceramics with this coating structure were tested. The chromium was suggested to provide a bonding surface for the gold which then provides a soldering surface for a indium based solder.

(a) Solder applied directly to the HR dielectric (b) View through the unsoldered surface

Figure 5.20: InSn solder applied to an HR mirror with an ultrasonic soldering iron

These samples had InSn solder applied to the gold surfaces, see Figure 5.21. The sample on the left of this image shows the YAG without solder applied with a uniform chromium surface visible on the back surface. The sample on the right had InSn applied to its back surface with an ultrasonic soldering iron. Discolouration due to indium ingress is clearly visible. To confirm the ingress wasn't caused by the use of ultrasonics, solder was also applied to the gold surface by heating the sample on a hot plate. The result is the middle sample in the figure, which still shows visible indium ingress. Clearly this coating structure is not appropriate for a RCL gain medium.

A coating structure similar to that presented in [8] was then tested. This consisted of a Al_2O_3 capping layer followed by 300 nm of silver to act as a broadband reflector, 1000 nm of nickel to act as a buffer between the silver and the indium and finally 300 nm of gold to provide a soldering surface. This structure is shown in Figure 5.22.

5.5.3 Soldering Procedure

The procedure to mount a gain medium slab to a gold plated copper heat sink is outlined here. First the heat sink surface was cleaned with acetone and isopropanol to remove any oil or grease that had built up on the surface. Indium-tin foil was then placed on the surface to be soldered. A hot plate was used to heat the heat sink and solder to 130°C in a nitrogen atmosphere.

Once at temperature an ultrasonic soldering iron was used to tin the surface of the heat sink with a thin layer of solder. The tinned heat sink was then allowed to cool to room

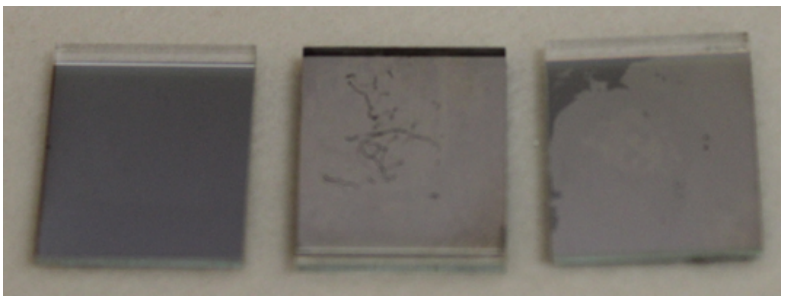

Figure 5.21: YAG ceramic samples with Cr and Au layers deposited on the back surface. The sample on the left has not been soldered, the middle sample had InSn melted onto the gold layer with a hot plate and the sample on the right had InSn solder applied with an ultrasonic soldering iron.

Figure 5.22: Sputtered layers applied to the base of the gain medium.

temperature. Once cold the gain medium was placed on the soldered surface and the temperature slowly ramped back to 130°C. The gradual temperature ramp was to limit the temperature difference between the slab and the heat sink, if the slab does not reach the melting point of the solder the solder will not adhere to it and will instead just flow around it. Once at temperature the gain medium was moved gently over the surface to 'iron' the solder flat. The heat sink and slab were then allowed to cool back to room temperature before being removed from the nitrogen atmosphere.

5.5.4 Soldering Results

To test the soldering procedure outlined above it was carried out on a 50 mm diameter, 6 mm thick Nd:YAG ceramic disk which was AR coated at 808 nm and 1064 nm on one surface and HR coated on the other at the same wavelengths. As this disk already had a thin film of silver applied it was decided to sputter it with 200 nm of silver followed by 1 μm of nickel and then 300 nm of gold to provide the soldering surface.

After soldering there was no visible discolouration in the metallic layer, see Figure 5.23, unlike Figure 5.21. Furthermore, the uniformity of the reflectivity map, Figure 5.24, is now unchanged from the unsoldered case, Figure 5.17. This is in stark contrast with what was found in the ceramic that had been bonded to a heat sink without the nickel and gold buffer layers, see Figure 5.18.

The mechanical strength of this soldered join was also considerably greater than that of both the compressed indium-slab bond and a melted indium join. This suggests the quality of the join was higher, and thus the thermal interface was been improved. This should reduce the thermal impedance at the gain medium heat sink interface.

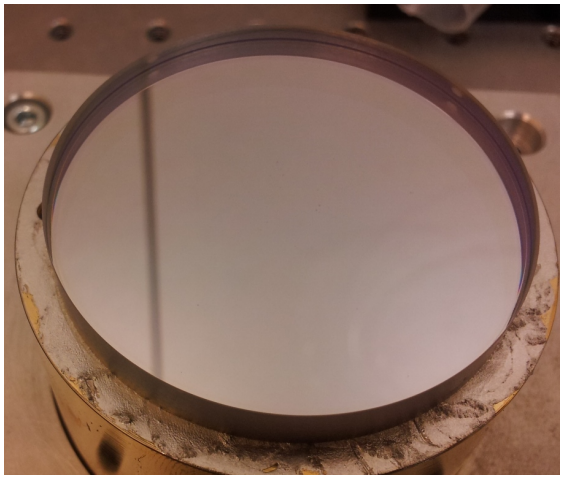

Figure 5.23: The soldered slab. Note the lack of discolouration of the silvered surface.

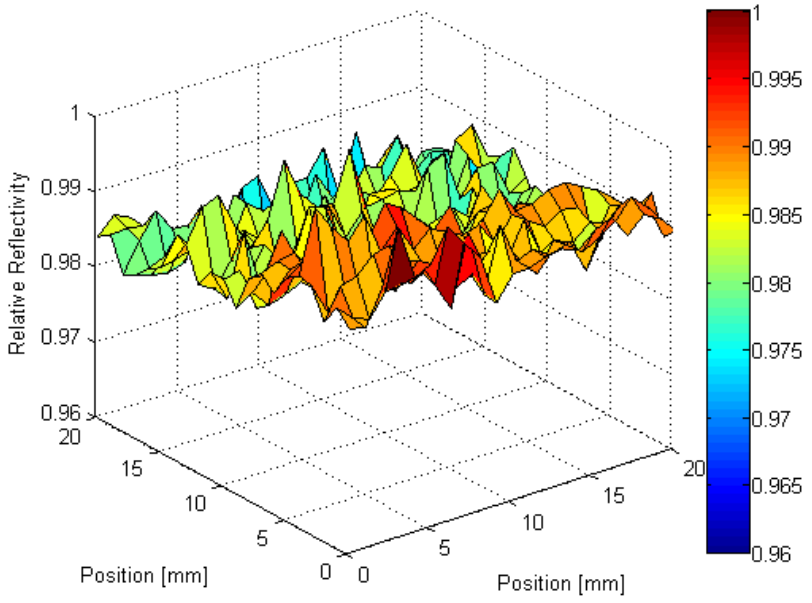

Figure 5.24: Reflectivity map of the soldered ceramic with the new metal stack.

The thermal interface in a face cooled system therefore needs to be considered carefully. Not only does it have to provide a mechanical join whilst supporting a large heat flux but it must do so without interacting with the optical properties of the dielectric layers, either through ingress or during the mounting procedure. In the RCL this problem is exacerbated by the need for uniformity over a large area, a single 'sweet spot' on the slab cannot be used, unlike in traditional laser architectures.

5.6 Measuring Small Signal Gain

The amplifier experiments that first revealed the power drop were repeated with the soldered slab. Figure 5.25 compares the stability of the power output of the amplifier as the periscope rotates between the two slab mounting techniques. Not only is the output considerably more stable, with a standard deviation of 1.6% as opposed to 10.4%, but the power drop has also reduced.

Figure 5.26 shows that whilst a power drop does still occur it is considerably smaller than what was the case with the older coating structure. This is consistent with the gain loss mechanism being dependent on temperature. Whilst the thermal interface has been improved so the temperature rise in the slab was decreased it still remains non zero as Nd:YAG has a finite thermal conductivity.

The saturation intensity, the intensity required to reduce the gain coefficient by a factor of two, can be calculated for a given gain medium with Equation 5.3 [14]. For Nd:YAG

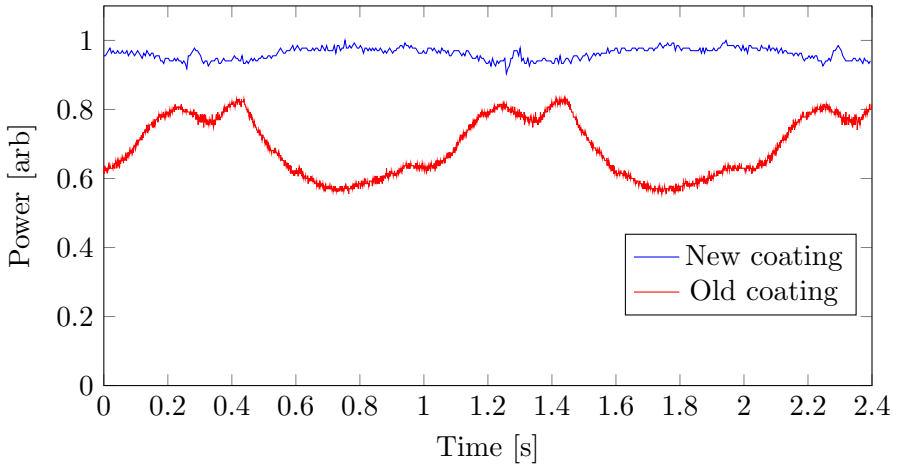

Figure 5.25: The power output of the amplifier with the improved coating has a much smaller modulation depth than previously, incident pump power 119W

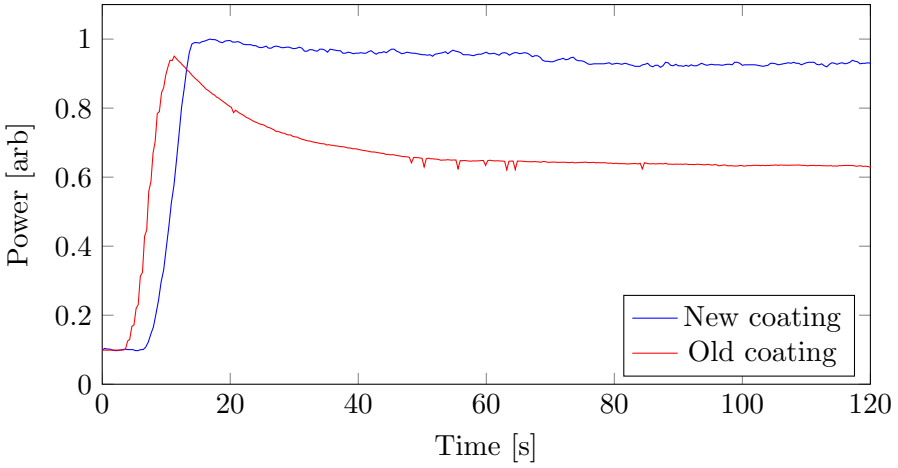

Figure 5.26: The reduction in gain over time is also considerably smaller with the new coating structure.

and a beam waist of 700 μm a power of 44.6 W is required to saturate the gain. As the seed beam was 0.5 W the amplification it experiences can be taken to be the small signal gain which can be calculated with Equation 2.23.

$$I_{\text{sat}} = \frac{h\nu}{\sigma\tau_f} \tag{5.3}$$

The small signal gain has been plotted with experimentally measured values in Figure 5.27. At pump power levels less than 120 W the experimental results show a linear dependence on the pump power. The theoretical prediction, which assumes a top hat pump profile, shows a higher level of gain than that which was observed. This is expected as in reality more Gaussian like profiles were being used. The plot also show evidence of a reduction in the small signal gain as the azimuthal velocity is increased, this is expected when there is little stimulated emission as discussed in §3.5.2.1. Furthermore,

the nonlinear nature of the curves below 120 W suggests there is a decrease in gain efficiency as the pump power is increased, which is in agreement with Equation 5.1.

The predicted change in small signal gain is the reciprocal of the change in threshold predicted in §3.5.2.1. The result of the Gaussian analysis is plotted in Figure 5.28. The predicted 0.9dB change in gain between the 0.19 m s^{-1} and 1.51 m s^{-1} cases and the 0.3dB change between 0.19 m s^{-1} and 0.75 m s^{-1} are in good agreement with Figure 5.27.

Before entering the slab the seed beam had an M^2 of 1.12, Figure 5.29 shows the beam quality post 10dB of amplification. The average M^2 over a rotation period increased to 1.35 and if the one outlier is ignored shows good uniformity.

Above 120 W of pump power the small signal gain no longer increases linearly as the pump power is increased. This point is independent of azimuthal velocity and therefore

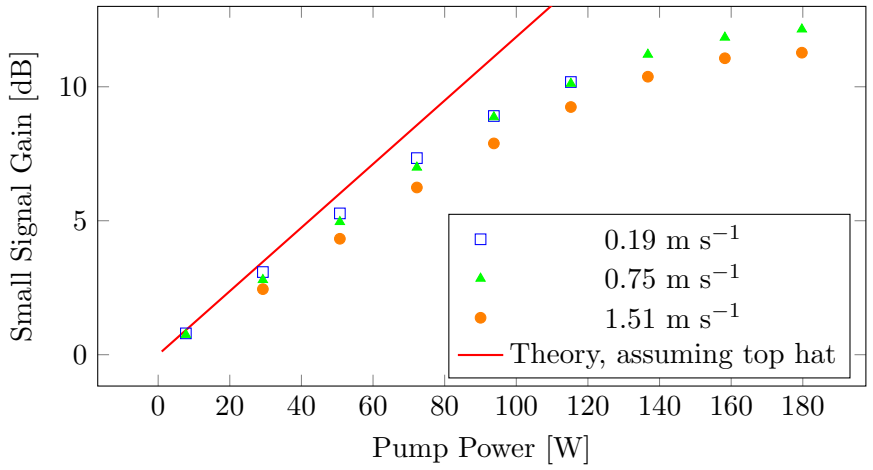

Figure 5.27: The small signal gain reduced as azimuthal velocity was increased as expected.

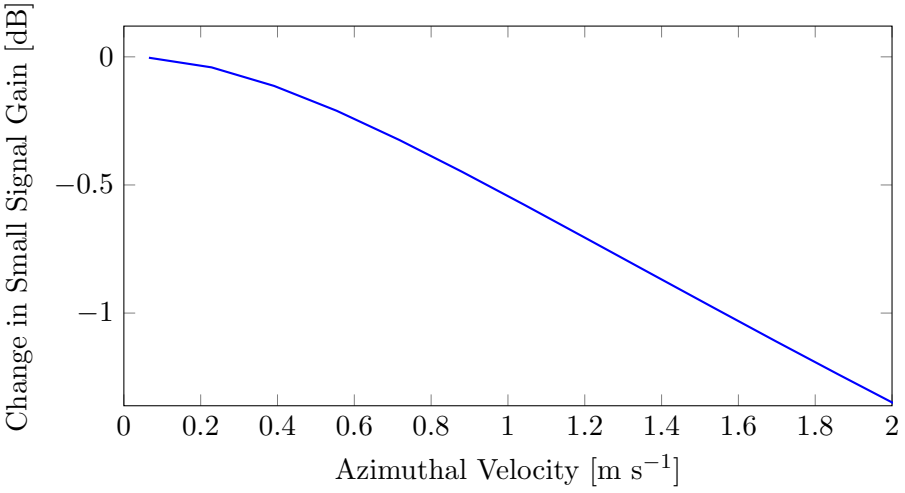

Figure 5.28: Predicted change in small signal gain with azimuthal velocity.

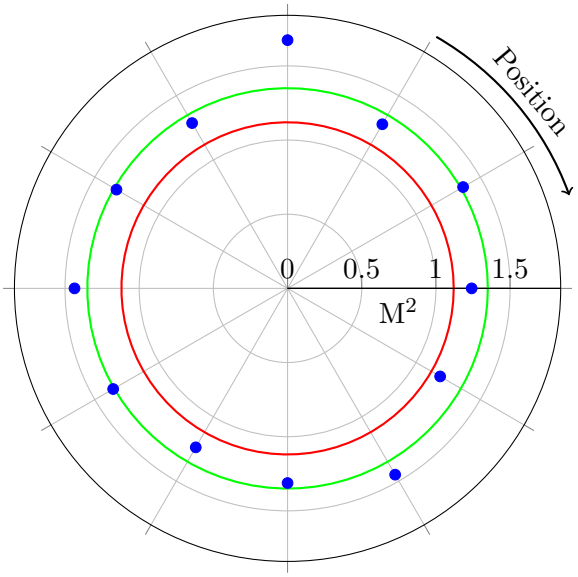

Figure 5.29: The beam quality of the beam after being amplified by 10dB. The azimuthal velocity was 0.75 m s^{-1} and 115 W of amplifier pump power was used. The seed M^2 is given by the red line and the average is shown in green.

is independent of temperature. In a similar RCL amplifier system parasitic lasing was observed above a pump power of the order of 110 W.

The seed laser was completely isolated from the amplifier with a beam block when the parasitic lasing was found. When the pump power was increased to over 107 W a spike indicative of lasing appeared in the power versus rotation trace, which widened and increased in amplitude as the pump power was increased further. It is therefore likely parasitic lasing is occurring at these power levels which acts to clamp the available gain for the seed laser.

The surface providing feedback to cause lasing is not currently known as the laser crystal is obscured by the rotating components. The parasitic beam initialises at a single point on the rotation cycle indicating the moving parts are influencing the parasitic beam. It is therefore likely this surface is being obscured by the mechanical assembly.

It is also possible at these gain levels that ASE is extracting stored energy and thereby reducing the small signal gain. If ASE propagates parallel to the top of the slab it is possible for it to be reflected back into the slab when it meets the curved edge. This has been seen to happen in thin disk amplifiers where it has been solved by adding a chamfer to the outside edge [15].

5.7 Thermal Wedging

In §3.5.1.3 it was proposed that the relative motion between the pump beam and gain medium would result in the generation of a thermal wedge. The angle of the proposed wedge would evolve as the intracavity periscope rotates. The preliminary calculations performed there suggested the effect would be small, here results from FEA thermal simulations and experiments are presented to check this initial analysis.

5.7.1 Experimental Results

Under the influence of a rotating wedge a beam will precess around the propagation axis, see Figure 5.30. In the case of the RCL a rotating wedge can be induced by either the imperfect periscope or through thermal effects due to the unusual temperature profile found in the gain medium.

With the beam profiler described in §4.4 it was possible to determine the pointing stability of an amplified beam over a rotation of the periscope. By varying the pump power or the rotation rate it is possible to change the temperature rise experienced by a pumped spot. The strength of any thermal wedge can therefore be changed by manipulating these parameters. If this change has a significant effect on the radial component of the wedge it will manifest as an increase in the rate at which the radius of the beam path changes as it travels through a focus. If the radial component of the thermal wedge is insignificant there will not be any change in this variation in radius as it will be only influenced by the quality of the periscope.

Figure 5.31 shows the change in the radius of the circle swept out as the laser mode travels through a focus whilst the rotation rate was changed. In this plot the minimum of each data set has been aligned to compensate for change in waist position created by change in thermal lens within the slab. The circle swept out collapsed to a single spot at the focus for all the rotation rates as expected. The slower the azimuthal velocity

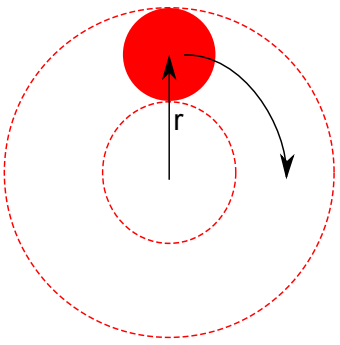

Figure 5.30: Path of a beam which has passed through a rotating wedge. It was possible to measure r with the diagnostic described in §4.4.

the larger the radius swept out away from focus. This is consistent with the thermally induced wedge having a measurable radial component.

In Figure 5.32 the radius of the swept out circle is changed by changing the pump power whilst the rotation rate is kept constant. Like in Figure 5.31 the points of smallest radius have been aligned. Again reducing the temperature rise in the pumped spot reduced the swept out radius away from focus.

For the case where the slab is pumped with 115 W and the periscope is moved with an azimuthal velocity of 1.51 m s^{-1} the angle created by the increase in radius is 6 milliradians. This has been calculated by considering the red triangle sketched in Figure 5.32. The divergence angle for this beam leaving the waist created by this lens is 10

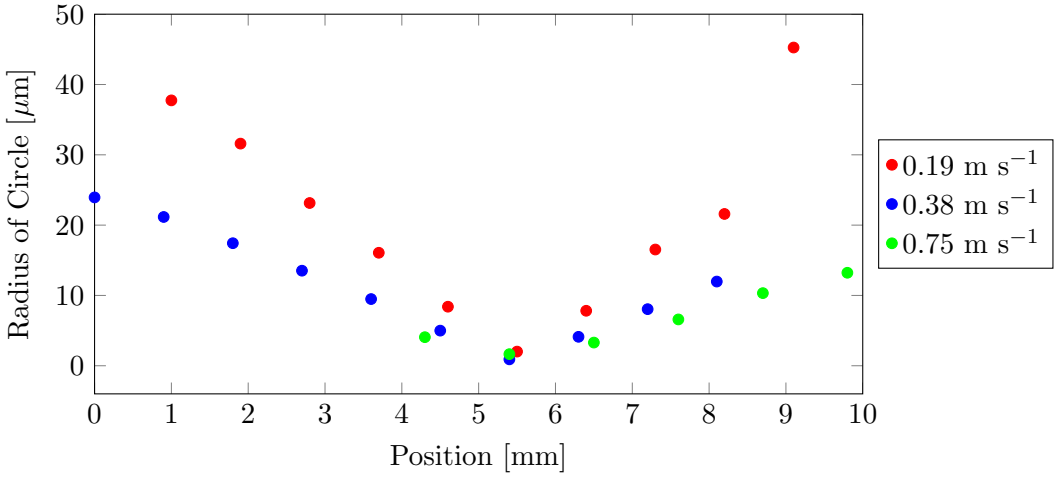

Figure 5.31: Change in the radius swept out by the amplified beam under 51 W pump power for different rotation rates.

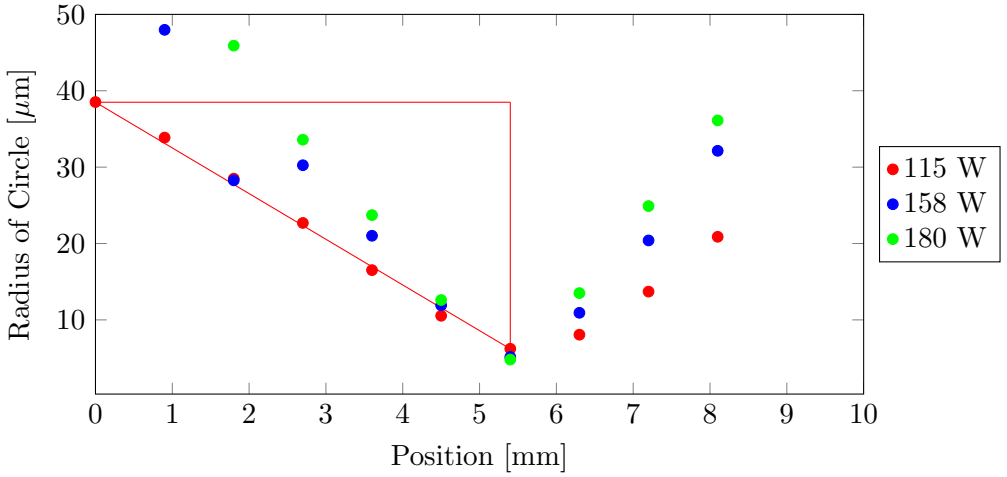

Figure 5.32: Change in the radius swept out by the amplified beam under different pump powers whilst the pump beam is moved with an azimuthal velocity of 1.51 m s^{-1}. The red triangle was used to calculate the divergence the radius swept out.

milliradians. If this were to occur within a laser resonator an angular change of the order of the divergence angle will have consequences for the resonators performance, see §3.5.1.3.

Furthermore, this experiment has only detected changes in the radial direction. The thermal wedge will also steer the beam in the azimuthal direction, see Figure 5.33. The total angular shift experienced by the beam will thus be larger than that calculated above. Inside a laser resonator this thermally induced angle evolves with the rotation of the periscope and acts to misalign the laser. It is not possible to account for this angle with a stationary component and results in the need for a 'compromise' alignment. Whilst the power output of the laser can be made stable with such a compromise alignment, this is at the expense of beam quality. The presence of a larger than expected thermal wedge could thus explain the rapid increase in M^2 seen in Figure 5.5 as pump power was increased.

By deliberately angling a stationary resonator mirror it was hoped the beam quality could be improved at a single point on the rotation cycle at the expense of power stability and beam quality elsewhere. To test this a resonator was constructed and the output coupler angled. Figure 5.34 shows the M^2 under 59 W of pumping and producing 9.6 W. When aligned for power stability the average M^2 was 1.26. Applying a wedge to an optic provided a slight improvement in M^2.

Figure 5.35 shows the same procedure applied when the resonator was producing 22 W under 94 W of pump power. In this case the power stability optimized average M^2 was 2.2, by applying a wedge this was reduced to 1.4 at one point on the cycle, providing evidence a thermal wedge was acting to reduce the beam quality at high pump powers.

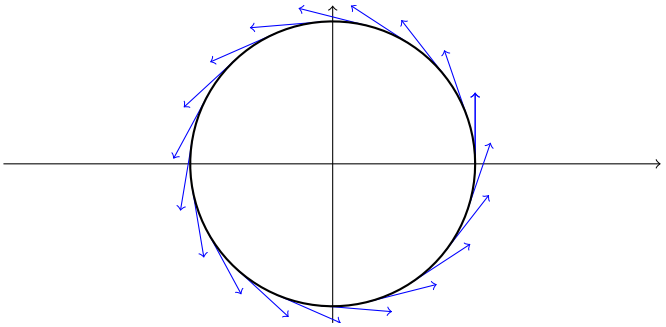

Figure 5.33: The circle represents the path of the laser mode over the surface of the gain medium. The arrows are tangential to it and indicate a thermal wedge will change the radius of the swept out circle as will as the angle of the laser in the azimuthal direction.

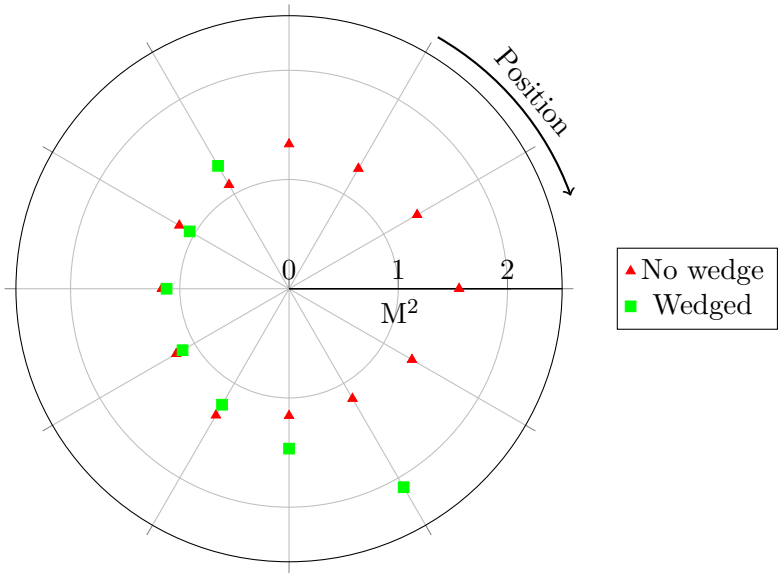

Figure 5.34: A slight improvement in M^2 was seen by applying a deliberate wedge under 59 W of pump power.

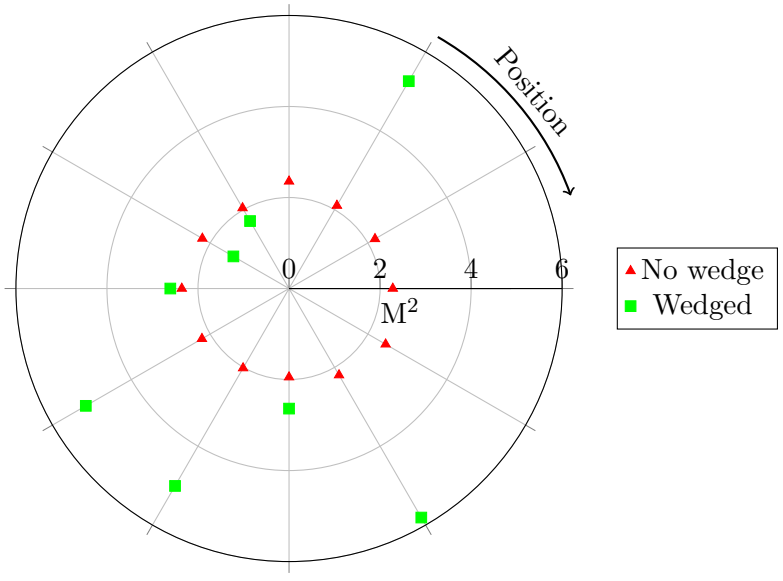

Figure 5.35: Under 94 W of pump power deliberate wedging had a greater effect on the M^2.

5.7.2 FEA Analysis

§3.5.1.3 predicts the thermally induced wedge should be of the order of 50 microradians for the 27 W heating power generated by the 750 μm waist, a wedge of this order is an order of magnitude less than the 450 microradian divergence angle. A wedge of this size does not explain the effects seen above. FEA analysis was therefore performed to verify the temperature rise found with Equation 3.5 and by extension the angle found with Equation 3.10. In particular this analysis will allow the effect of repeated pump passes over a given spot to be taken into account.

The FEA analysis was performed for a 50 mm square, 6 mm thick sample under the influence of a 500 micron waist Gaussian pump beam using a C++ program written by P C Shardlow. The model assumes all the heat deposited into the gain medium is extracted through the bottom surface into a perfectly conducting heat sink. It calculated the evolution of temperature over the entire slab, see Figure 5.36.

The average temperature through the depth of the slab of a pumped spot is shown in Figure 5.37. The predicted temperature rise, as calculated by Equation 3.5 is included. The FEA shows good agreement with this expression when the pump is passed once over cold material. In this situation the modelled temperature profile does not explain the larger than expected thermal wedge seen above.

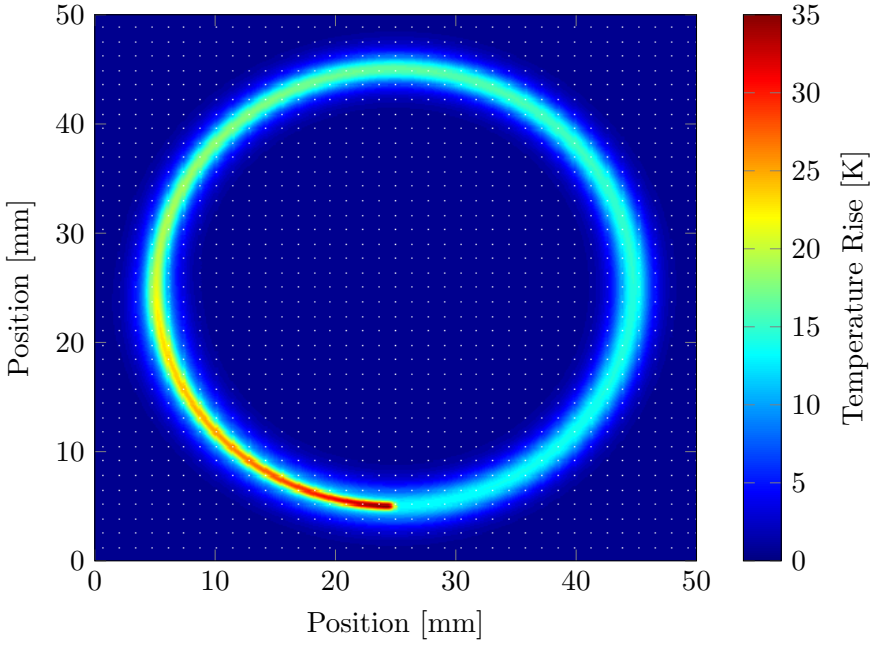

Figure 5.36: FEA software was used to calculate the temperature of a square slab heated by moving pump beam. This is the mean temperature through a 6 mm piece of Nd:YAG which has been heated by a 180 W source moving at 1.51 m s^{-1} after 5 rotations

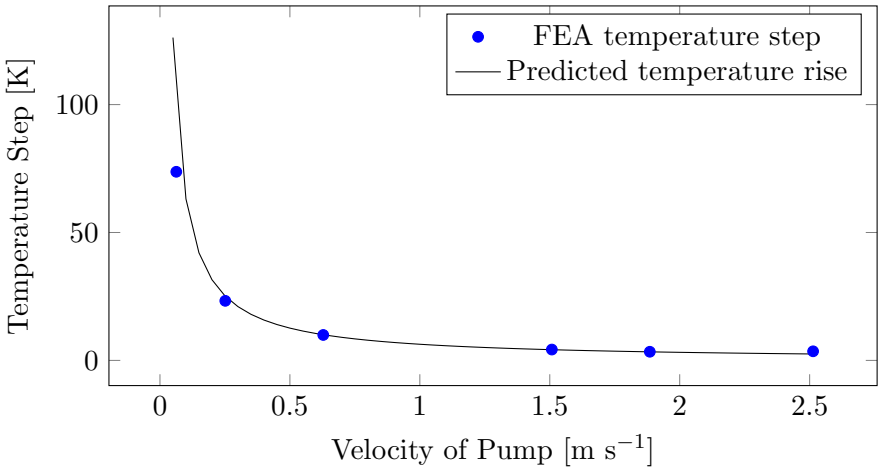

Figure 5.37: The FEA results show good agreement with Equation 3.5. These results are for 80 W of heating power

The change in temperature over the point of maximum temperature in the azimuth direction has been plotted in Figure 5.38 for multiple passes of the pump beam. Whilst the absolute temperature the slab reaches changes as the pump is repeatedly passed over it until a steady state is reached, the size of the temperature step does not change with repeated passes of the pump beam. The distance the temperature step occurs over is defined by the leading edge of the pump and this remains unchanged as repeated passes are made. The strength of the thermal wedge does therefore not change as the laser gain medium heats up.

Figure 5.38 also shows the width of the temperature step is constant with repeated passes. However it indicates that the temperature change occurs over a beam waist, half the value used in Equation 3.10. This is due to the previous assumption that the wedge

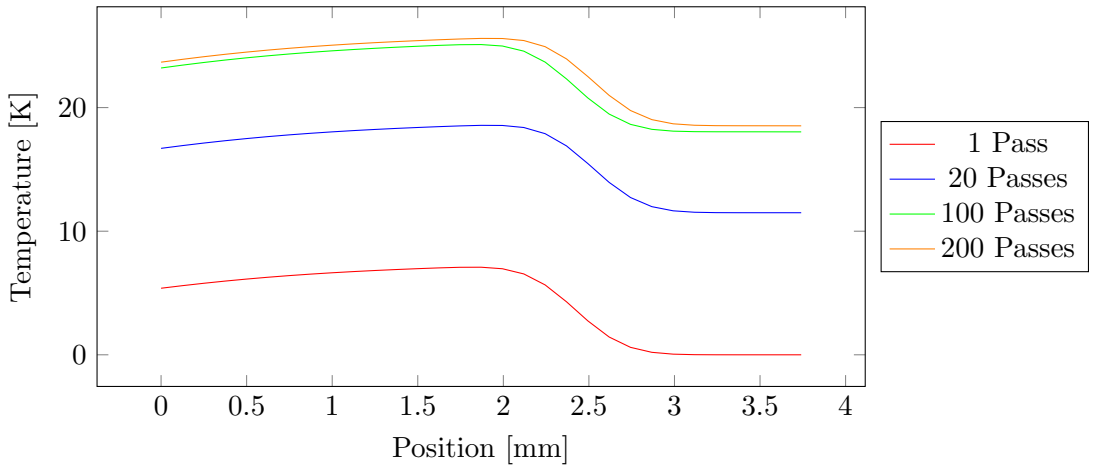

Figure 5.38: The absolute temperature of the pumped region increases with each pass until a steady state is reached, here the pump was moved at 1.51 m s^{-1} and the heating power was 115 W. The change in position of the temperature stop is an artefact of the time step used in the FEA analysis.

occurs over a beam diameter as opposed to a beam radius being incorrect. Making this modification and combining with Equation 3.9 gives the following expression for the thermal wedge angle.

$$\alpha = 2\frac{Q}{C_v \pi^2 w_p^2 r_{rot} \Omega}\frac{dn}{dT} \tag{5.4}$$

A 1064 nm beam of radius 700 μm, like that in §5.2, has a divergence angle of 490 microradians. Under an azimuthal velocity of 2.64 m s^{-1} and a heating power of 43 W Equations 5.4 and 3.11 predict a deflection angle of 90 microradians. 43 W of heating power corresponds to a pump power of 180 W, which is where the beam quality was seen to start to degrade in Figure 5.5. Under a heating power of 72 W, equivalent to a pump power of 300 W which resulted in an M^2 of 11 in Figure 5.5, the deflection angle is 150 microradians. A wedge of this size would be expected to have a detectable effect on the resonator's performance however the observed effect is larger than a wedge of this order would suggest.

Any asymmetry in the radial temperature distribution due to one side being closer to the slab edge will also contribute to a change in the radius of the circle being swept out by the output beam and would explain the larger than expected edge found above. Figure 5.39 shows the temperature distribution in the radial direction under the same conditions as used to produce Figure 5.38. Whilst Figure 5.38 shows a thermal gradient after repeated pump passes beyond a beam waist, the thermal profile exposed to a laser mode matched to the pump beam is unchanged. There is also no asymmetry in this direction suggesting the observed radial wedge is due to the radial element of the azimuthal wedge illustrated in Figure 5.33.

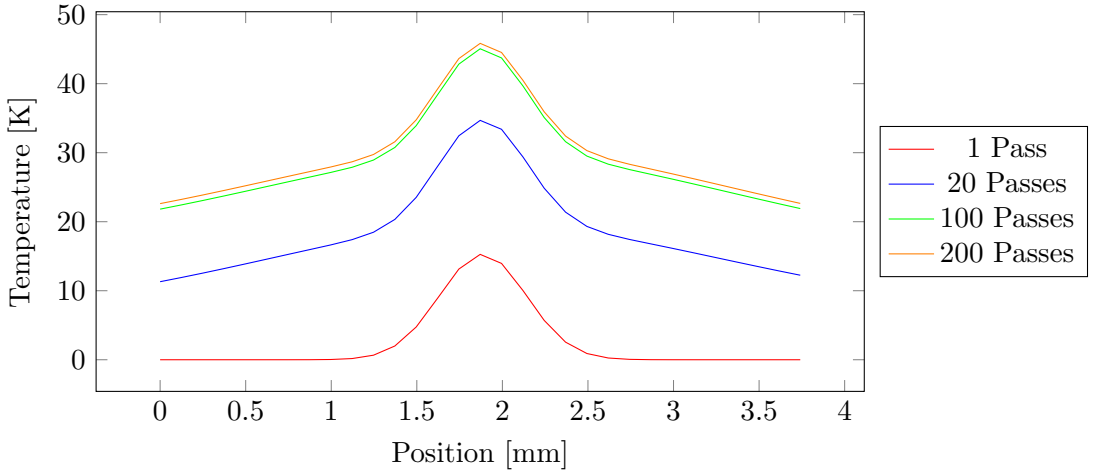

Figure 5.39: The radial temperature distribution dose not include any asymmetry. Here the pump was moved at 1.51 m s^{-1} and the heating power was 115 W.

Whilst the FEA analysis showed the thermal wedge is a factor of two larger than that predicted in §3.5.1.3 it is not enough to explain the experimental observations. These

considerations did not include any contributions from the thermal expansion of the slab which will also act to increase the deflection angle.

5.8 Conclusion

In this chapter results gathered with the use of a 400 W, 808 nm pump source were presented. Using this to drive a telescopic resonator 120 W of 1064 nm light was generated from an end pumped Nd:YAG laser. Using the RCL strategy power regimes that normally require more complicated optical arrangements within a solid-state laser have been accessed with an early prototype.

An M^2 of 1.1 was achieved at low power but this was not maintained at the higher power levels, becoming 11 when generating 100 W. It was proposed this reduction in beam quality was due to a combination of the thermal lens due to the instantaneous heating effect changing the overlap between the pump beam and laser mode and potentially driving the resonator unstable, and the presence of a thermal wedge.

Whilst the presence of a larger than expected thermal wedge was detected by measuring the change in the radius of the circle swept out by the laser mode and FEA analysis indicated that the temperature step was a factor of 2 stronger than that predicted by Equation 3.10 this was not severe enough to cause the rapid rise in M^2 at high power levels. Analysis conducted so far has ignored contributions from thermally induced expansion as these are normally considered to be small so it is still unlikely to explain the beam degradation when these factors are included. The cause of the beam degradation is thus most likely a combination of factors, including the thermal wedge, and some other thermal effect which is currently unknown.

The mechanical assembly and gain medium were then reconfigured to form an amplifier. When first operated a drop in gain was observed as the temperature of the slab increased. The amount of power drop had a dependence on the position of the beam on the slab. This suggested a variation in thermal properties across the Nd:YAG slab, because of this the coatings and process used to bond the slab to the heat sink were investigated.

The optical coatings were found to have been damaged by the original mounting process. By replacing the metallic stack with layers designed to protect the dielectric coatings and then soldering in an oxygen free environment the gain drop associated with temperature was drastically reduced. With the new coating arrangement 12dB of gain was generated before the onset of parasitic lasing prevented a further increase.

References

[1] P. Sarkies, "A stable YAG resonator yielding a beam of very low divergence and high output energy," *Optics Communications*, vol. 31, pp. 189–192, Nov. 1979.

[2] M. Frede, R. Wilheim, and M. Brendel, "High power fundamental mode Nd: YAG laser with efficient birefringence compensation," *Optics Express*, vol. 12, pp. 3581–9, July 2004.

[3] J. Lu, H. Yagi, K. Takaichi, T. Uematsu, J.-F. Bisson, Y. Feng, A. Shirakawa, K.-I. Ueda, T. Yanagitani, and A. A. Kaminskii, "110 W ceramic Nd3+ : Y3Al5O12 laser," *Applied Physics B*, vol. 79, no. 1, pp. 25–28, 2004.

[4] W. A. Clarkson, "Thermal effects and their mitigation in end-pumped solid-state lasers," *Journal of Physics D: Applied Physics*, vol. 34, p. 2381, 2001.

[5] Y. Sato and T. Taira, "Temperature dependencies of stimulated emission cross section for Nd-doped solid-state laser materials," *Optical Materials Express*, vol. 2, no. 8, pp. 514–522, 2012.

[6] Fan and T.Y., "Heat generation in Nd:YAG and Yb:YAG," *IEEE Journal of Quantum Electronics*, vol. 29, pp. 1457–1459, June 1993.

[7] L. Zapata, S. Massey, R. J. Beach, and S. Payne, "High average power Yb: YAG laser," in *Solid State and Diode Laser Technology Review*, 2001.

[8] L. Zapata, R. Beach, S. Mitchell, and S. Payne, "Yb Thin-Disk Laser Results," in *Solid State and Diode Laser Technology Review*, Lawrence Livermore National Lab., CA (US), 2002.

[9] G. Humpston and D. M. Jacobson, *Principles of Soldering.* ASM International, 2004.

[10] A. Moore and D. Tabor, "Some mechanical and adhesive properties of indium," *British Journal of Applied Physics*, vol. 299, 1952.

[11] R. B. Belser, "A Technique of Soldering to Thin Metal Films," *Review of Scientific Instruments*, vol. 25, no. 2, p. 180, 1954.

[12] S. Choe, W. So, and C. Lee, "Low temperature fluxless bonding technique using In-Sn composite," *2000 Proceedings. 50th Electronic Components and Technology Conference (Cat. No.00CH37070)*, pp. 114–118, 2000.

[13] B. E. Noltingk and E. A. Neppiras, "Ultrasonic soldering irons," *Journal of Scientific Instruments*, vol. 28, pp. 50–52, Feb. 1951.

[14] W. Koechner, *Solid State Laser Engineering.* New York: Springer, 6th ed., 2006.

[15] A. Antognini, K. Schuhmann, F. D. Amaro, F. Biraben, A. Dax, A. Giesen, T. Graf, T. W. Hansch, P. Indelicato, L. Julien, C.-Y. Kao, P. E. Knowles, F. Kottmann, E. Le Bigot, Y.-W. Liu, L. Ludhova, N. Moschuring, F. Mulhauser, T. Nebel, F. Nez, P. Rabinowitz, C. Schwob, D. Taqqu, and R. Pohl, "Thin-Disk Yb:YAG Oscillator-Amplifier Laser, ASE, and Effective Yb:YAG Lifetime," *Quantum Electronics, IEEE Journal of*, vol. 45, pp. 993–1005, Aug. 2009.

Chapter 6

Overcoming Detrimental Thermal Phenomena with Motion

6.1 Introduction

To illustrate the effectiveness of the RCL architecture at overcoming thermally induced phenomena a number of experiments were conducted, these are presented in this chapter. First the thermally induced stresses present in a pumped laser are discussed by considering stress induced birefringence. The case where the periscope is held stationary is compared with the rotating case to demonstrate the thermal loading reduction experienced in RCL like architectures.

A method of predicting the thermal lens strength under rotation is then presented. The approach outlined assumes the RCL is operating within the adiabatic regime with respect to heat flow and the generated refractive index profile is thus due to a temperature profile that matches the pump beam.

The aberating quality of the unusual thermal profile expected in the RCL, see §5.7.2, was investigated with a 1064 nm probe beam. Attention was also paid to the potential for variation in the quality of the thermal lens over a rotation cycle. By making use of the beam profiler described in §4.4 it was possible to detect fluctuations in the probe beam's beam quality.

6.2 Stress Induced Birefringence

An indicator of the thermal load on a non-birefringent laser gain medium, such as YAG, is the amount of stress induced birefringence. Whilst in a birefringent crystal the birefringent axes are orthogonal this is not the case for stress induced birefringence.

A birefringent crystal can be orientated to enforce linear polarization on a laser mode, this cannot be done with the more complicated birefringence profile induced by thermal stress.

Stress-induced birefringence is linked to thermal gradients within a gain medium. As density is temperature dependant a material with a temperature gradient across it will attempt to expand by different amounts. As the hotter material is constraint by the surrounding cooler material this results in a stress distribution across the material. In a laser rod the cylindrical symmetry results in stress and birefringence with radial and tangential axes, see Figure 6.1 [1].

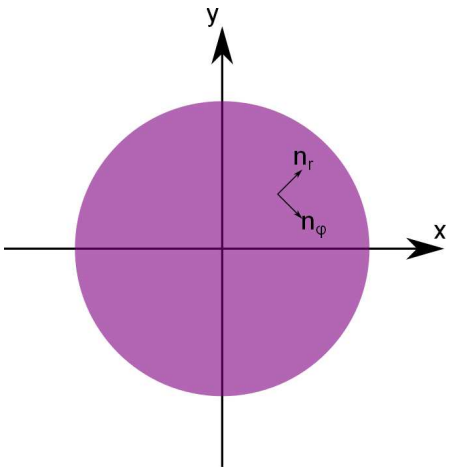

Figure 6.1: The stress distribution follows has radial and tangential components.

If a linearly polarized beam interacts with the stressed gain medium the cylindrical birefringence distribution will act to depolarize the beam. Importantly, different parts of the beam experience different levels of depolarization as the x and y components of the birefringence vary over the beam. Figure 6.2 shows the result of passing a polarized HeNe beam through both a pumped Nd:YAG rod and a polariser crossed with the HeNe beam's polarization, illustrating the complexity of the induced birefringence profile.

The output of a laser is defined by the mode that minimises the losses of the resonator. By introducing a polarization dependent loss it is therefore possible to force a laser to produce a polarized output. The Fresnel equations show a polarization dependent loss can be straight forwardly produced by inserting an uncoated window into the resonator at Brewster's angle. If any other elements within the resonator act to change the polarization state the Brewster window will create a loss by removing some of the S-polarization state from the resonator. This can be measured allowing the amount of stress induced birefringence to be quantified.

To measure the depolarization loss of an RCL a Brewster window was inserted in to the resonator described in §5.2. The points where the laser output was at a maximum over

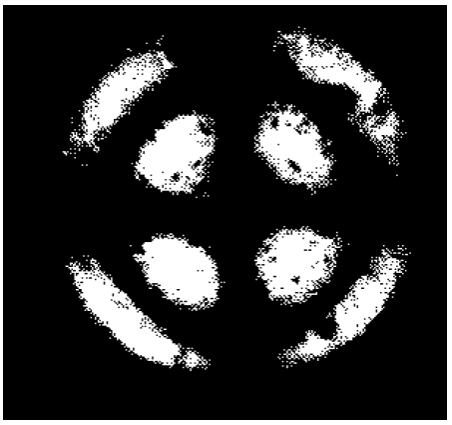

Figure 6.2: Stress in induced birefringence in a Nd:YAG rod, from [2].

a rotation period were then considered. These values corresponded to the points where the Fresnel romb like rhomboid prism was aligned to the incident polarization. At these points an incident beam receives a phase shift aligned to the polarization axis, retarding the beam without affecting its polarization state. Any depolarization at these points are thus due to stress-induced birefringence and not the rotating prism. Figure 6.3 shows how the depolarization loss was reduced as the rotation rate was increased for a number of different pump powers.

When the slab was pumped with 53 W of pump power and the periscope was held stationary the round trip depolarization loss was 8% of the output power. With an azimuthal velocity of 0.19 m s^{-1} this was reduced by an order of magnitude to 0.77%. Whilst motion created a drastic reduction in the stresses inside the laser crystal they were not completely removed. Any inherent stress in the Nd:YAG will create a result in

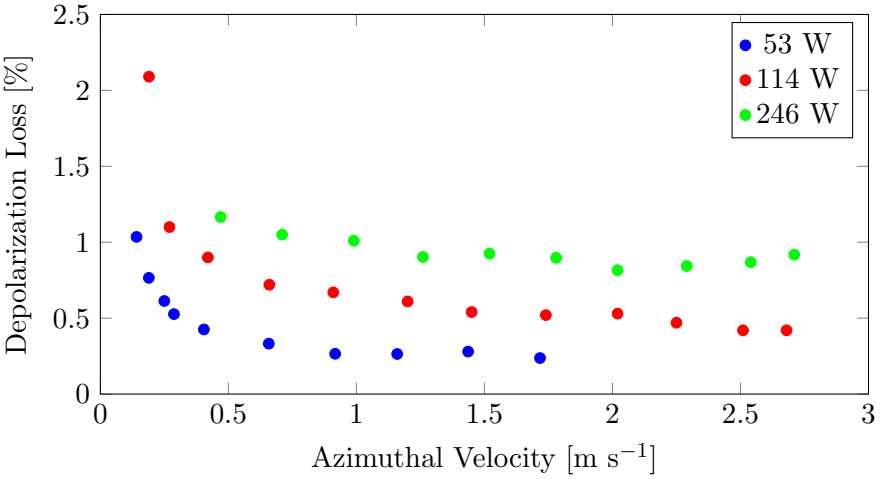

Figure 6.3: The introduction of motion reduced the depolarization losses when the resonator was running in a polarized mode under different pump powers. When the azimuthal velocity was 0 m s^{-1} the depolarization loss was 8% for 53 W of pump power.

some birefringence and thus a loss if the birefringent axis are not aligned to the incident polarization. However Figure 6.3 shows the minimum loss has a power dependence. This minimum loss appears to scale linearly with the pump power, which matches the behaviour of the expected temperature rise according to Equation 3.5.

Figure 6.4 shows the temperature rise inside the slab as predicted by Equation 3.5 for the pump powers used to generate Figure 6.3. Whilst the relative difference in temperature matches the relative change in birefringence losses at high azimuthal velocities the sharpness of the fall in induced birefringence seen even under high pump powers does not match.

Above 0.5 m s^{-1} for all the pump powers shown on Figure 6.3, there is only a small further decrease in birefringence losses while Figure 6.4 suggests that it is possible to reduce the temperature by a considerable amount by increasing the velocity further. The reduction in stress is much sharper than that expected by considering the temperature rise alone, particularly at high pump powers.

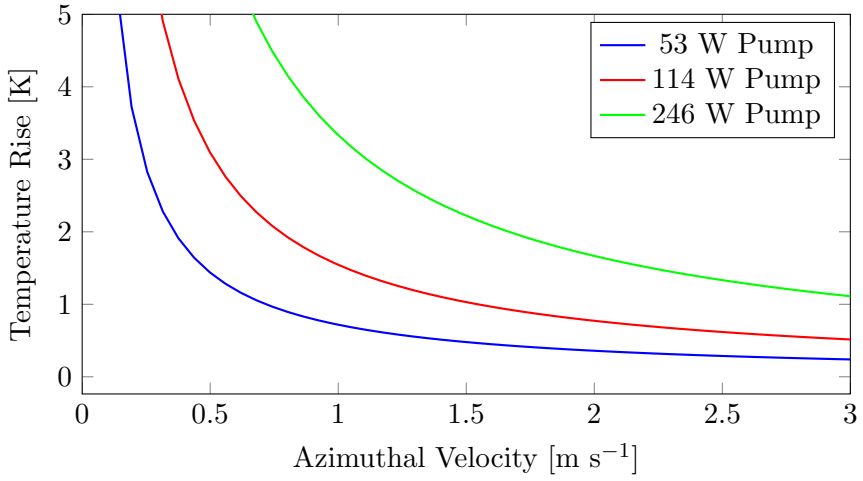

Figure 6.4: Temperature change calculated with Equation 3.5.

This indicates the absolute temperature may no longer be the determining factor. As stated above the presence of temperature gradients are the cause of the stresses as opposed to the temperature rise itself. If the temperature rise is uniform the induced stress will be small regardless of the absolute temperature rise. The observed rapid decay of stress and then plateau as azimuthal velocity is increased suggests that the RCL is influencing the temperature distribution by transitioning into the adiabatic limit.

In the adiabatic limit heat does not flow so the temperature profile is defined by the pump beam, resulting in less extreme temperature gradients. Clearly as the heated material is still constrained by surrounding cold material a stress related to the absolute temperature rise will still be induced. This agrees with the increase in minimum stress with pump power observed in Figure 6.3.

The adiabatic limit was discussed in §3.5.1.2 and Figure 6.5, which is a plot of Equation 3.8, shows the percentage of thermal energy generated in a pump spot that moves 1 mm within a dwell time of the pump spot. At 0.5 m s^{-1} in Nd:YAG 3.6% of the thermal energy moves this far and whilst further increases in velocity decrease this further the reductions are small. At velocities of this order the adiabatic limit is thus reached.

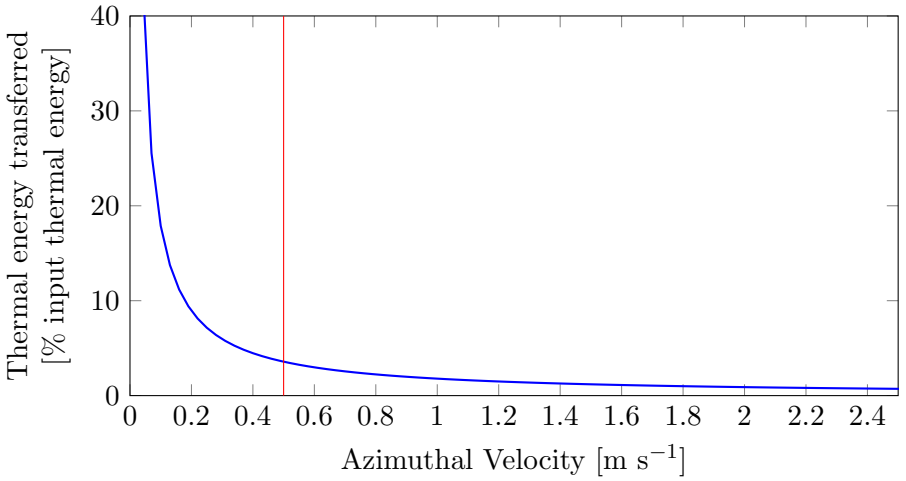

Figure 6.5: Percentage of heat energy that moves 1000 microns within the pump dwell time. The red line marks 0.5 m s^{-1}.

The adiabatic limit occurring at 0.5 m s^{-1} agrees with the observed behaviour of the stress-induced birefringence presented in Figure 6.3 and provides evidence that temperature gradients become more severe once heat flows. The behaviour of stress induced birefringence losses under different pump powers, and azimuthal velocities, indicates not only is the reduction in temperature associated with motion of benefit to laser operation but operating in the adiabatic regime also gives improvements. The thermal profile created by the pump profile appears to result in less stress than that created once the heat starts to flow through the gain medium.

6.3 Predicting Thermal Lens Strength

The thermal lens is a key property of a solid state laser and needs to be considered when designing a high power resonator, see §2.6.3.1. In a laser rod the thermal lens strength can be determined by considering the temperature distribution in a cylinder which is heated centrally under the approximation all heat flow is radial. Clearly this is not the case for an RCL, here a method to predict the strength of thermal lens within a RCL is outlined.

6.3.1 Theoretical Prediction

Within the adiabatic limit the temperature distribution seen by a laser mode matches the profile of the pump source in the radial direction. The leading edge in the azimuthal direction will also match this profile but the trailing edge will be modified by the presence of previously heated material reducing the strength of any thermal gradients. As the lensing in the radial direction are strongest they are the main consideration when considering resonator stability. By approximating the radial temperature distribution with an appropriate parabola it is therefore possible to model this as a spherical lens and thus determine its effect on a resonator.

The focal length of the parabolic refractive index profile given in Equation 6.1 can be found by considering Equation 6.2 [3]. Here r is the distance from the centre of the refractive index profile, n_0 is the refractive index at the centre of the profile, l is the length of the heated material, and k is a constant describing the parabola.

$$n(r) = n_0 \left(1 - \frac{2r^2}{k^2}\right) \tag{6.1}$$

$$f \cong \frac{k^2}{4n_0 l} \tag{6.2}$$

If the pump beam is assumed to be Gaussian in shape the temperature profile leads to a refractive index profile given by

$$n(r) = \Delta T \exp\left(-2\frac{r^2}{w^2}\right) \frac{dn}{dT} \tag{6.3}$$

Taking the first two terms of the Taylor expansion of Equation 6.3 leaves

$$n(r) = \Delta T \left(1 - \frac{2r^2}{w^2}\right) \frac{dn}{dT} \tag{6.4}$$

which is in the same form as Equation 6.1. This parabolic approximation has been plotted with the Gaussian in Figure 6.6. Whilst the approximation is good within half a beam waist of the centre of the profile the rate of change in refractive index becomes faster beyond this point. This approximation will thus lead to the prediction of a stronger thermal lens than is actually generated.

Comparing Equations 6.1, 6.2 and 6.4 gives the following expression for the thermal lens focal length.

$$f = \frac{w^2}{4\Delta T l} \left(\frac{dn}{dT}\right)^{-1} \tag{6.5}$$

In the RCL ΔT can be calculated with Equation 3.5 in the adiabatic limit. Re-expressing this in terms of the azimuthal velocity of the pump beam and substituting in to Equation

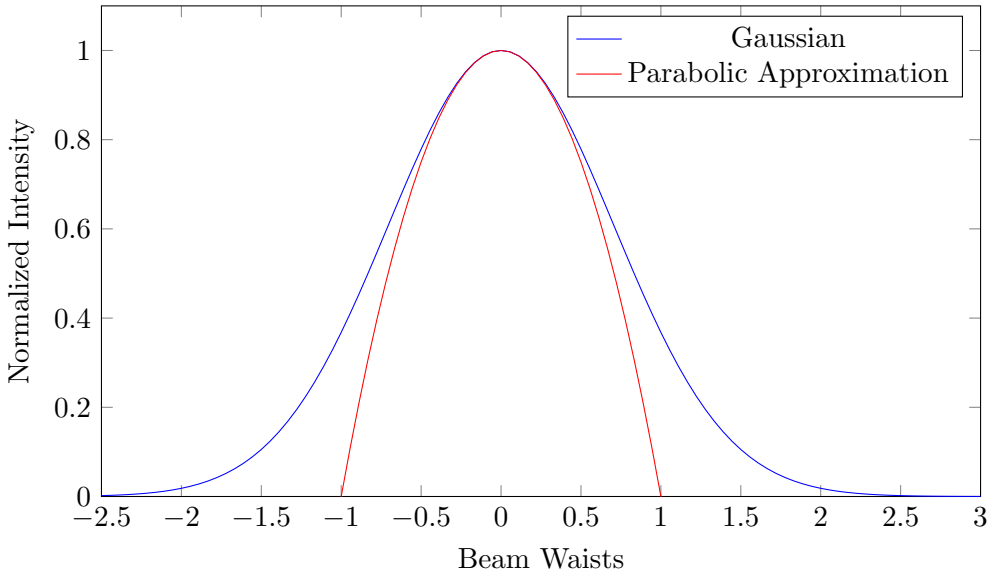

Figure 6.6: A Gaussian profile can be approximated by a parabola, however the approximation becomes less accurate beyond half a beam waist from the centre.

6.5 results in the expression for the thermal lens given by Equation 6.6.

$$f = \frac{w^3 C_v \pi v}{8 P_{\text{heat}}} \left(\frac{dn}{dT}\right)^{-1} \tag{6.6}$$

Comparing this with Equation 6.7, which gives the thermal lens focal length for the case of an edge cooled rod under a Gaussian pump beam [4], allows the reduction in focal length to be calculated.

$$f_{\text{rod}} = \frac{\pi \kappa w^2}{P_{\text{heat}}} \left(\frac{dn}{dT}\right)^{-1} \tag{6.7}$$

$$\frac{f_{\text{RCL}}}{f_{\text{Rod}}} = \frac{w C_v v}{16 \kappa} \tag{6.8}$$

Equation 6.8 has been plotted for Nd:YAG in Figure 6.7 and clearly shows the drastic reduction in thermal lens power associated with the decrease in temperature rise associated with the introduction of motion to the laser system. Whilst larger beam waists experience a greater reduction in thermal lens strength from motion a velocity of 1 m s^{-1} increases the thermal lens focal length by 4.5 for a beam waist of 300 μm. This reduction is equivalent to reducing the heat load by a factor of 4.5, which would allow an increase in output power of the same amount in the common case of a solid state laser being limited by the thermal lens.

This equation indicates that choosing a material with a low thermal conductivity will improve the performance of an RCL relative to the rod case of a rod made of the same material. This is due to the increase in time where the adiabatic limit applies when

heat flow is slower. This indicates the RCL architecture would be an effective way of improving performance when a material with a low thermal conductivity needs to be used, for example to access a particular wavelength.

6.3.2 Experimental Results

To test Equation 6.6 the resonator in Figure 6.8 was constructed and pumped with a 60 W diode producing a 450 μm pump radius in the Nd:YAG slab. This resonator had a mode waist that varies with the thermal lens as shown by Figure 6.9. The point of thermal roll over was determined for a number of azimuthal velocities and are shown in Figure 6.10. Here the only source of heating was assumed to be the quantum defect.

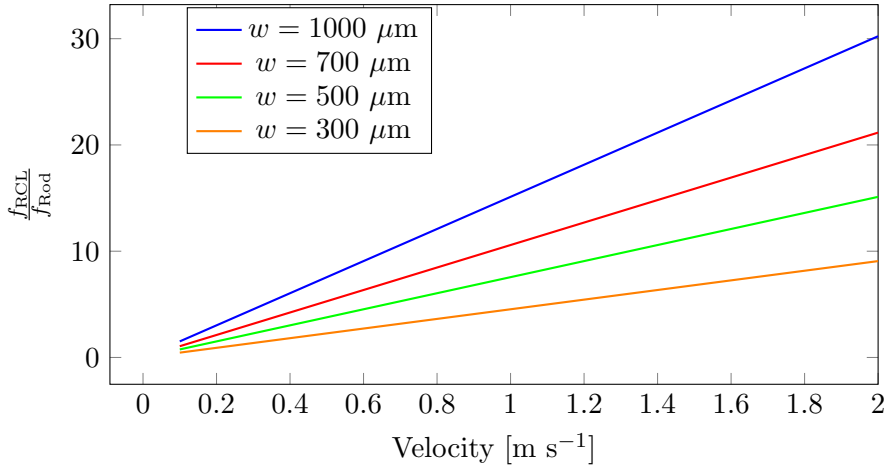

Figure 6.7: Ratio of predicted thermal lens strength for a Nd:YAG rod and RCL.

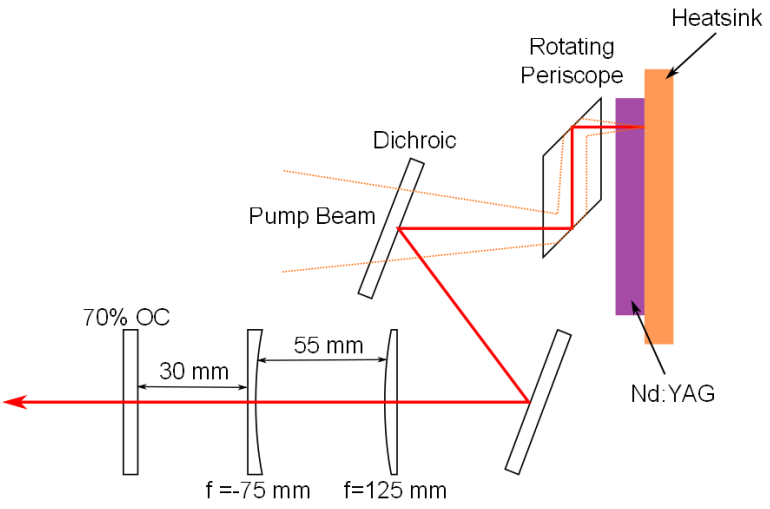

Figure 6.8: The resonator used to find the point of thermal roll over. The distance between the positive lens and the Nd:YAG was 300 mm.

The resonator was considered to be unstable if the thermal lens power was greater than 1.9 m^{-1}, as shown by the red line in Figure 6.9. RTM analysis showed a thermal lens stronger than this would prevent a mode being resonant. Using this value for f in Equation 6.6 and rearranging allows the heating power that renders the resonator unstable to be calculated. This has also been included in Figure 6.10.

Equation 6.6 predicts the RCL will go unstable for a lower pump power than was observed. Whilst the increase in heating power was seen to once again be linear, see §4.2, the measured value was a factor of three higher than that predicted, also shown on

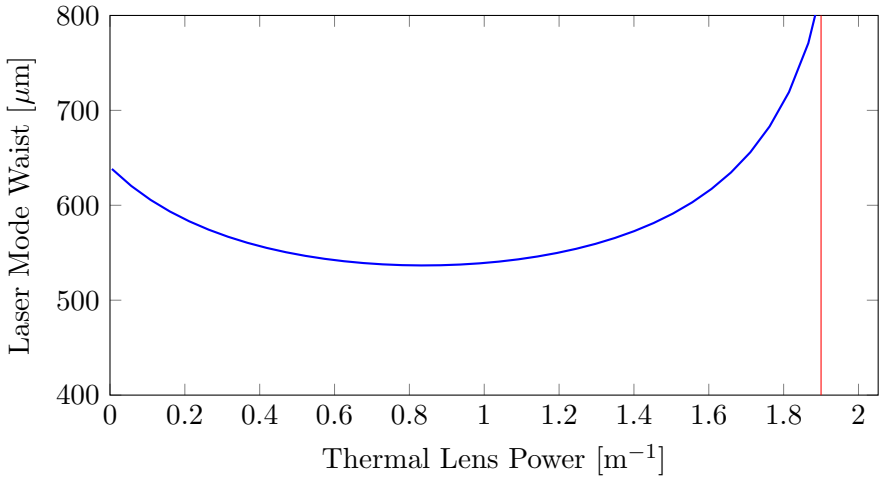

Figure 6.9: Resonator mode waist in the slab as a function of heating power, the red shows the thermal lens strength that is assumed to make the resonator unstable.

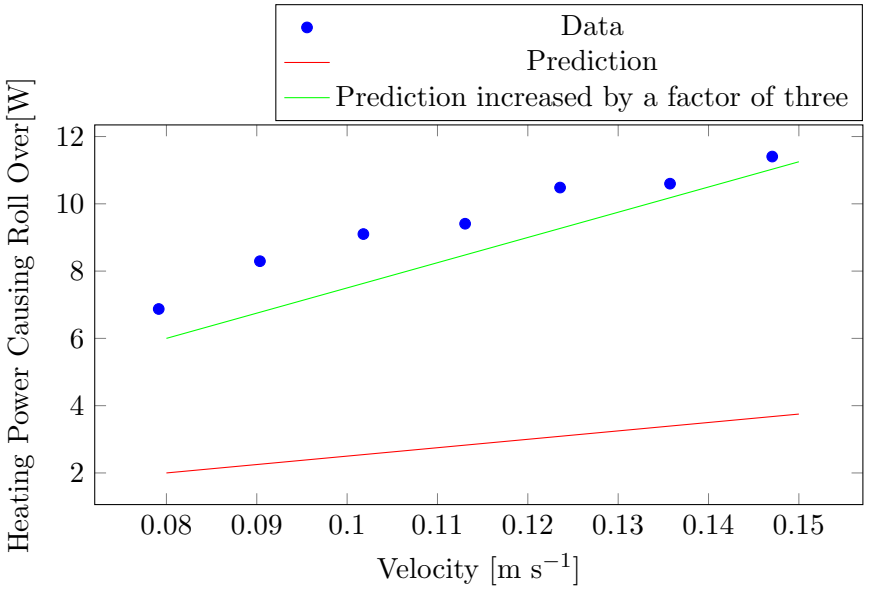

Figure 6.10: Thermal roll over plotted against azimuthal velocity, the red line represents the expected point of roll over given by Figure 6.9.

Figure 6.10. The thermal lens was thus weaker than predicted. The parabolic approximation made in deriving Equation 6.6, see Figure 6.6, will have produced a stronger thermal lens than a Gaussian beam and thus an earlier point of instability. Furthermore, the Gaussian pump beam is in its self an approximation of the actual pump beam shape which is a super Gaussian and has a profile with shallower gradients than that of a Gaussian further reducing the thermal lensing effect.

6.4 Thermal Aberration of a Probe Beam

Whilst the strength of the thermal lens can render a laser unstable this can be compensated for in a particular operating window with an appropriate resonator design. Aberrations introduced by this lens are not as straightforward to correct for, aspherical components have been used to do this but they require careful characterisation of the thermal lens to be successful [5]. The degradation a beam experiences after passing through the pumped spot in an RCL, independent of any focusing effects, is therefore of interest.

6.4.1 Experimental Set-up

To demonstrate the reduction of thermally induced aberrations in an RCL a probe beam was passed through the pump spot. To make the probe beam available to diagnostics after being passed through the pump spot it was incident on the Nd:YAG slab at a small angle away from the normal. It was then separated from the incident probe beam with a knife edge mirror, and deposited on a power meter after being passed through an uncoated optic which was used to provide power to the beam profiler described in §4.4, see Figure 6.11. In this experiment a 6 mm thick, 50 mm diameter Nd:YAG slab was used and a rhomboid prism acted as a monolithic periscope, producing a radius of rotation of 20 mm.

Before placing the slab into this experiment the the probe beam and pump light were measured with a beam profiler at the intended slab position. This served two purposes, allowing the amount of overlap between the two beams at a single prism orientation to be determined as well as showing how well the beam waists were matched. The pump beam was found to have a waist of 750 μm and the probe beam a waist of 600 μm. However, as this only confirmed overlap between the pump and probe beams at a single point it does not ensure the two beams are collinear.

To ensure this probe beam was aligned to the centre of the pump beam over an entire rotation the probe was generated by a separate Nd:YAG laser operating at 1064 nm so it would experience gain if it passed through the pumped region. The power of the returned probe beam could then be analysed over a rotation of the periscope. Once

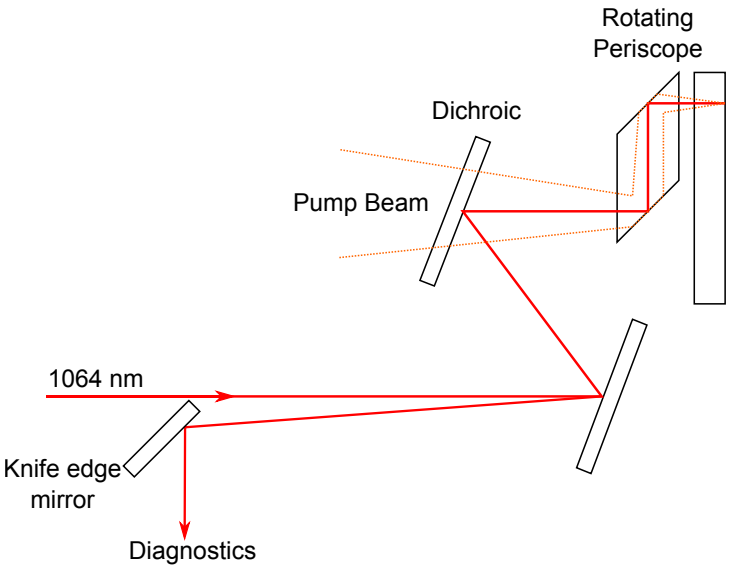

Figure 6.11: Experimental set up to investigate aberrations experienced by a probe 1064nm beam

the power fluctuations were minimised the probe was considered aligned with the pump beam. Figure 6.12 shows the output power returned by the slab after completing this alignment procedure. The uniform unpumped trace indicates uniform reflection over a rotation and the uniform amplified trace indicates that the beams are aligned and the gain is also uniform over a cycle.

The probe beam had an M^2 of 1.12 which was unchanged when passed through the rotating periscope and unpumped slab. Beam quality is thus maintained by the delivery and rotating optics and there are no aberrating features present in the regions of the unpumped slab interrogated by the probe beam. Any variation observed over a rotation

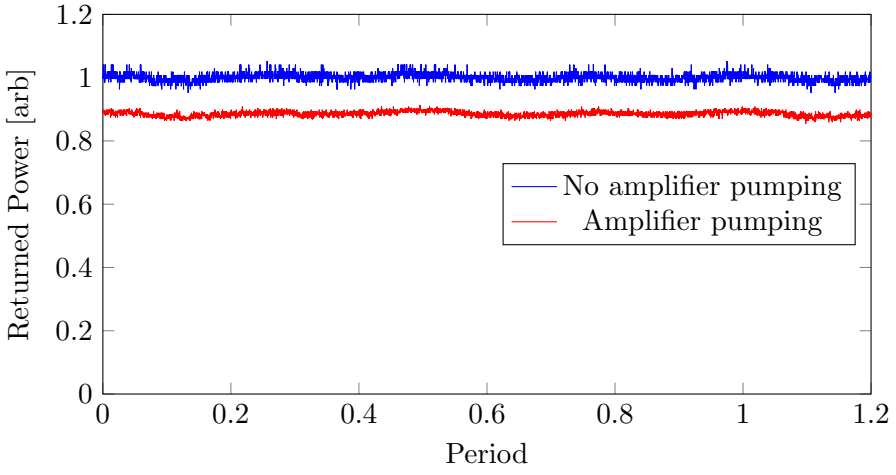

Figure 6.12: The power returned from the rotating amplifier was did not have its modulation depth increased.

trace once the slab is pumped are thus the result of variations in the thermal profile over the pumped region.

6.4.2 Results

Figure 6.13 shows how the M^2 evolves as the pump power, and thus thermal load, is increased when the pump spot and laser mode were moved at 0.38 m s^{-1}. When the incident pump power is less than 51 W there was no degradation in M^2 except for one outlier. As the thermal load was increased further the probe beam suffers thermal aberrations and the M^2 increases. However, the degradation was considerably less than that experienced by the stationary case which produces an M^2 of 2.2 when 15 W of pump light were incident on the slab.

Figure 6.14 shows the average beam quality over a rotation period under different operating conditions. As stated above the beam degradation was severe when the periscope was kept stationary, effectively operating the RCL as a traditional end pumped laser. The beam quality rapidly decayed to 1.97 under 16.3 W of incident pump light. Whereas even moderate rotation speeds are capable of preserving the probe beam's quality under these pump conditions. At higher rotational rates a slight improvement in the seed beams M^2 was seen as the centre of the seed beam saw more gain due to the pump distribution, effectively sharpening it, without being influenced by thermal effects. An M^2 of 1.06 was measured under 16.3 W of pump light whilst rotating at 0.75 m s^{-1} a significant improvement on the 1.97 found for the stationary case.

Whilst there is a rapid increase in the beam quality once motion is introduced, Figure 6.14 shows that at higher rotation rates there are diminishing returns. Again the reduction in performance improvements occurs above 0.5 m s^{-1}. The difference in M^2 between the 0.75 m s^{-1} and 1.5 m s^{-1} cases was only 0.05 under 158 W of pump power. Equation 3.5 predicts a reduction in temperature rise from 2.9 K to 1.4 K which is not dissimilar to the 4.4 K to 2.1 K drop which resulted in a decrease in M^2 of 0.34 between 0.75 m s^{-1} and 0.36 m s^{-1} found under 116 W of pump power. It is therefore likely the heat distribution created by heat flow had a more aberating effect than that under the adiabatic regime.

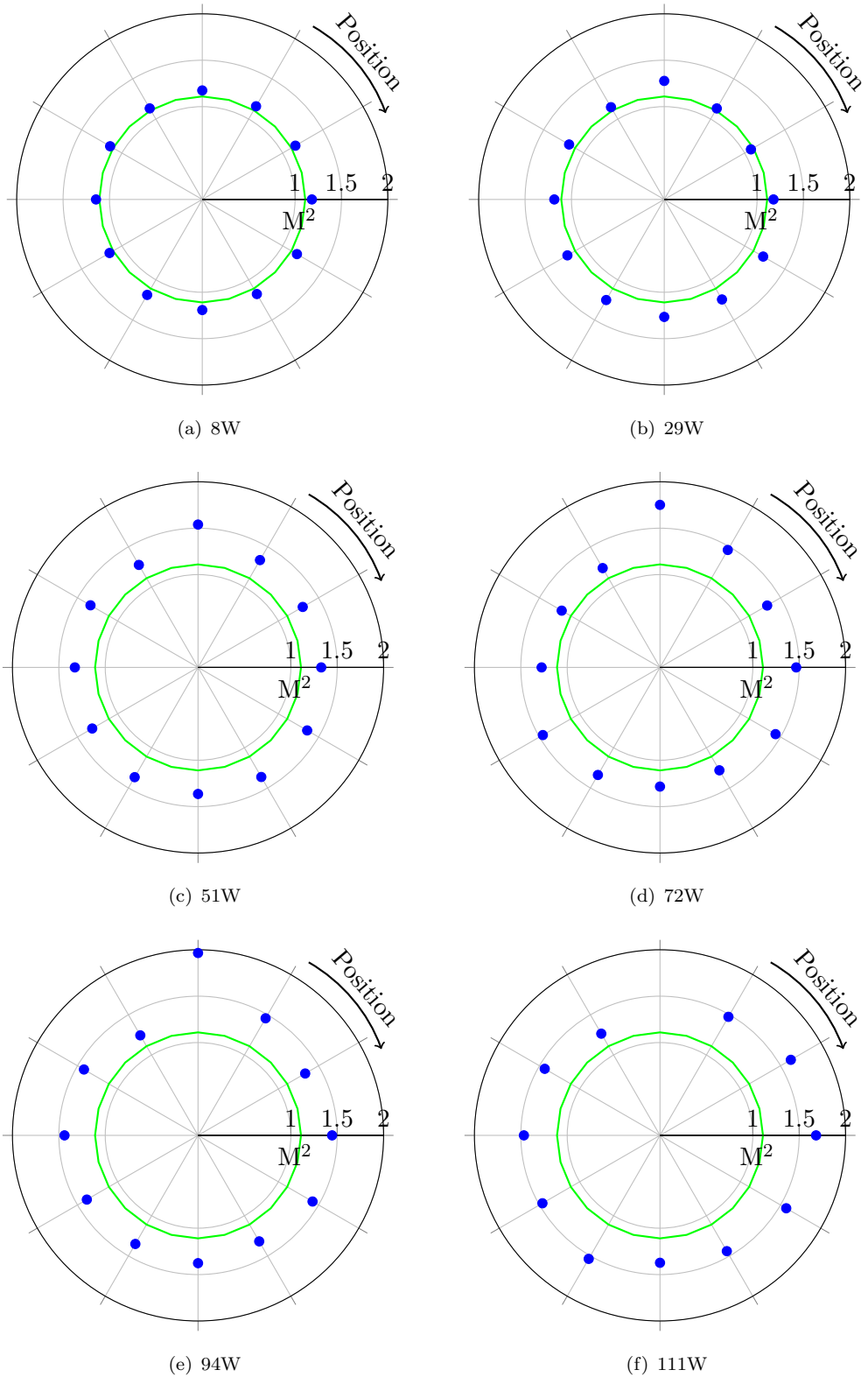

(a) 8W (b) 29W

(c) 51W (d) 72W

(e) 94W (f) 111W

Figure 6.13: M^2 degradation with a velocity of 0.38m s^{-1} as the incident pump power is changed, the green line represents the seed M^2.

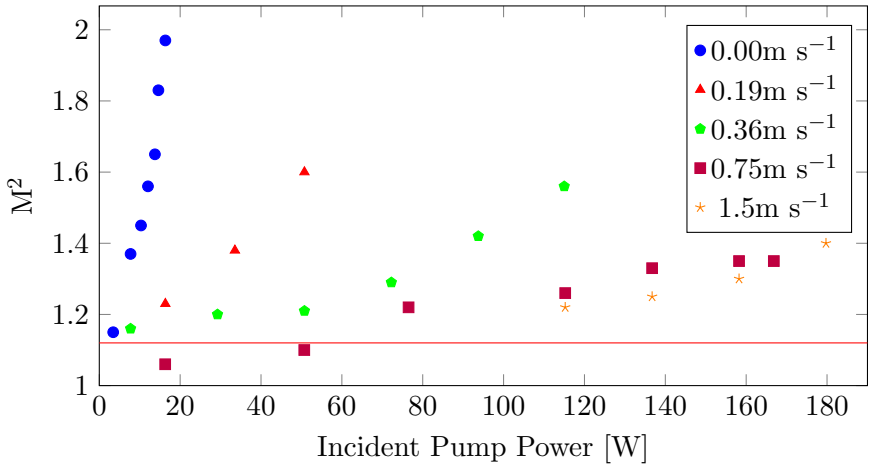

Figure 6.14: Beam degradation as a function of incident pump power at different rotational speeds, the red line represents the unamplified seed beam.

6.5 Thermal Scaling Limits

To determine the scaling limits of the RCL it is useful to consider the situation where the periscope is spinning fast enough to result in a ring of heated material with negligible azimuthal variation. In this situation the heat flow in the azimuthal direction will be small. If heat flow in the axial direction is also ignored the temperature distribution due to radial flow can be calculated, see Figure 6.15. By not considering axial heat flow the heat sinking arrangement in the RCL is not taken into account, giving a worst case description of the temperature profile.

The radial part of the steady state heat equation in polar coordinates is

$$\frac{d}{dr}\left(r\frac{dT}{dr}\right) = 0 \tag{6.9}$$

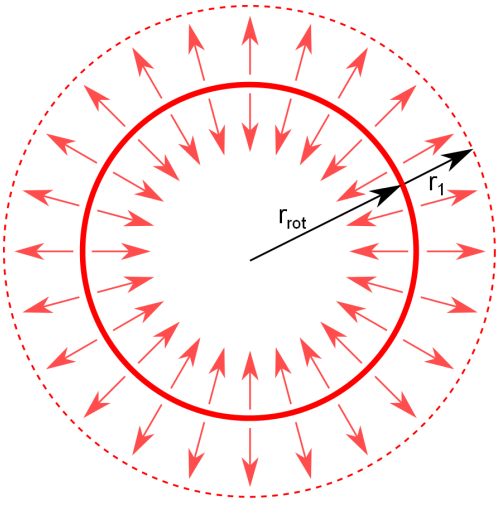

Figure 6.15: Heat flow is assumed to be radial.

The general solution to which can be found via the separation of variables and is

$$T(r) = A\ln(r) + B \tag{6.10}$$

Where A and B are constants of integration. If it is assumed the width of the pumped spot is small compared to r_1 the heat flux can be modelled as coming from a infinitesimally narrow ring and thus can be treated as a Neumann boundary. The constant heat flux through the boundary is described by Equation 6.11 where k is the thermal conductivity of the material and q is the heat flux [6].

$$q(r_{\text{rot}}) = -k\frac{dT}{dr} \tag{6.11}$$

If a second boundary r_1 away from the pumped ring is considered to be at constant temperature T_0 both A and B can be found, leaving

$$T(r) = \frac{T_0}{2} + \frac{qr_{\text{rot}}}{2k}\ln\left(\frac{r_{\text{rot}} + r_1}{r}\right) \tag{6.12}$$

If r_{rot} is large and there is no asymmetry in the radial temperature distribution, a situation likely in an RCL and suggested by the FEA analysis in §5.7.2, the heat flow will be mirrored on the other side of the Neumann boundary. The temperature at r_{rot} is thus given by

$$T(r_{\text{rot}}) = T_0 + \frac{qr_{\text{rot}}}{k}\ln\left(1 + \frac{r_1}{r_{\text{rot}}}\right) \tag{6.13}$$

As r_{rot} increases the temperature at the Neumann boundary tends to

$$T(r_{\text{rot}}) = T_0 + \frac{qr_1}{k} \tag{6.14}$$

For a constant pump power, q is reduced as the surface area the flux enters the system is increased. In the high speed limit the area of this surface is the circumference of the circle swept out by the rotating periscope multiplied by the depth of the slab if heat generation is assumed to be uniform over its depth. The area of this surface increases linearly with r_{rot}, reducing the temperature rise.

The volume exposed to pump light in an RCL determines its temperature rise in the high speed limit. Comparing the heated volume with a rod case gives an indication of the power scaling potential of the RCL architecture. The volume heated in the high speed RCL is as follows, where l is the length the pump beam travels within the slab.

$$V_{\text{heated}} = 4\pi r_{\text{rot}} w_p l \tag{6.15}$$

Comparing Equation 6.15 with the pumped volume in a traditional laser rod gives the following expression for the increase in volume when using an RCL. In a thermally limited system this gives the increase in usable pump power and thus the power scaling potential of the RCL technique.

$$V_{\text{ratio}} = \frac{4r_{\text{rot}}}{w_p} \tag{6.16}$$

The RCL allows an increase in the volume exposed to heating without increasing the lasing volume. This results in a drastic increase in the thermal mass without the problems associated with large volumes of excited material outlined in 2.6.3. Importantly the displacement of the periscope acts as a power scaling mechanism beyond the high speed limit as it increases the volume of material directly exposed to heat. This scaling approach is limited only by the practicalities of large gain media and the pump brightness required to avoid aperaturing through the length of the periscope.

If it is assumed that the pump beam fills the first reflecting surface of the periscope with beam radius w_a and that the gain medium is as close as possible to it the distance from the first periscope aperture to the focus of pump is

$$z = d + l + \frac{w_a}{2} \tag{6.17}$$

Here l is the distance beyond the periscope the focus is, see Figure 6.16, and d is the displacement introduced by the periscope.

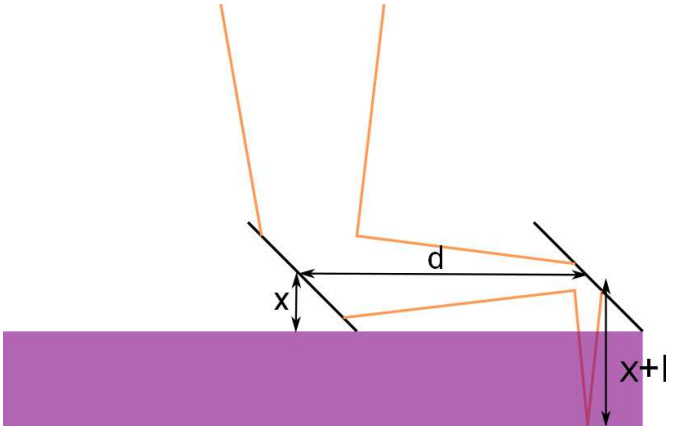

Figure 6.16: The size of the periscope determines the minimum pump brightness.

Using Equation 6.17 in Equation 2.40 it can be shown that the displacement introduced by the periscope, d, must satisfy the following expression.

$$d = z_R \left(\left(\frac{w_a}{w_0} \right)^2 - 1 \right)^2 - l - \frac{w_a}{2} \tag{6.18}$$

w_0 is the focused spot size and z_R is the Rayleigh range which is given by

$$z_R = \frac{\pi w_0^2}{\lambda \mathrm{M}^2} \tag{6.19}$$

This constraint provides the limit on the scaling potential of the RCL due to the available pump brightness.

By introducing a more complicated beam path, for example by including a second smaller periscope to rotate the pump laser pair around the exit axis of the main periscope, the heated volume could be drastically increased without increasing the size of the gain medium. However, this does not remove the pump brightness limitation as the path within the periscope would be necessarily increased.

6.6 Conclusion

In this chapter a series of experiments which demonstrated the reduction of thermally induced deleterious effects were presented. First stress induced birefringence was considered as a convenient measure of the amount of stress the thermal load was placing on the gain medium. This was done by using a Brewster window to force the resonator to operate in a linearly polarized mode. The losses from this surface where then measured when the rotating periscope was acting as an optical retarder allowing the change in polarization due to induced stresses to be determined. The induced stresses reached a minimum when the thermal processes became adiabatic.

A theoretical prediction of the thermal lens strength followed, which underlined the dramatic increase in thermal load handling ability that motion creates in comparison to a traditional laser rod. Experimental results indicate that the thermal lens was in fact weaker than predicted, which was consistent with the parabolic approximation used in the analysis.

To investigate the aberating nature of the thermal lens independently of its focal length, a probe beam was used to interrogate the pumped spot on the RCL slab. The beam degradation was severe when the periscope was kept stationary with the M^2 degrading rapidly from the 1.12 seed to 1.97 under 16.3 W of incident pump light. Whereas even moderate rotation speeds were capable of preserving the probe beam's quality under these pump conditions. With an azimuthal velocity of 1.51 m s^{-1} the aberrations introduced by the pump spot resulted in an increase in M^2 to 1.4 under 180 W of pumping, demonstrating a dramatic improvement in heat handling ability.

A comparison between the heated volumes in a traditional laser rod and the RCL was also presented. This showed the new power scaling mechanism available to RCL like architectures in the form of the radius of rotation. This approach to power scaling is

limited by pump brightness as the pump light must be coupled into the gain medium though the periscope and the practicalities of large gain media.

Geometric considerations of the periscope arrangement provided a condition on the pump brightness that must be satisfied to avoid aperaturing the pump beam. The need for bright pump sources is common across many laser architectures and the available brightness from diode sources has improved dramatically recently. Whilst their brightness is now starting to rival that of fibre lasers and thin disk sources they do not offer the energy storage potential of a solid state gain medium [7]. Pairing a modern diode with a RCL will therefore allow the generation, or amplification, of high average power laser pulses in a more straight forward manner than has been previously possible.

References

[1] W. A. Clarkson, N. S. Felgate, and D. C. Hanna, "Simple method for reducing the depolarization loss resulting from thermally induced birefringence in solid-state lasers," *Optics Letters*, vol. 24, p. 820, June 1999.

[2] J. D. Foster, "Thermal Effects in a Nd:YAG Laser," *Journal of Applied Physics*, vol. 41, no. 9, p. 3656, 1970.

[3] W. Koechner, *Solid State Laser Engineering*. New York: Springer, 6th ed., 2006.

[4] M. E. Innocenzi, "Thermal modeling of continuous-wave end-pumped solid-state lasers," *Applied Physics Letters*, vol. 24, no. 19, p. 2253, 1990.

[5] S. C. Tidwell, J. F. Seamans, and M. S. Bowers, "Highly efficient 60-W TEM_00 cw diode-end-pumped Nd:YAG laser," *Optics Letters*, vol. 18, p. 116, Jan. 1993.

[6] M. S. Gockenbach, *Partial Differential Equations: Analytical and Numerical Methods*. SIAM, 2nd ed., 2010.

[7] R. K. R. Huang, B. Chann, J. Burgess, M. Kaiman, R. Overman, J. D. Glenn, P. Tayebati, and B. B. Rd, "Direct diode lasers with comparable beam quality to fiber, CO2, and solid state lasers," in *SPIE LASE*, p. 824102, International Society for Optics and Photonics, 2012.

Chapter 7

Conclusions and Future Work

7.1 Conclusion

After introducing the basic principles behind lasing in §2, along with the challenges faced by the laser community to generate ever brighter laser sources, this thesis introduced a new approach to improve the thermal load handling characteristics of a solid state laser. Solid state lasers offer a distinct advantage over other laser architectures in the pulsed regime. The large energy storage offered by a solid state host, coupled with the relatively large mode sizes when compared to a fibre and high single pass gain when compared to a thin disk, makes them ideally suited to generating short, intense, laser pulses.

Whilst a solid state laser is capable of both storing a large amount of energy and extracting it very quickly, at high average powers the thermal load imparted by the lasing process inhibits their performance. An analysis conducted by Tidwell et al found that even if thermal lensing could be overcome an end pumped Nd:YAG rod cannot be pumped by more than 70 W from a single end (assuming an absorption coefficient of 4.1 cm^{-1}) before suffering from thermal fracture [1]. With modern pump sources a lower absorption coefficient can be used whilst maintaining overlap with the laser mode over the pumped region which will increase the maximum pump power. However the authors note that this reduction in stress does not decrease linearly with an increase in absorption length and the allowed pump power increases slowly. There are thus fundamental limits to the further power scaling of a traditional laser rod.

In §3 the Rotating Cavity Laser was introduced. Optically this new laser architecture acts as an end pumped laser but introduces motion to separate the lasing process from thermal processes in space, much like a QCW laser separates them in time. This chapter included an analysis of the expected effects introducing moving parts to a laser resonator would have as well as a discussion of previous examples of moving media lasers. By

keeping the gain medium stationary, unlike in previous work, the practicality of the system was improved by removing the need to cool the gain medium with gaseous helium. Preliminary calculations found that whilst motion would have a drastic impact on the temperature rise its adverse effects on the lasing process would by comparison be small, giving the RCL advantages over other solid state lasers.

In §4 results from the first demonstration of an RCL were presented. The first prototype was restricted to low azimuthal velocities and was used to show that any detrimental effects from introducing motion to a laser resonator did not overshadow the beneficial thermal properties. By replacing the mechanical components the regime where laser threshold is effected by motion was explored and results confirming the behaviour of laser threshold predicted in §3.5.2.1 were presented. Q-switched operation was also demonstrated and the motion was found not to effect the energy storage properties of the Nd:YAG when operating at 1 kHz.

Beam quality measurements conducted for the source in §4.3 were found to be influenced by the pointing instability and the finite exposure time of the measuring system. Under the assumption any variations in the laser mode in an RCL are cyclic it was possible to reconstruct beam profiles from measurements of multiple rotation periods. The beam profiler that was constructed could resolve any variations in beam quality over a rotation.

The resonator described in §5 made use of a more powerful pump source than that used in §4. With this it was possible to pump beyond the stress fracture limit predicted in [1] and generate 120 W at 1064 nm from an end pumped Nd:YAG laser. Whilst excellent beam quality was found at low powers the M^2 became poor as the pump power increased.

The system was reconfigured as an amplifier which revealed a fault with the bond between the Nd:YAG ceramic and the heat sink. This was corrected by making use of a nickel buffer layer and soldering in a nitrogen atmosphere. With an improved thermal interface it was possible to generate 12 dB of small signal gain for 180 W of pump power. Parasitic lasing prevented the generation of more gain.

The pointing stability of the amplified beam was used to extract information about the thermal wedge induced by the unusual temperature profile created by motion. FEA analysis suggested that earlier predictions underestimated the strength of this wedge by a factor of two. It was postulated that this thermal wedge was adversely affecting the beam quality at high powers and that by compensating for this wedge it is hoped the beam quality at high power will be drastically improved.

§6 presented a series of experiments which demonstrate the reduction of thermally induced deleterious effects. Both stress induced birefringence and the aberrating nature of the thermal lens were shown to be drastically reduced by operating in the adiabatic regime. The marked decrease in thermal aberration under rotation found with the probe

beam when compared to the stationary case indicate the system could be usefully used as a final stage amplifier.

A theoretical prediction of the thermal lens strength was also included. This underlined the dramatic increase in thermal load handling ability motion creates in comparison to a traditional laser rod. Experimental results indicate that the thermal lens was in fact weaker than predicted which was consistent with the parabolic approximation used in the analysis as well as the use of a super Gaussian pump profile in the experiment. Furthermore, the theoretical model assumed the system was within the adiabatic limit, the presence of any axial heat flow in the experiment would also have reduced the strength of the measured thermal lens.

The power scaling potential of the RCL was also considered by comparing the heated volume with that of a traditional laser rod. Unlike in other laser rod the RCL allows this volume to be increased whilst leaving the size of the lasing region unchanged. By increasing the displacement introduced by the rotating periscope the thermal mass can be increased, and thus the pump power can be increased without inducing detrimental effects. This scaling technique is limited by the practicalities of large gain media and the need to have the pump collinear with the laser mode before entering the periscope which has the potential to act as an aperture.

The need to have large gain media to continue power scaling can be removed by introducing more complicated motion to the system. For example, a second rotating periscope can be used to trace circles around current beam path. This would drastically increase the volume of the gain medium used. However, this does not alleviate the constraint on the pump brightness and an expression was derived that must be satisfied for the pump to be able to fit through the periscope.

In conclusion, whilst good beam quality has not yet been demonstrated at the 100 W level from an RCL it is felt that by overcoming the thermally induced misalignment triggered by the moving heat spot the increase in beam quality can be reduced. Once this artefact is removed from the laser system it is hoped any other causes of beam degradation will become apparent allowing good beam quality to be realised. The energy storage potential of a solid state gain medium could then be used to produce high pulse energy at high average power, a capability which is non trivial to implement in other laser designs. Furthermore, in an amplifier configuration this misalignment manifests as beam steering of the output which can be compensated for with an active optic. Importantly the gain spot in the Nd:YAG slab was found to have a minimal aberrating effect on the seed beam indicating a promising future for this technique as a final stage amplifier.

7.2 Future Work

7.2.1 Polarization Compensation

An immediate consequence of using a rhomboid prism as a rotating periscope was the variation in polarisation properties over a rotation cycle. In the future this constraint could be avoided by either replacing the prism with a pair of suitably ruggedized mirrors and thereby avoid relying on total internal reflection, or by including an extra optical element to compensate for it. Clearly any polarization compensating component needs to be synchronised to the rotation of the prism. This can be done by making it part of the monolithic periscope.

Attaching a piece of appropriately orientated birefringent material to the front of the prism will undo the phase shift imparted by the total internal reflections. The length of this component can be calculated with Equation 7.1 which has been derived by considering the phase shift between two waves experiencing different refractive indexes. λ_0 is the vacuum wavelength and $\Delta\phi$ is the required phase shift in radians.

$$l = \frac{\Delta\phi\lambda_0}{2\pi\Delta n} \tag{7.1}$$

A BK7 rhomboid prism introduces a phase shift of 77.26°, see §3.4.2.2, and quartz has a $\Delta n = 0.00873$ [2]. A 26 μm thick layer of quartz will thus correct for the phase shift. A thicker piece of quartz would be more practical and as long as the thickness is increased in increments that introduce a phase shift of 2π a dimension that facilitates its manufacture can be chosen. A suitable piece of quartz can therefore be bonded directly to the rhomboid prism making the unit suitable for operation in a polarized resonator.

7.2.2 Alignment Compensation

The variation in alignment created by both the thermal wedge and the imperfect periscope are cyclic, making them straightforward to predict. Furthermore the changes are slow, gross variation in the output power occurs over the order of a rotation period, 50 ms if the system is rotating at 20 Hz. Variations in the power output can therefore be readily compensated for by modulating the pump power as the periscope rotates. However, if a thermal wedge is responsible for the poor beam quality at higher pump powers this will not act to improve it.

The change in angular alignment at high power could be compensated for by placing an intracavity optic on a piezoelectric mirror mount. This would remove the need for a compromise alignment as the mirror would be able to track the evolving wedge. The cyclic nature of this would remove the need for high speed electronics as the required

motion can be determined from the previous rotation period reducing the cost and complexity of the active system.

7.2.3 Final Stage Amplifier

The amplifier experiments in §5 only explored the small signal regime due to the lack of a suitable high power seed. The low gain efficiency associated with Nd:YAG make it more suitable as a final stage amplifier. This would allow more of the energy stored within the crystal to be usefully extracted, importantly the level of thermally induced aberrations should remain unchanged. In this configuration the amplifier could form a useful device with the ability to further amplify both high power CW and pulsed sources.

The minimal aberrations experienced by the seed under a pump power of 100s of Watts suggest operation at higher pump powers is possible. Furthermore, identifying and removing the source of the feedback causing parasitic lasing should allow an increase in the available small signal gain.

7.2.4 Other Gain Media and Wavelengths

The 1% doped, 6 mm thick Nd:YAG slab is capable of absorbing 91% of the incident pump light in a single pass if the effective absorption coefficient is taken to be 41 mm^{-1} with a pump bandwidth of 3 nm [1]. However the 400 W source has a bandwidth of 0.7 nm allowing the 808 nm absorption peak to be better targeted, the slab can therefore be reduced in thickness whilst still maintaining an acceptable level of pump absorption. Reducing the thickness of the gain medium will further encourage axial heat flow as the thermal profile tends to that found in a thin disk.

The thickness of the disk could also be reduced by using a Yb:YAG gain medium which is the strategy adopted in high power thin disks. The higher dopant levels, and hence shorter absorption lengths, would allow complete pump absorption in less material than would be required for Nd doped YAG. Importantly the disk thickness would not have to be reduced to the levels seen in a thin disk allowing mechanical rigidity to be retained.

The low cross section 946 nm transition in Nd:YAG may also be better able to be exploited in an RCL geometry. Output powers of this transition have been thermally limited to 10s of Watts in non-guiding architectures and 105 W has been achieved in a planar waveguide geometry [3]. The reduction in thermal loading associated with the RCL could thus allow further power scaling without the need for guiding, simplifying the device while removing the beam quality astigmatism and giving the potential for the generation of more intense pulses.

7.3 Closing Remarks

Finally, perhaps the best example of the improvement in thermal load handling the introduction of motion provides, occurred when the mechanical system failed. Whilst being pumped with 85 W, delivered to a 700 μm spot in an amplifier configuration, the drive motor malfunctioned. The interlock set to turn off the pump diode in this situation also failed. The resulting heat load caused the stress fracture limit of the Nd:YAG slab to be exceeded resulting in a catastrophic failure, see Figure 7.1. Not only did the ceramic crack cleanly into multiple pieces but it also caused either the solder to re-flow or the delamination of the metallic layers bonding the slab to the heat sink; resulting in it coming free from its mount. When rotating not only was the amplifier undamaged when pumped by over twice this power, but it was able to provide gain whilst degrading a probe beam from an M^2 of 1.1 to 1.4. This stark difference in behaviour clearly shows the effectiveness of motion as a thermal load mitigating technique.

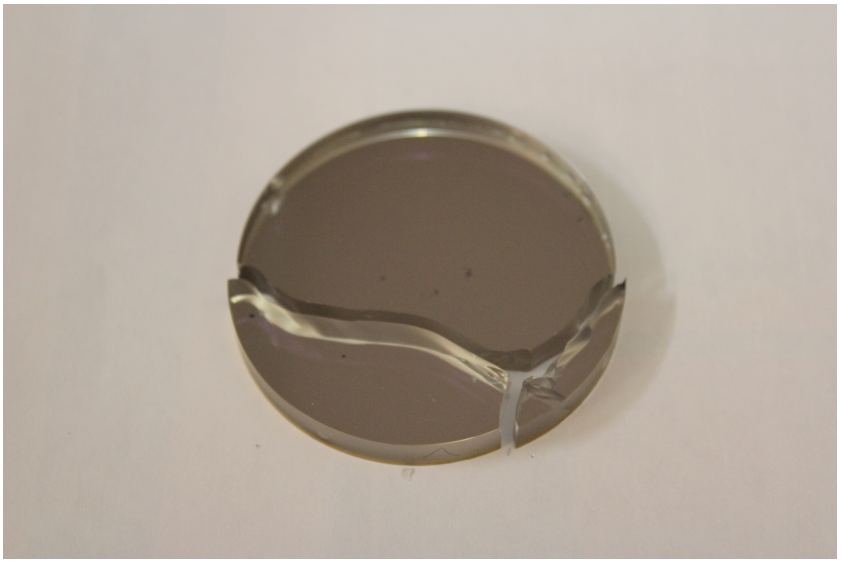

Figure 7.1: When the periscope failed to rotate the resultant temperature rise overcame the stress fracture limit of the Nd:YAG slab.

References

[1] S. C. Tidwell, J. F. Seamans, M. S. Bowers, and A. K. Cousins, "Scaling CW diode-end-pumped Nd:YAG lasers to high average powers," *Quantum Electronics, IEEE Journal of*, vol. 28, pp. 997–1009, Apr. 1992.

[2] G. Ghosh, "Dispersion-equation coefficients for the refractive index and birefringence of calcite and quartz crystals," *Optics Communications*, vol. 163, pp. 95–102, May 1999.

[3] S. P. Ng and J. I. Mackenzie, "Power and radiance scaling of a 946 nm Nd:YAG planar waveguide laser," *Laser Physics*, vol. 22, pp. 494–498, Feb. 2012.